N 84 - 18726

INVERSION ALGORITHMS FOR THE MICROWAVE REMOTE SENSING

OF SOIL MOISTURE

by

Gary D. Hancock

Department of Electrical Engineering
University of Arkansas
Fayetteville, Arkansas 72701

March 1984

INVERSION ALGORITHMS FOR THE
MICROWAVE REMOTE SENSING OF
SOIL MOISTURE

Experiments with Swept Frequency Microwaves

Gary Duke Hancock
University of Arkansas

ABSTRACT

Two experiments were performed employing swept frequency microwaves for the purpose of investigating the reflectivity from soil volumes containing both discontinuous and continuous changes in subsurface soil moisture content. Discontinuous moisture profiles were artificially created in the laboratory while continuous moisture profiles were induced into the soil of test plots by the environment of an agricultural field. The reflectivity for both the laboratory and field experiments was measured using bi-static reflectometers operated over the frequency ranges of 1.0 to 2.0 GHz and 4.0 to 8.0 GHz.

Reflectivity models that considered the discontinuous and continuous moisture profiles within the soil volume were developed and compared with the results of the experiments. This comparison shows good agreement between the smooth surface models and the measurements. In particular the comparison of the smooth surface multi-layer model for continuous moisture profiles and the field experiment measurements points out the sensitivity of the specular component of the scattered electromagnetic energy to the movement of moisture in the soil.

Although the agreement of the smooth surface reflectivity and the measurement is good, the smooth surface models do not adequately explain the frequency dependence exhibited by the measured reflectivity of both experiments. In order to account for the frequency dependence of the measurement, a specular

transmission coefficient for a rough surface is derived and incorporated into the reflectivity models. The roughness corrected models gave improved agreement with the measurements indicating that swept frequency microwave measurement techniques can be used to account for both moisture gradients within the soil and structures at the soil surface. Most notable about the roughness corrected models and the measurements is that coherent phase effects due to the interference of a subsurface reflection from the moisture gradients and a surface reflection can occur in the presence of surface roughness.

TABLE OF CONTENTS

LIST OF FIGURES

LIST OF FIGURES (CONT.)

LIST OF FIGURES (CONT.)

LIST OF FIGURES (CONT.)

LIST OF FIGURES (CONT.)

CHAPTER 1

INTRODUCTION

Two experiments employing broad-spectrum electromagnetic waves were conducted to investigate the moisture of soil volumes. Bistatic reflecto-meters were used to measure the scattered electromagnetic energy at the specular angle. The experiments characterized the soil volumes by measuring reflectivity as a function of frequency for the ranges of 1.0 to 2.0 and 4.0 to 8.0 GHz. One experiment was conducted in the laboratory and involved soil volumes with artifically created moisture profiles, while the other experiment was conducted in the field and examined soil volumes with moisture profiles under the influence of the environment.

Soil moisture content affects the microwave reflectivity of the soil through changes in the complex permittivity. If the soil surface is smooth and the moisture content of the subsurface uniform, then the reflectivity of the soil is directly related to the complex permittivity and in turn to the moisture content. However, soil surfaces in nature are seldom smooth, and the moisture content posesses gradients which are seldom in a state of equilibrium. The irregularities in the soil surface give a frequency dependent roughness effect to the reflectivity, while gradients in the complex permittivity produce subsurface reflections that must be accounted for in the total reflectivity of the soil volume. It is the purpose of this paper to describe, model, and therefore explain the microwave reflectivity of soil volumes that have both roughness at the surface boundary and moisture gradients within the volume.

Chapter 2 provides background material that examines soil composition and structure. Included in the material is the effect of both a smooth and rough surface on the reflection of electromagnetic energy.

1

The description of the laboratory experiment is given in Chapter 3. In this chapter the reflection coefficient using a two-layer model of a soil volume with a smooth surface is developed. This smooth surface model is then compared with the results of the experiments.

Chapter 4 deals with the field experiment conducted at the University of Arkansas Experimental Station with the help of members of the Agronomy Department. The two-layer model of Chapter 3 is extended to a multi-layer model to account for permittivity gradients in the soil subsurface. The field experiment is described, and the results of the experiment are compared to the smooth surface multi-layer model.

The effects of surface roughness are incorporated into the models of Chapter 5, and the roughness corrected models are compared to the results of both experiments.

The conclusions of the experiments as well as recommendations for future instrumentation and experiments are given in Chapter 6.

CHAPTER 2

BACKGROUND

2.1 Soil Composition and Structure

The microwave reflectivity of soil surface is directly dependent
on the complex permittivity of the soil (Waite et. al., 1973). The complex
permittivity of the soil is in turn dependent on the moisture content
of the soil volume (Lundien, 1971; Newton, 1977; Wang and Schmugge, 1978).

Soil volumes may exhibit layers or stratifications giving rise to
discontinuities in soil moisture. Under the influence of the environment
each layer may in turn possess moisture gradients. Of particular interest
is the effect of the soil moisture profile on microwave reflectivity
as the spatial variation in soil moisture introduces gradients and discon-
tinuities in the complex permittivity. The majority of work involving
electromagnetic waves in layers, or strata, and permittivity gradients
has been for application to waveguide and atmospheric propagation (Collin,
1966; Brekhovskikh, 1960; Wait, 1962). Investigations dealing with layered
materials, and in particular soils, show that discontinuities in permittivity
due to soil moisture content can be detected using microwave swept frequency
technqiues (Lundien, 1972 and Waite et al., 1973). Simulation studies
of the emissivity from a three-component soil model in which a transitional
permittivity layer is sandwiched between two homogeneous layers indicate that
the reflectivity is determined by the permittivity gradient in the transitional
layer and that it may be possible to estimate the deep distribution of
the soil permittivity (Wilheit, 1976; Basharinov and Shutko, 1977).

A further complication to the composition of the soil is that the
moisture content in the surface zone of an agricultural field exhibits
long term time variations as well as diurnal changes in which the soil

3

surface dries during the day and partially rewets during the evening and night (Jackson, 1973). The movement of moisture within the soil profile is governed by the demands of the atmosphere and the ability of the soil to deliver water. The ability of the soil to deliver water is in turn influenced by its texture and structure. Soil texture refers to the predominate size range of the particles comprising the soil (Reid, 1977), and for a given soil will remain essentially constant (Hillel, 1971). Soil structure is the mutual arrangement, orientation, and organization of the particles of the soil and is also used to refer to the geometry of the pore spaces (Hillel, 1971). It is possible to recognize three types of soil structures. These are single-grained, massive, and aggregated structures. The soil particles are unattached in a single-grained structure. In a massive structure the soil particles are bonded into large massive blocks. The aggregated structure is an intermediate state in which the soil particles are organized into small clods called aggregates.

Soil structure is dynamic and can change with time as a result of changes in the environment. The surface soil zone in an agricultural field is tilled, exposed to rainfall, and compacted due to traffic all of which subject the soil surface zone to structural change. Tilling the soil can create a loose dry surface layer which reduces evaporation losses of the soil (Jackson, 1973). The beating action of rain can cause the surface to develop a crusting layer or seal that inhibits the movement of moisture through the surface. Compaction of the soil has the effect of reducing the size of interaggregate pores which reduces the ability of free water to move within the soil (Hillel, 1971).

The roughness of the surface soil structure acts to scatter incident electromagnetic energy. This roughness effect yields a specular and diffuse component in the scattered energy. The specular component is

a function of the surface height variance, while the diffuse component
is a function of both the variance and the correlation of the surface
structural heights (Peake, 1959; Beckmann and Spizzichino, 1963; Waite
et al, 1973).

In summary, the microwave reflectivity is a function of the composi-
tion and structure of the soil, both of which may be dynamic processes.
The permittivity of the soil can possess discontinuities and gradients
due to the layering and spatial variability of soil moisture. The soil
structure can affect the movement of soil moisture as well as the scattering
of the electromagnetic energy.

2.2 Reflection Coefficient from a Smooth Surface

Consider a plane wave with an electric field E_i incident on a boundary
of infinite extent between media as shown in Figure 2.1. For horizontal
polorization the field will take form

$$\bar{E}_i = E_o \, e^{-\gamma_A (\bar{n}_i \cdot \bar{r})} \, \bar{a}_3 \tag{2.1}$$

where E_o is the magnitude of the electric field, $\bar{n}_i$ a unit vector in the
direction of propagation, $\bar{r}$ the position vector, $\bar{a}_z$ a unit vector perpen-
dicular to the plane of incidence, and γ_A the propagation factor. Defining
the reflection and transmission coefficients at the origin as

$$\Gamma_\perp = \frac{E_r}{E_i}$$
, the ratio of the reflected and incident fields

$$\tau_\perp = \frac{E_r}{E_i}$$
, the ratio of the transmitted and incident electric fields

The form of the reflected and transmitted electric fields is then
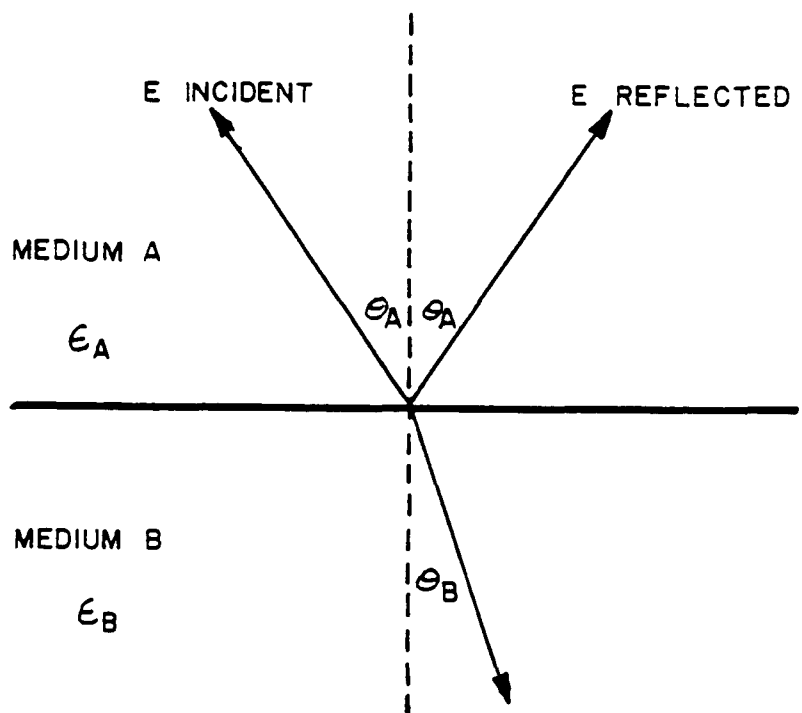
Figure 2.1 Geometry of a plane boundary

$$\bar{E}_r = \Gamma_\perp E_o e^{-\gamma_A (\bar{n}_r \cdot \bar{r})} \bar{a}_3 \qquad (2.2)$$

$$\bar{E}_T = \tau_\perp E_o e^{-\gamma_B (\hat{n}_r \cdot \bar{r})} \bar{a}_3 \qquad (2.3)$$

where γ_B is the propagation factor in medium B and $\bar{n}_r$ and $\bar{n}_t$ are unit vectors in the direction of propagation for the reflected and transmitted electric fields. By applying the boundary conditions it can be shown that the angle of incidence will equal the angle of reflection and that the angle of transmission θ_B will be related to the angle of incidence θ_A by Snells' law (Kraus and Carver, 1973).

$$\sin \theta_B = \frac{\gamma_A}{\gamma_B} \sin \theta_A$$

It can further be shown that the horizontal reflection coefficient will be given by

$$\Gamma_\perp = \frac{\cos \theta_A - \sqrt{\frac{\hat{\epsilon}_B}{\epsilon_A} - \sin^2 \theta_A}}{\cos \theta_A + \sqrt{\hat{\epsilon}_B / \epsilon_A - \sin^2 \theta_A}} \qquad (2.4)$$

and the transmission coefficient will be related by the boundary condition

$$\tau_\perp = 1 + \Gamma_\perp \qquad (2.5)$$

A similiar development can be shown for vertical polarization. (Stratton, 1941; Ramo, et al., 1967).

The propagation factor for the media is given by

$$\gamma_i^2 = \frac{\omega^2}{C^2} \hat{\epsilon}_i \quad , \quad i = A \text{ or } B \tag{2.6}$$

where ω is the angular frequency, C the velocity of light and $\hat{\epsilon}_i$ the complex relative permittivity. The propagation factor γ_i can be written as a complex term

$$\gamma_i = \alpha_i + j\beta_i \tag{2.7}$$

where α_i = attenuation factor

β_i = phase factor

Both α_i and β_i can be solved in terms of the complex permittivity yielding

$$\alpha_i = \frac{2\pi}{\lambda_o} \left[\frac{\sqrt{(\epsilon_{r,i})^2 + (\epsilon_{I,i})^2} - \epsilon_{r,i}}{2} \right]^{1/2}$$

$$\beta_i = \frac{2\pi}{\lambda_o} \left[\frac{\sqrt{(\epsilon_{r,i})^2 + (\epsilon_{I,i})^2} + \epsilon_{r,i}}{2} \right]^{1/2}$$

where

λ_o = free space wavelength

$\epsilon_{r,i}$ = real part of the complex permittivity for i = A or B.

$\epsilon_{I,i}$ = Imaginery part of the complex permittivity for i = A or B.

If $\epsilon_{r,i} > \epsilon_{I,i}$ which is normal condition for soils (Lundien, 1971), then the phase factor can be approximated by

$$\beta_i \approx \frac{2\pi}{\lambda_o} \sqrt{\epsilon_{r,i}}$$

2.3 The Scattering of Electromagnetic Waves from Rough Surfaces

A plane wave incident on a plane surface of infinite area is reflected
in the specular direction as given by Snell's law. A plane surface of finite
area will introduce diffraction effects giving a lobe structure to the reflected
field. The main lobe resulting from the effects of diffraction is referred
to as the coherent or specular component of the scattered field. The addition
of random surface structures, or roughness, decreases the specular component
and produces an incoherent or diffuse component of the scattered field. The
scattered field will remain coherent (specular component dominant) for surfaces
with roughness of small height deviations. As the surface become progressively
rougher there will be a continuous transition in the scattered field from
coherent to incoherent (Beckmann and Spizzichino, 1963).

The model of particular interest for the specular component of the scattered
field is the small perturbation theory which is an extension of the Rayleigh method
for the solution of the scattered field from surfaces with random roughness.
The Rayleigh method represents the scattered field as an infinite series
of plane waves in the form

$$\sum_{m,n} E(m,n)$$

where E is a plane wave with direction determined by the integers m and n.
Each of the scattered fields is determined by satisfying the exact boundary
condition at the surface (Beckman, and Spizzichino, 1963). The Rayleigh
method will theoretically be exact since it uses the exact boundary condition.
In practice the infinite series generated by the solution of the Rayleigh

9

method converges readily only for small height deviation, and small height is the restriction for both the Raleigh method and the small perturbation method.

The surface $z = \zeta(x, y)$ for the small perturbation theory is random and may vary only a small amount from $z = 0$. The equation of the surface is expanded as a two-dimensional Fourier series with random coefficients. The statistics of the Fourier coefficients are used to determine the frequency spectrum or roughness distribution function of the surface.

The scattered electric field of the small perturbation theory takes the form

$$E_{x, y, \text{ or } 3} = \sum_{mn} N_{mn} E(m, n, 3)$$

where N_{mn} is the magnitude of the scattered electric field $E(m, n, z)$. The integers m and n are summed from $-\infty$ to $+\infty$ and give the direction of propagation for an infinite set of plane waves. A detailed development of the small perturbation theory is contained in Waite, et al., (1973) and Stiles (1974). The development of the method states that if the perturbations of the surface are largely uncorrelated, then the effective rough surface reflection coefficients are

$$\Gamma_{h,v}^{R} = \Gamma_{h,v} e^{-a \left(\frac{2 \pi h \cos \theta_0}{\lambda} \right)^2}$$

(2.9)

10

where

$\Gamma_{h,v}^{R}$ = Effective rough surface specular reflection coefficient for either horizontal or vertical polarization.

$\Gamma_{h,v}$ = smooth surface reflection coefficient for either horizontal or vertical

h^2 = Mean square surface height

θ = Angle of incidence

The results of the small perturbation theory given by equation 2.9 are the same as those of Beckman and Spizzichino (1963), Ament (1953), and Davies (1954) using the Kirchoff or physical optics model for a randomly rough surface of zero mean and normal distribution. The Kirchoff model assumes that the field at any point on the rough surface can be approximated by the field that would appear on a plane tangent to that point. This tangent plane approximation requires that the slopes of the surface structures be small or that their radius of curvature be large.

Experimental investigations of the specular reflection from rough surfaces satisfying the requirements of the small perturbation theory (Waite, et. al., 1973 and Stiles, 1974) as well as from surfaces purposely violating the theory (Hancock, 1976) substantiate the exponetial dependence of the reflection coefficient on wavelength and indicate that frequency diversity can be used to correct for roughness.

CHAPTER 3

DISCONTINUOUS MOISTURE PROFILES

The investigation of coherent effects due to a permittivity gradient within the soil volume began with laboratory experiments involving artificially created layered soil media. These layered media consisted of differing depths of dry soil material with a moisture content varying from 3% to 6% by weight over saturated soil material with moisture contents ranging from 30% to 40% moisture by weight. The following sections present the derivation of a two-layer model, a description of the experiment, and the results of the experiment explained in terms of the two-layer model.

3.1 Theory

The following is a solution for the reflection of a plane electromagnetic field from a two-layered medium. The solution is for horizontal polarization, however, the model can be expanded to include vertical polarization. The model derivation is similar to Lundien, 1972.

3.1.1 The Reflection Coefficient of the Two-Layer Model

For the purposes of this simple model it is assumed that the field is reflected from a non-homogeneous medium that can be separated into two homogeneous layers with horizontal area of infinite extent. Figure 3.1 shows the geometry of the problem. Medium B is relatively thin while the underlying layer is sufficiently thick that it may be considered infinite in depth. Medium A is air, or free space, in which the field has an incident component, a reflected component due to the air-soil interface, and an infinite sum of components while medium C has only

E INCIDENT E REFLECTED

MEDIUM A

ϵ_A

MEDIUM B

ϵ_B

MEDIUM C

ϵ_C
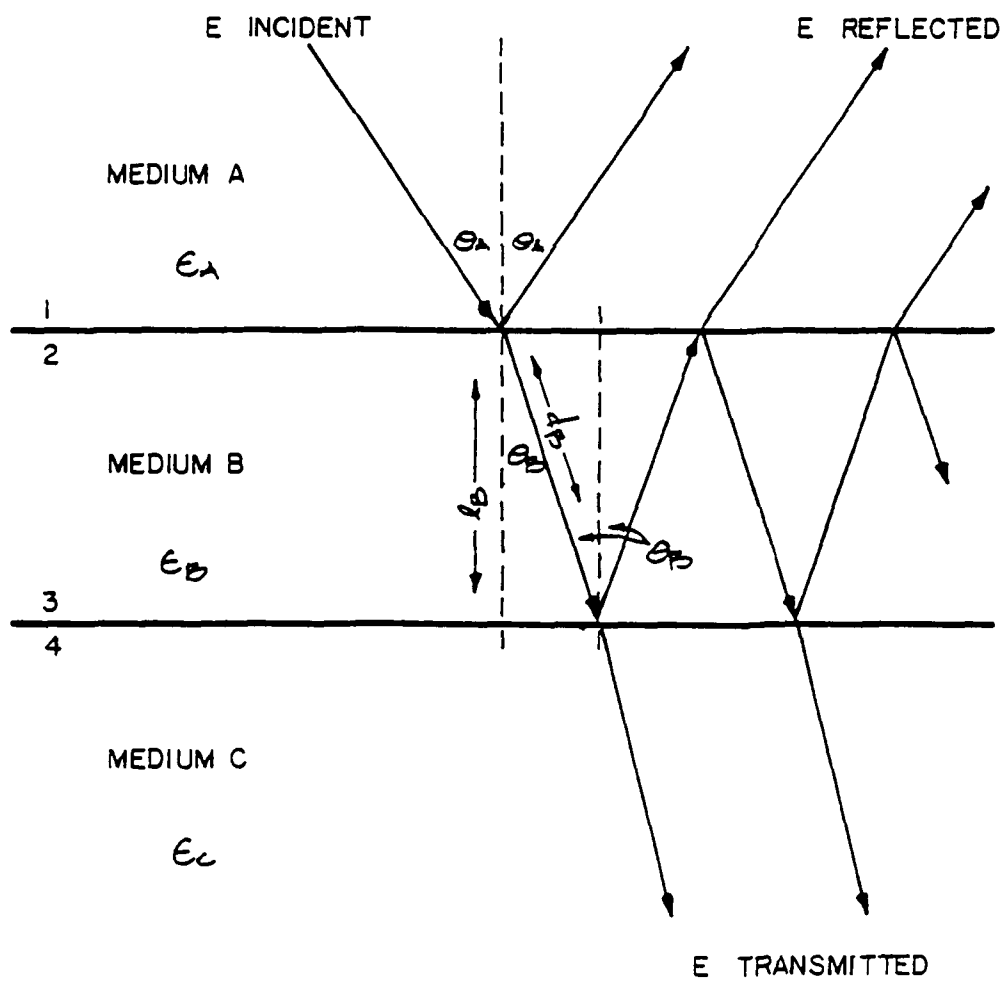
E TRANSMITTED

Figure 3.1 Geometry of the two-layer model.

transmitted components. It is also assumed that the permittivity $\hat{\epsilon}_C$ of medium C is greater than the permittivity $\hat{\epsilon}_B$ of medium B.

The incident field is expressed in the form

$$\bar{E}_i = E_0 e^{-\gamma_A (\bar{n} \cdot \bar{r})} \, \bar{a}_3$$

where E_0 is the magnitude of the electric field, γ_A is the propagation factor in medium A, $\bar{n}$ is a unit vector in the direction of propagation, $\bar{r}$ is the position vector, and $\bar{a}_z$ is a unit vector perpendicular to the plane of incidence indicating horizontal polarization. The total reflection coefficient in medium A (see Appendix A) is given by

$$\Gamma_{TOTAL} = \frac{\Gamma_1 + \Gamma_3 e^{-2\gamma_B d_B}}{1.0 + \Gamma_1 \Gamma_3 e^{-2\gamma_B d_B}} \tag{3.1}$$

Reflection coefficient Γ_1 is due to the abrupt change in permittivity between the A and B media and while Γ_3 is the reflection coefficient due to the interface between the B and C media. The total reflection coefficient given by equation 3.1 may be viewed as a surface reflection summed with a subsurface reflection that is altered in phase and attenuated in magnitude due to the thickness and dielectric properties of medium B.

The surface reflection coefficient Γ_1 for horizontal polarization is given by

$$\Gamma_1 = \frac{\cos\Theta_A - \sqrt{\dfrac{\hat{\epsilon}_B}{\hat{\epsilon}_A} - \sin^2\Theta_A}}{\cos\Theta_A + \sqrt{\dfrac{\hat{\epsilon}_B}{\hat{\epsilon}_A} - \sin^2\Theta_A}} \tag{3.2}$$

The subsurface reflection coefficient Γ_3 can likewise be related to the angle of incidence Θ_A in medium A giving

$$\Gamma_3 = \frac{\sqrt{1 - \frac{\hat{\epsilon}_A}{\hat{\epsilon}_B} \sin^2\Theta_A} - \sqrt{\frac{\hat{\epsilon}_C}{\hat{\epsilon}_B} - \frac{\hat{\epsilon}_A}{\hat{\epsilon}_B} \sin^2\Theta_A}}{\sqrt{1 - \frac{\hat{\epsilon}_A}{\hat{\epsilon}_B} \sin^2\Theta_A} + \sqrt{\frac{\hat{\epsilon}_C}{\hat{\epsilon}_B} - \frac{\hat{\epsilon}_A}{\hat{\epsilon}_B} \sin^2\Theta_A}} \qquad (3.3)$$

It is important to note that the reflection coefficients at the layer interfaces, Γ_1 and Γ_3, are functions of the ratio of the permittivities of the media comprising the boundaries and not the magnitude of a specific permittivity.

3.1.2   Reflectivity of Two-layer Model

The power reflectivity ρ is defined as

$$\rho = \Gamma_{TOTAL} \Gamma^*_{TOTAL} = |\Gamma_{TOTAL}|^2$$

and can be expressed in terms of the two-layer model as

$$\rho = \frac{|\Gamma_1|^2 + |\Gamma_3|^2 e^{-4\alpha_B d_B} + 2|\Gamma_1||\Gamma_3| e^{-2\alpha_B d_B} \cos(2\beta_B d_B + \Theta_1 - \Theta_3)}{1.0 + |\Gamma_1|^2 |\Gamma_3|^2 e^{-4\alpha_B d_B} + 2|\Gamma_1||\Gamma_3| e^{-2\alpha_B d_B} \cos(2\beta_B d_B - \Theta_1 - \Theta_3)} \qquad (2.4)$$

where $\Theta_1 = \tan^{-1}\left(\frac{Im \, \Gamma_1}{Re \, \Gamma_1}\right)$

$\Theta_3 = \tan^{-1}\left(\frac{Im \, \Gamma_3}{Re \, \Gamma_3}\right)$

15

α_B = attenuation factor of medium B

β_B = phase factor of medium B.

$|\Gamma_1|^2 = \Gamma_1 \Gamma_1^*$

$|\Gamma_3|^2 = \Gamma_3 \Gamma_3^*$

If the real part of the permittivity for each medium is much greater than the imaginary part, which is the normal case for soils (Lundien, 1971), then the real part of the reflection coefficient will also be much greater than the imaginary part for the condition

$$\hat{\epsilon}_C > \hat{\epsilon}_B > \hat{\epsilon}_A$$

The phase angles ϑ_1 and ϑ_2 will then be negligible allowing the approximation of $\cos(2\beta_B d_B)$ to be used in equation 3.4. The minima of equation 3.4 will occur when

$$\cos(2\beta_B d_B) = -1$$

or when $2\beta_B d_B$ is an odd multiple of π

$$2\beta_B d_B = (2n+1)\pi \qquad (3.5)$$

The reflectivity minimum may then be expressed as

$$\rho_{min} = \left[\frac{|\Gamma_1| - |\Gamma_3| e^{-2\alpha_B d_B}}{1.0 - |\Gamma_1||\Gamma_3| e^{-2\alpha_B d_B}} \right]^2 \qquad (3.6)$$

For this condition the propagation distance d_B can be obtained by noting that

$$\beta_B = \frac{2\pi}{\lambda_B} = \frac{2\pi \sqrt{\epsilon_{r,B}}}{\lambda_o}$$

16

then

$$d_B = (2n+1) \frac{\lambda_B}{4} \qquad (3.7)$$

Equation 3.7 shows that when the propagation distance d_B in medium B is an odd multiple of a quarter-wavelength the surface and subsurface components of the reflectivity will be 180° out of phase.

The propagation distance can be related to the vertical depth, ℓ_B in medium A by the approximation

$$\ell_B = \frac{\lambda_0 \sqrt{\varepsilon_{r,B} - \sin^2\Theta_A}}{4 \; \varepsilon_{r,B}} \; (2n+1) \qquad cm. \qquad (3.8)$$

or

$$\ell_B = \frac{30 \sqrt{\varepsilon_{r,B} - \sin^2\Theta_A}}{4 \; \varepsilon_{r,B} \; f_0(GHz)} (2n+1) \qquad cm.$$

where $\varepsilon_{r,B}$ is the real part of the complex permittivity for medium B.

It is possible for the minimum reflectivity to be zero which would give the appearance of no boundary. This condition will occur if

$$|\Gamma_1| = |\Gamma_3| e^{-2\alpha_B d_B}$$

This, in turn, requires

$$|\Gamma_3| > |\Gamma_1|$$

which states that the subsurface component must be greater than the surface component of the reflectivity. This condition leads to a relationship between the relative permittivities of media B and C

for subsurface dominance of the reflectivity

$$|\epsilon_c| = \left(\frac{|\epsilon_B|}{\cos\theta_A} - \tan\theta_A\right)^2 + \sin^2\theta_A \qquad (3.9)$$

For normal incidence ($\theta_A = 0^\circ$), the above expression reduces to

$$|\epsilon_c| > |\epsilon_B|^2 \qquad (3.10)$$

Equation 3.9 and 3.10 indicate the non-linear relationship of the permittivities in the volume for subsurface dominance of the total reflectivity.

3.2 Laboratory Experiment

The reflectivity of abrupt moisture profiles was measured in the laboratory with a bistatic reflectometer employing swept frequency techniques over the frequency ranges of 1.0 to 2.0 GHz and 4.5 to 8.0 GHz.

3.2.1 Description of Experiment

A block diagram of the system is shown in Figure 3.2. The microwave power for the frequency range of interest is generated by the sweep oscillator and conveyed to the transmitting antenna via coaxial cable. A directional coupler is used to sample the transmitted power and provide feedback leveling to the sweep oscillator as well as a reference to the network analyzer. The microwave power is radiated from the transmitting antenna, reflected by the soil target, and gathered by the receiving antenna. Square law crystal detectors are used to
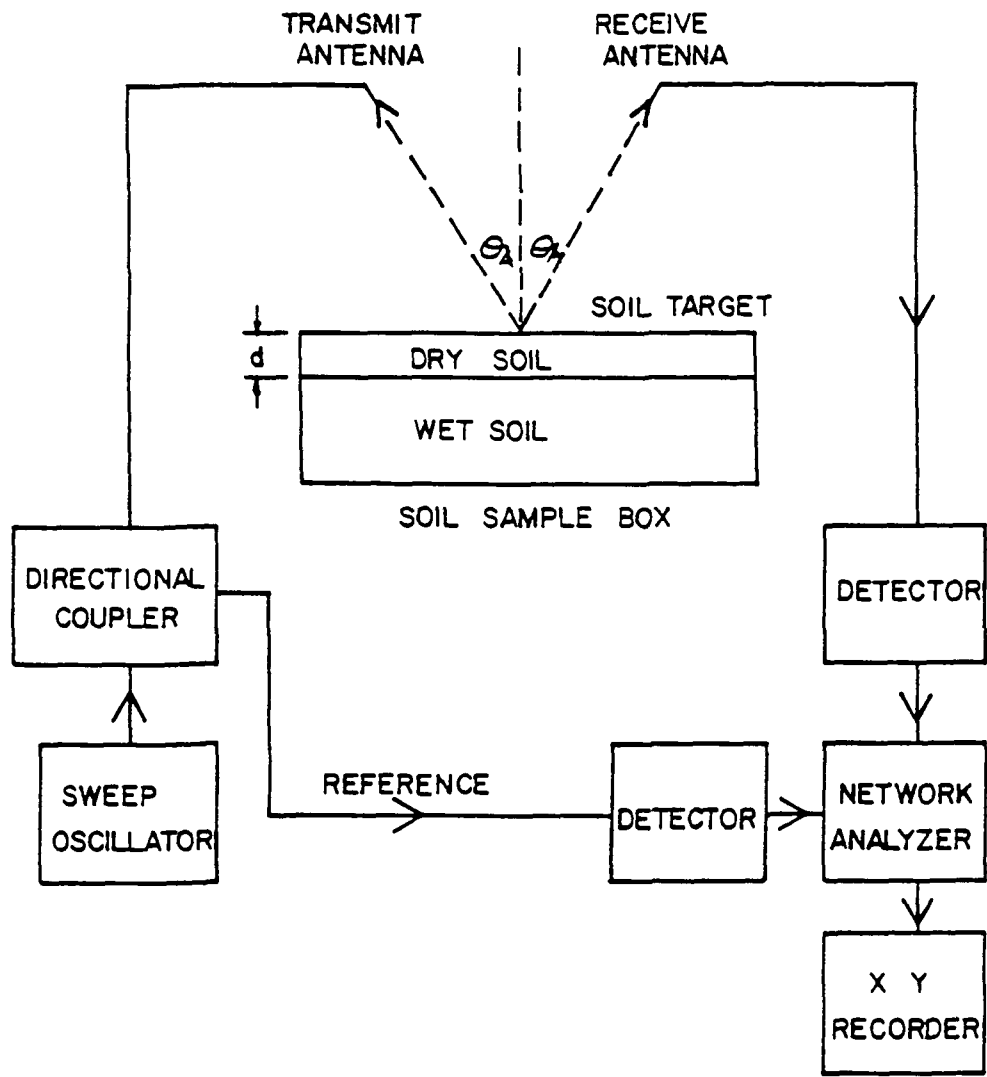
Figure 3.2 Block diagram of laboratory bistatic reflectometer system.

develop a voltage porportional to power for both the reference and the signal received from the soil target surface. These voltages are fed to the network analyzer which ratios the two voltages. This ratio is then recorded by an X-Y plotter as a function of transmission frequency.

All equipment other than the bistatic reflectometer support frame and soil sample box is commercial. The sweep oscillator is an Alfred Model 650 mainframe with oscillator plug-in units for the frequency ranges of 1-2 GHz (wavelengths from 30 to 15 cm), 4-8 GHz (wavelengths from 7.5 to 3.75 cm) and 8-12 GHz (wavelengths 3.75 to 2.5 cm). The network analyzer system is an Alfred Model 8000 oscilloscope with an Alfred Model 7051 Sweep Network Analyzer plug-in unit. The transmitting and receiving antennas are identical for each frequency range and are standard gain waveguide horn antennas.

The bistatic reflectometer support apparatus is constructed of wood and consists of a basic framework centered about the soil sample box. Brace arms are attached to the sides of the soil sample box for the support and mounting of the antennas. This brace arm arrangement permits the antennas to be rotated about the central axis of the sample box at a constant radius of 1.8 meters. A more detailed description of this bistatic reflectometer system is given in Hancock, 1976.

The soil sample box is also constructed of wood and has dimensions of 112 x 112 x 30 centimeters. Wet soil was added to the box to the necessary height, a thin plastic sheet was spread over the wet soil, and dry soil was added filling the sample box. The thin plastic sheet clearly defined the moisture boundary and prevented moisture from redistributing from the wet soil into the drier upper soil layer. This method gave dry soil layers of specific depths over wet soil.

Laboratory system calibration is accomplished by placing an aluminum sheet over the soil sample box. This metal sheet simualtes a ground of infinite conductivity. A swept frequency measurement of the power reflected from the metal plate is used to elminate resonances. The reflectivity of the plate is one, therefore we may express tne soil reflectivity as

$$|\Gamma_{soil\ sample}|^2 = \frac{|\Gamma_{soil\ sample}|^2}{|\Gamma_{metal\ plate}|^2} = \frac{\left(\frac{P_r}{P_t}\right)_{soil\ sample}}{\left(\frac{P_r}{P_t}\right)_{metal\ plate}}$$

where $\left(\frac{P_r}{P_t}\right)$ is the ratio of the received power to the transmitted power given by the network analyzer. Since the network analyzer expresses the ratioed power in decibels the more appropriate equation is

$$|\Gamma_{soil\ sample}|^2 dB = \left(\frac{P_r}{P_t}\right)_{sample} dB - \left(\frac{P_r}{P_t}\right)_{plate} dB \qquad (3.11)$$

Data recording simply involves plotting a swept frequency measurement of the reflected power from the metal calibration plate as it lay atop the soil sample box. The metal plate is removed and the measurement repeated for the bare soil sample. Data reduction was accomplished by determining the differences between the two recorded curves as given by equation 3.11.

The texture of the soil used in the laboratory experiment was clay loam. Soil moisture content was determined using wetness

$$\omega = \frac{mass\ of\ water}{mass\ of\ soil} \times 100\%$$

In order to obtain the proper degree of soil wetness, dry soil and water were combined in a concrete mixer. The use of the concrete mixer gave a good homogeneous soil and water mixture as well as facilitating large volume soil preparations. This method of soil preparation resulted an aggregated soil structure for the laboratory experiment.

3.2.2 Results of Experiment

In this section three representative reflectivity curves from the laboratory experiment are shown to illustrate the coherent effect of the dry upper soil layer and discontinuous boundary. Each of these reflectivity curves were obtained from a soil volume consisting of thin dry soil layer with an uncompacted agregated structure over a saturated subsurface soil volume. The three reflectivity measurements are shown by the dashed curves of Figures 3.3, 3.4, and 3.5, respectively. In these figures the solid curves are reflectivities obtained from the two-layer model with surface permittivity $\hat{\varepsilon}_B$=3.0-j .05, and subsurface permittivity $\hat{\varepsilon}_C$=30 - j 1.7, and angle of incidence θ_A=30°. This results in reflection coefficients at the interfaces of the layers of -.31 + j .004 and -.54 + j.007 for Γ_1 and F_3, respectively. An examination of the values for the reflection coefficients shows the imaginary part to be much less than the real part for each coefficient.

Figure 3.3 shows the calculated and measured reflectivities for an abrupt permittivity transition at a depth of 1.9 cm. As previously stated the measured reflectivity extends only over the frequency ranges of 1.0 to 2.0 GHz and 4.5 to 8.0 GHz while the calculated reflectivities are continuous over the span of 1.0 to 8.0 GHz. The gap in the measured reflectivity in the frequency range of 6.45 to 6.65 GHz is due to the reflectivity minimum exceeding the dynamic range of the network analyzer

22
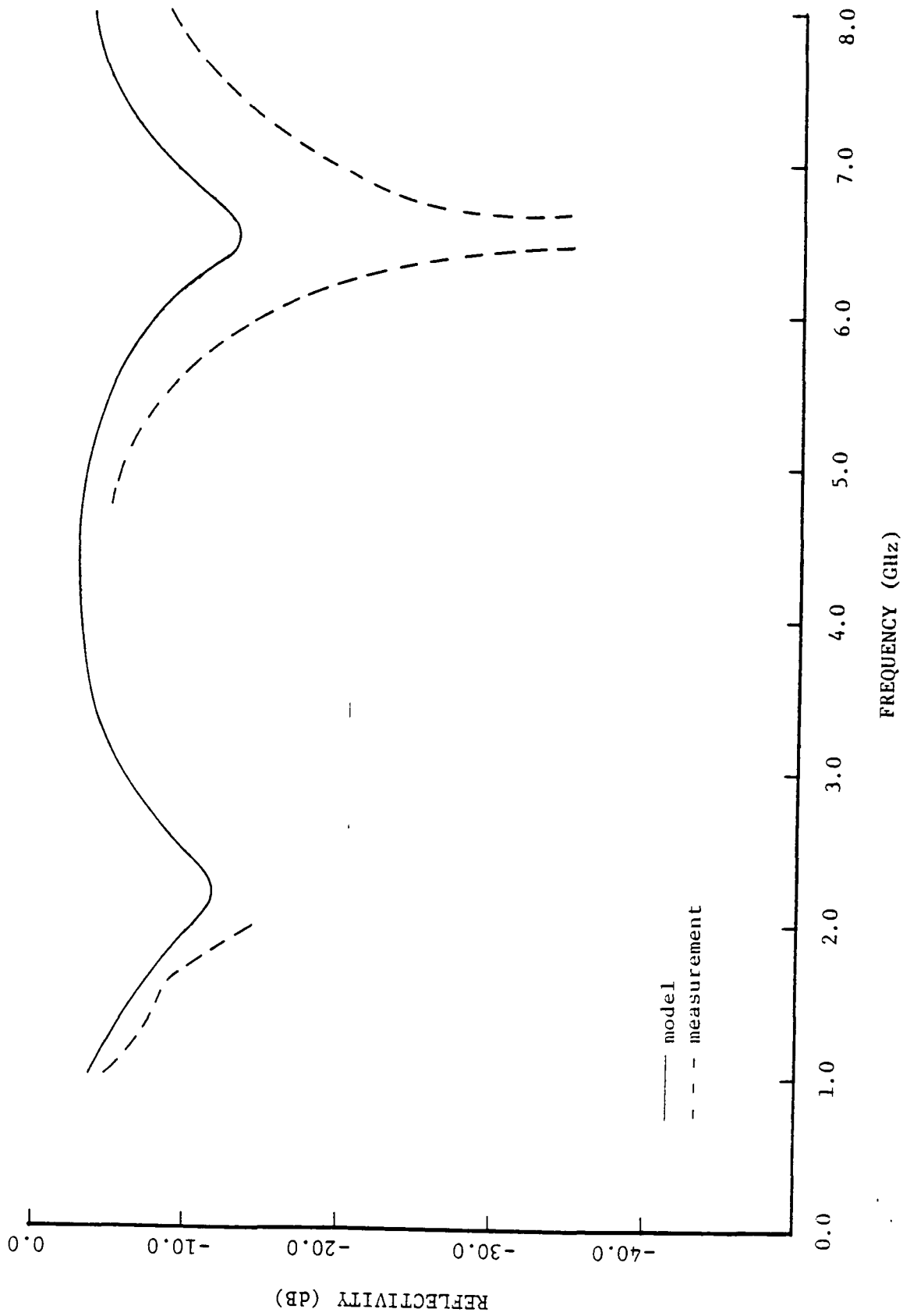
Figure 3.3 Comparison of two-layer model and measurement for dry layer depth of 1.9 cm.

23

used in the experiment. Both the model and measured reflectivity indicate minima at frequencies of 2.2 and 6.6 GHz. These frequencies correspond to one and three-quarter wavelengths in the dry soil medium. However, there is a difference in the magnitude at the minima and an increasing offset with frequency between the two reflectivity curves particularly over 4.5 to 8.0 GHz range. The subsurface component of the model reflectivity is dominant at the minima, but the measured reflectivity shown by the depth of the minima especially about 6.6 GHz indicates that the surface and subsurface components are nearly equal. This characteristic will also be seen in the other reflectivity measurements presented in this section. This phenomena as well as the increasing offset with frequency is attributed to roughness at the air - soil boundary and will be discussed more fully in Chapter 5.

The reflectivity curves of Figure 3.4 are for a soil volume with a dry layer depth of 3.0 cm. The model reflectivity shows three minima at frequencies corresponding to one, three, and five quarter-wavelengths as related to the dry soil medium. A comparison of the two reflectivity curves shows good agreement between model and measurement except for a difference in the magnitude of the minima and an offset between the curves that increases with frequency.

The thickness of the upper dry soil layer for the reflectivity curves of Figure 3.5 is 3.6 cm. The reflectivity of the model shows minima at frequencies of 1.15, 3.45, 5.7 and 8.0 GHz. Similar to Figures 3.3. and 3.4, the minima occur for wavelengths where the subsurface component is in phase opposition to the surface reflected component of the surface. The depths traversed by the field in the upper soil

24
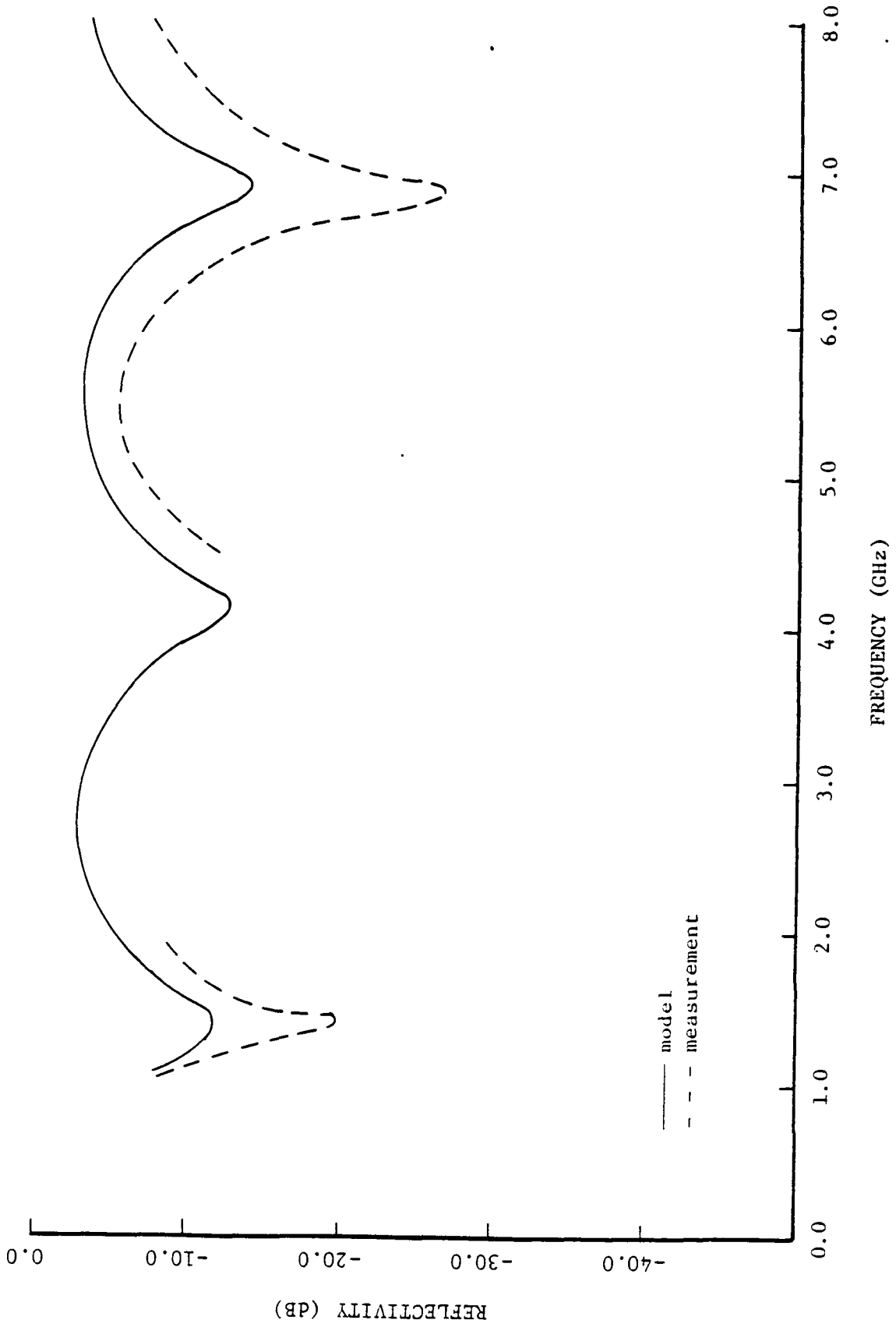
Figure 3.4 Comparison of two-layer model and measurement for dry layer depth of 3 cm.

REFLECTIVITY (dB)

FREQUENCY (GHz)

———— model

– – – measurement

0.0   1.0   2.0   3.0   4.0   5.0   6.0   7.0   8.0

0.0   -10.0   -20.0   -30.0   -40.0

25
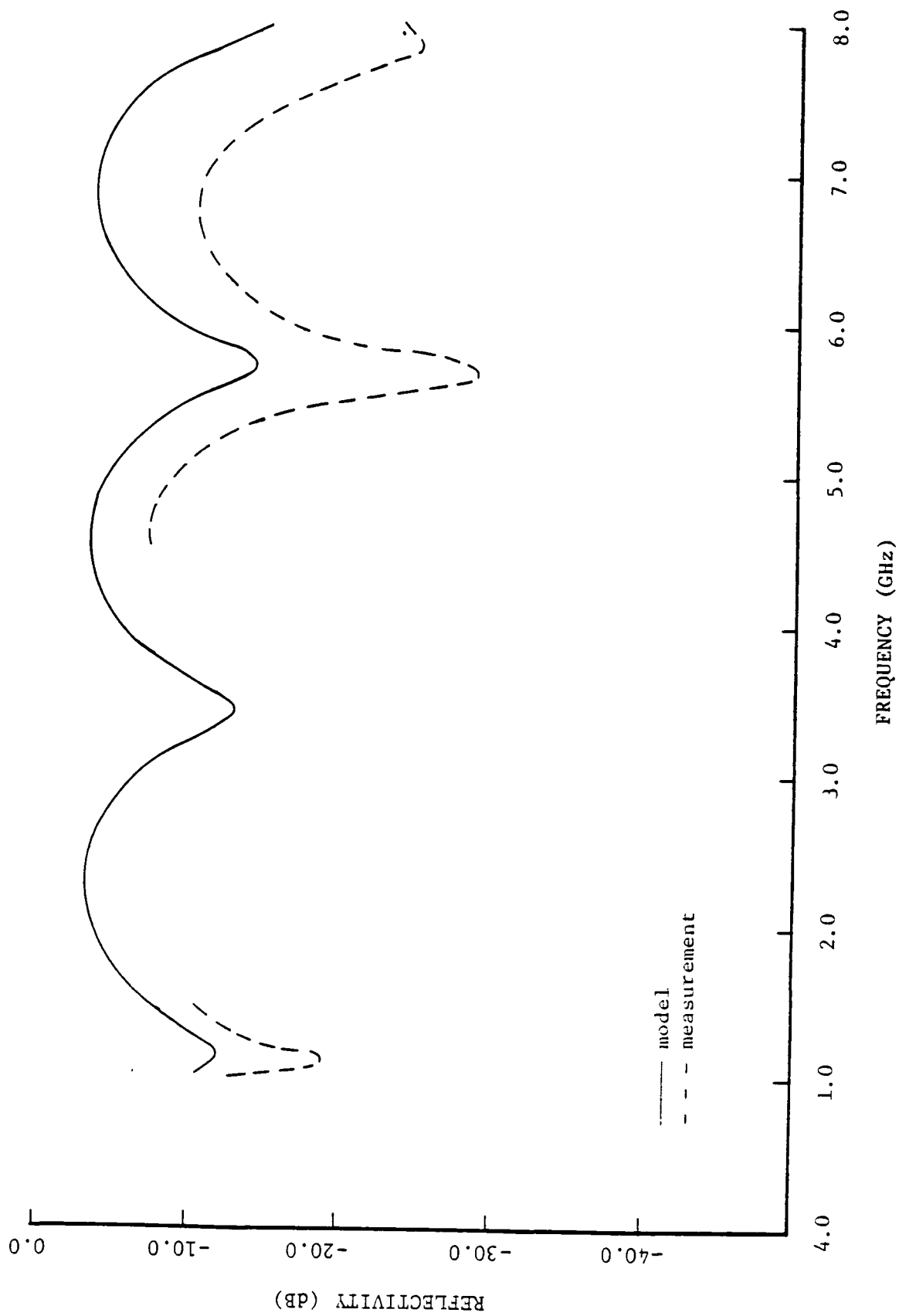
Figure 3.5 Comparison of two-layer model and measurement for dry layer depth of 3.6 cm.

medium can be related to one, three, five, and seven quarter-wavelengths, respectively. The comparison of the model and the measurement in Figure 3.5 yields the same results as the comparisons in Figures 3.3 and 3.4: good overall agreement with discrepancies in the reflectivity at the minima and an offset that increases with frequency.

In conclusion, coherent effects can occur for abrupt soil moisture profiles created in laboratory. The two-layer model for a smooth surface gives good overall agreement with the measurement. The discrepancies between the model and measured reflectivities will be further resolved in Chapter 5. The question remains as to the possibility of coherent effects occurring under more realistic soil moisture profiles. This question will be the subject of the following chapter.

CHAPTER 4

CONTINUOUS MOISTURE PROFILES

4.1 Theory

The previous chapter was concerned with plane waves incident on homogeneous layered soils separated by plane boundaries. The concern of this chapter will be plane waves incident on non-homogeneous soil media. The term non-homogeneous is used to refer to a medium in which the complex permittivity changes as a function of depth, e.g. the soil moisture and permittivity vary with depth.

Care must be taken with the divergence relationship for the electric field in Maxwell's equations since the complex permittivity of these continuously varying profiles will be a function of depth, and thus will possess a gradient. The divergence relationship for a source-free region is given by

$$\nabla \cdot \hat{\epsilon} \bar{E} = \bar{E} \cdot \nabla \hat{\epsilon} + \hat{\epsilon} \nabla \cdot \bar{E} = 0 \qquad (4.1)$$

where $\qquad \nabla \hat{\epsilon} \neq 0$

Solving 4.1 for $\nabla \cdot \bar{E}$ and substituting into the wave equation

$$\nabla \times \nabla \times \bar{E} = \gamma^2 \bar{E} \qquad , \qquad \gamma^2 = \frac{w^2}{c^2} \hat{\epsilon}$$

which can also be expressed as

$$\nabla^2 \bar{E} + \gamma^2 \bar{E} - \nabla(\nabla \cdot \bar{E}) = 0$$

yields

$$\nabla^2 \bar{E} + \gamma^2 \bar{E} - \nabla(\bar{E} \cdot \frac{\nabla \hat{\epsilon}}{\hat{\epsilon}}) = 0 \qquad (4.2)$$

If $\hat{\epsilon}$, the complex permittivity, varies slowly with position such that $\nabla\hat{\epsilon}$ can be neglected then (4.1) will simplify to

$$\nabla^2 \bar{E} + \gamma^2 \bar{E} = 0 \tag{4.3}$$

which is the wave equation for a homogeneous medium. Thus, if the permittivity change is slight it may be ignored. Conversely, if the change with depth is abrupt the profile may be partitioned into two relatively homogenous regions as treated in the preceeding chapter. If the variation in permittivity falls between these extremes, a more exact solution of (4.2) must be used.

Closed form solutions of the reflected electric field can be obtained for specific permittivity profiles (Brekhovskikh, 1960 and Wait, 1962). However, the approach of this paper is to partition the region of continuous moisture variation into thin layers of infinite extent. Within each stratified layer the permittivity gradient can be neglected permitting the use of the homogeneous wave equation (4.3) for the solution of the electric field. This approach allows the two-layer model of the previous chapter to be extended to a multi-layer or continous approximation model.

4.2 Multi-layer Approximation to Continuous Moisture Profiles

The two layer model of the previous chapter will be extended to a multi-layer model for the approximation of the reflected electric field from continuous soil moisture profiles. For the purposes of the model the idealized soil moisture profile snown in Figure 4.1 is used along with the assumption that the only variation in soil moisture, and consequently soil permittivity, is with depth.
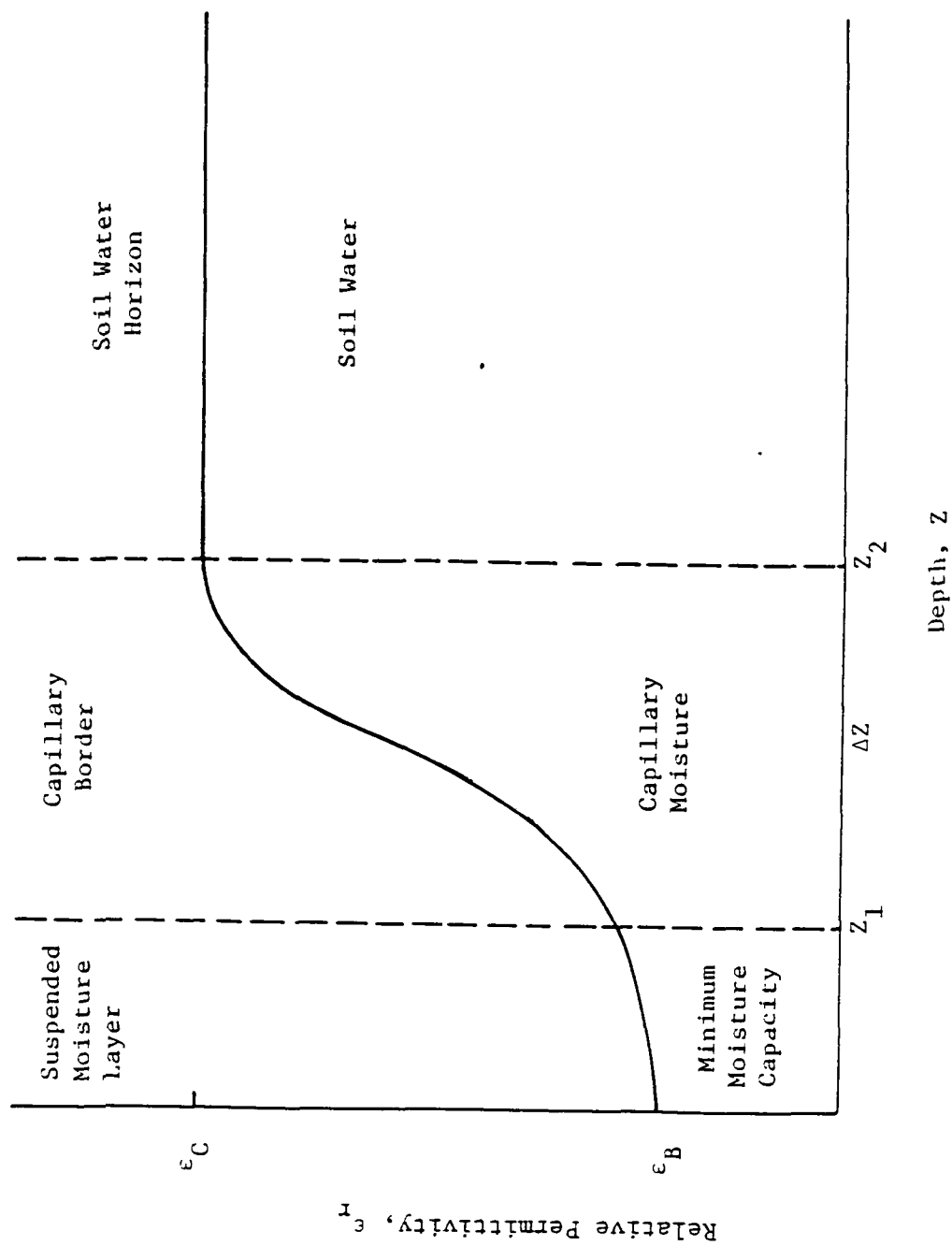
Figure 4.1 Idealized soil permittivity profile.

The moisture profile of Figure 4.1 is divided into three regions:
the suspended moisture layer, the capillary border, and the soil water
horizon. The depth of the suspended moisture layer and the capillary
border are considered finite while the depth of the soil water horizon
is assumed infinite. The suspended moisture layer and the soil water
horizon are treated as homogeneous media with uniform permittivities
separated by a non-homogeneous medium, the capillary border, which
has a transitional permittivity that is a function of depth. The initial
permittivity designations for the three regions are, $\widehat{\varepsilon}_B$ for the constant
permittivity of the suspended moisture layer, $\widehat{\varepsilon}_B'$ for the variable
permittivity of the capillary border, and $\widehat{\varepsilon}_c$ for the constant permittivity
of the soil water horizon. The model is further constrained such that

$$\widehat{\varepsilon}_c > \widehat{\varepsilon}_B' > \widehat{\varepsilon}_B$$

for all permittivities. This constraint restricts the model to surfaces
that have achieved an air dry condition.

The moisture profile of Figure 4.1 is repartitioned into N + 3
layers counting from zero at the air-soil boundary. Thus, layer 1
refers to the suspended moisture layer of permittivity $\widehat{\varepsilon}_B$, layer N
+ 2 relates to the soil moisture horizon of permittivity $\widehat{\varepsilon}_c$, and the
capillary border with transitional permittivity $\widehat{\varepsilon}_B'$ is divided into
N layers with N chosen such that the permittivity of each individual
layer is nearly uniform. Now the designations of the two-layer model
can be mapped into N + 1 sets as shown in Figure 4.2 to form the notation
for the multi-layer model. The horizontal polarization electric field
reflection coefficients for each boundary starting at the N + 1 set
are given as

31
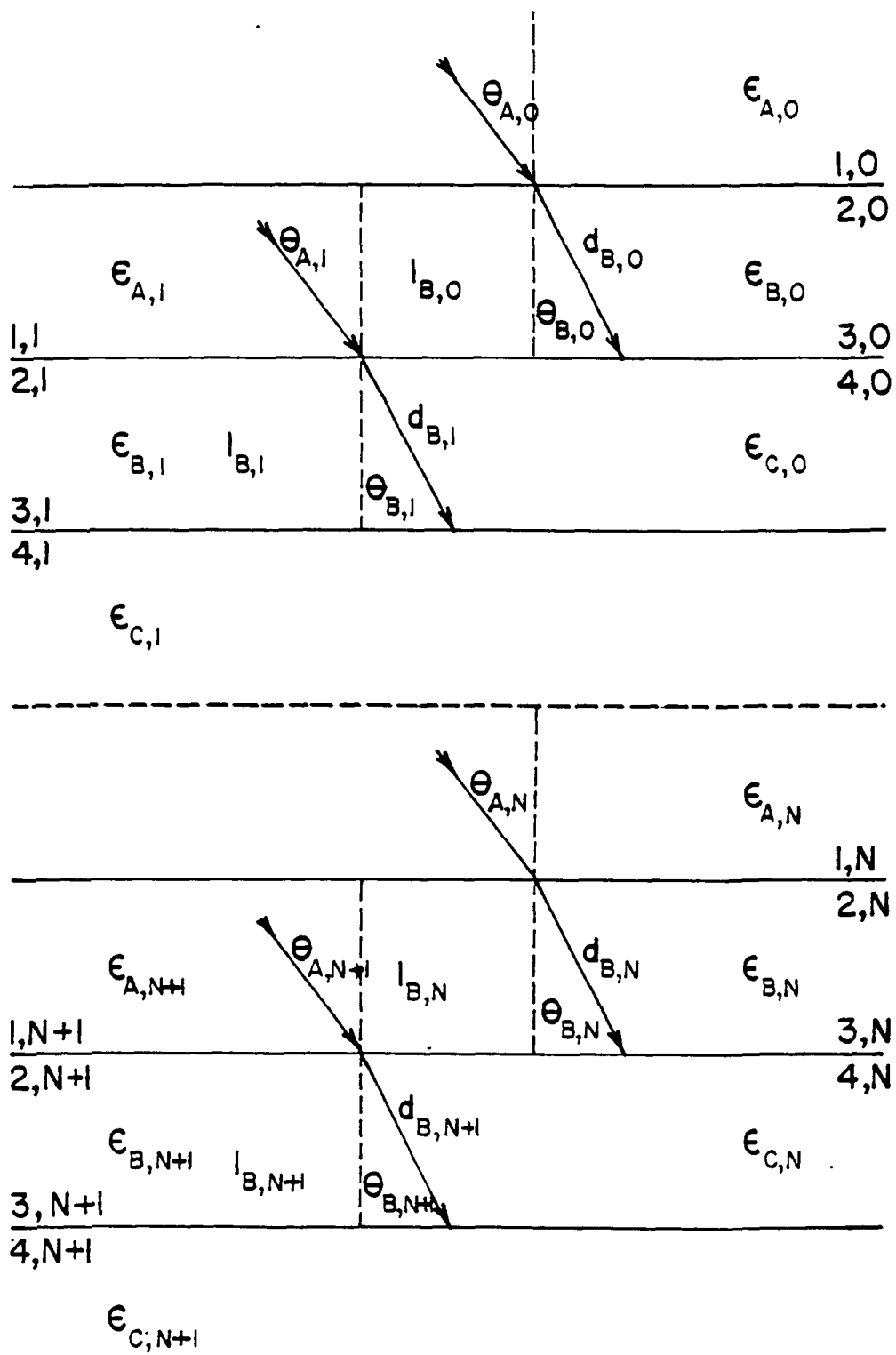
Figure 4.2 Designations of the multi-layers model.

32

$$\Gamma_{T,N+1} = \frac{\Gamma_{1,N+1} + \Gamma_{3,N+1}\, e^{-2\gamma_{B,N+1} d_{B,N+1}}}{1.0 + \Gamma_{1,N+1}\, \Gamma_{3,N+1}\, e^{-2\gamma_{B,N+1} d_{B,N+1}}}$$

$$\Gamma_{T,N} = \frac{\Gamma_{1,N} + \Gamma_{T,N+1}\, e^{-2\gamma_{B,N} d_{B,N}}}{1.0 + \Gamma_{1,N}\, \Gamma_{T,N+1}\, e^{-2\gamma_{B,N} d_{B,N}}}$$

$$\cdot$$
$$\cdot$$
$$\cdot$$

$$\Gamma_{T,n} = \frac{\Gamma_{1,n} + \Gamma_{T,n+1}\, e^{-2\gamma_{B,n} d_{B,n}}}{1.0 + \Gamma_{1,n}\, \Gamma_{T,n+1}\, e^{-2\gamma_{B,n} d_{B,n}}}$$

$$\cdot$$
$$\cdot$$
$$\cdot$$

$$\Gamma_{T,0} = \frac{\Gamma_{1,0} + \Gamma_{T,1}\, e^{-2\gamma_{B,0} d_{B,0}}}{1.0 + \Gamma_{1,0}\, \Gamma_{T,1}\, e^{-2\gamma_{B,0} d_{B,0}}} \tag{4.4}$$

where

$$\Gamma_{TOTAL} = \Gamma_{T,0}$$

$$\gamma_{B,n}^2 = \frac{w^2}{c^2}\, \hat{\epsilon}_{B,n}$$

with $\hat{\epsilon}_{B,n}$ = relative complex permittivity for layer B of set n, and

$\Gamma_{1,n}$ and $\Gamma_{3,n}$ the Fresnel reflection coefficients at the boundaries

of layer set n. Furthermore, it may be seen that the following relationships

between the reflection coefficients will hold.

$$\Pi_{1,N+1} = \Pi_{3,N}$$

$$\Pi_{1,N} = \Pi_{3,N-1}$$

$$\vdots$$

$$\Pi_{1,n} = \Pi_{3,n-1}$$

$$\vdots$$

$$\Pi_{1,1} = \Pi_{3,0}$$

where (for horizontal polarization)

$$\Pi_{3,n} = \frac{\sqrt{\hat{\varepsilon}_{B,n} - \sin^2\theta_0} - \sqrt{\hat{\varepsilon}_{c,n} - \sin^2\theta_0}}{\sqrt{\hat{\varepsilon}_{B,n} - \sin^2\theta_0} + \sqrt{\hat{\varepsilon}_{c,n} - \sin^2\theta_0}} \qquad (4.5)$$

$$\Pi_{1,0} = \frac{\cos\theta_0 - \sqrt{\varepsilon_{B,0} - \sin^2\theta_0}}{\cos\theta_0 + \sqrt{\varepsilon_{B,0} - \sin^2\theta_0}} \qquad (4.6)$$

with θ_0 = angle of incidence at the surface, $\hat{\varepsilon}_{B,n}$ and $\hat{\varepsilon}_{c,n}$ = relative complex permittivities of layer set n.

If the thickness of each layer in the transitional region is such that the ratio of the permittivities of the particular layer and the adjacent layers are less than 2, then the reflection coefficient at each boundary will be much smaller than unity. This allows the further simplification of the multi-layer model in the following manner.

$$\Pi_{T,N+1} = \Pi_{3,N} + \Pi_{3,N+1}\, e^{-2\gamma_{B,N+1}\, d_{B,N+1}}$$

$$\Pi_{T,N} = \Pi_{3,N-1} + \Pi_{T,N+1}\, e^{-2\gamma_{B,N}\, d_{B,N}}$$

$$= \Pi_{3,N-1} \sum_{i=N}^{N+1} \Pi_{3,i}\, e^{-2\sum_{m=N}^{i} \gamma_{B,m}\, d_{B,m}}$$

$$\vdots$$

34

$$\Gamma_{T,n} = \Gamma_{3,n-1} + \sum_{i=n}^{N+1} \Gamma_{3,i}\, e^{-2 \sum_{m=n}^{i} \gamma_{B,m} d_{B,m}}$$

.

.

$$\Gamma_{T,1} = \Gamma_{3,0} + \sum_{i=1}^{N+1} \Gamma_{3,i}\, e^{-2 \sum_{m=1}^{i} \gamma_{B,m} d_{B,m}} \tag{4.7}$$

where $\Gamma_{T,1}$ is the total reflection due to both the capillary border
and the soil water horizon. The reflection coefficient is presented
in this manner to show that it is a sum of reflections coupled with
attenuation and phase due to the electric fields traversing the non-
homogeneous permittivity region of the capillary border.

The exact closed form will be used to translate the subsurface
reflection through the suspended moisture layer to the surface since
the ratio of the permittivities at the air–soil boundary will be greater
than 2. The total reflection coefficient at the surface boundary will
be

$$\Gamma_{T,0} = \frac{\Gamma_{1,0} + \sum_{i=0}^{N+1} \Gamma_{3,i}\, e^{-2 \sum_{m=0}^{i} \gamma_{B,m} d_{B,m}}}{1.0 + \Gamma_{1,0} \sum_{i=0}^{N+1} \Gamma_{3,i}\, e^{-2 \sum_{m=0}^{i} \gamma_{B,m} d_{B,m}}} \tag{4.8}$$

where

This equation gives the multi-layer reflection coefficient in a form
similar to the two-layer result, except that the subsurface reflection
due to an abrupt change in permittivity in the two-layer model

35

has been replaced with a summation of reflections altered by the constant permittivity and depth of the suspended moisture layer.

The hypothesis presented is: if a frequency is found such that the total reflection is approximately zero, then a dominant portion of the reflections from the transitional region have added in phase such that a point within the capillary border appears as an abrupt change in permittivity. In essence, if a frequency is found at which a significant minimum exists, then the permittivity $\hat{\varepsilon}_c$ will be translated into the transitional permittivity region and the multi-layer model will reduce to the two-layer model for those frequencies near the minimum. At these frequencies the conditions that hold for the two-layer model will also hold to estimate certain parameters of the multi-layer model. One parameter in particular will be an estimate, or bound, of the suspended moisture layer depth which is given by

$$\ell = \frac{30 \sqrt{\varepsilon_{r,B} - \sin^2 \Theta_o}}{4 f_o \varepsilon_{r,B}} (2n+1) \quad cm.$$ (4.9)

where:

n = positive integer

f_o = frequency at minimum in Ghz

Θ_o = angle of incidence

$\varepsilon_{r,B}$ = real part of the soil crust permittivity

The equations and figures given in this section represent the model used to explain the microwave reflectivity data of the 1979 field experiment at the University of Arkansas (Hancock, 1980). Permittivities from the laboratory work of Lundien (1971) for Overstreet Silt Loam

36

were used to map moisture ground truth into soil permittivity as a
function of soil depth and this mapping is shown in Figure 4.3.

An estimate of the quarter-wavelength depth was obtained by using
the propagation term of eqn. 4.8

$$e^{-2\sum_{m=0}^{i} \gamma_{B,m} d_{B,m}}$$

The propagation factor, $\gamma_{B,n}$ can be expressed in terms of attenuation
and phase factors as

$$\gamma_{B,m} = \alpha_{B,m} + j\beta_{B,m}$$

where $\alpha_{B,n}$ is the attenuation factor.

In order to gain insight from the model as to what happens with
changes in soil moisture, a moisture profile with a constant slope
for the capillary border was constructed for this profile model

$$m = \begin{cases} m_0, & 0 \leq 3 < z_1 \\ \left(\frac{m_1 - m_0}{z_2 - z_1}\right)(3 - z_1), & z_1 \leq 3 < z_2 \\ m_1, & z_2 \leq 3 \end{cases} \quad \begin{array}{l} m_0 < m_1 \\ z_1 < z_2 \end{array} \tag{4.10}$$

m_0 corresponds to the moisture content of the suspended moisture layer,
m_1 the wetness of the soil water horizon, z_1 the depth of the suspended
moisture layer, and z_2 the depth at which the soil water horizon begins.
Figure 4.4 shows a sketch of this assumed moisture profile.
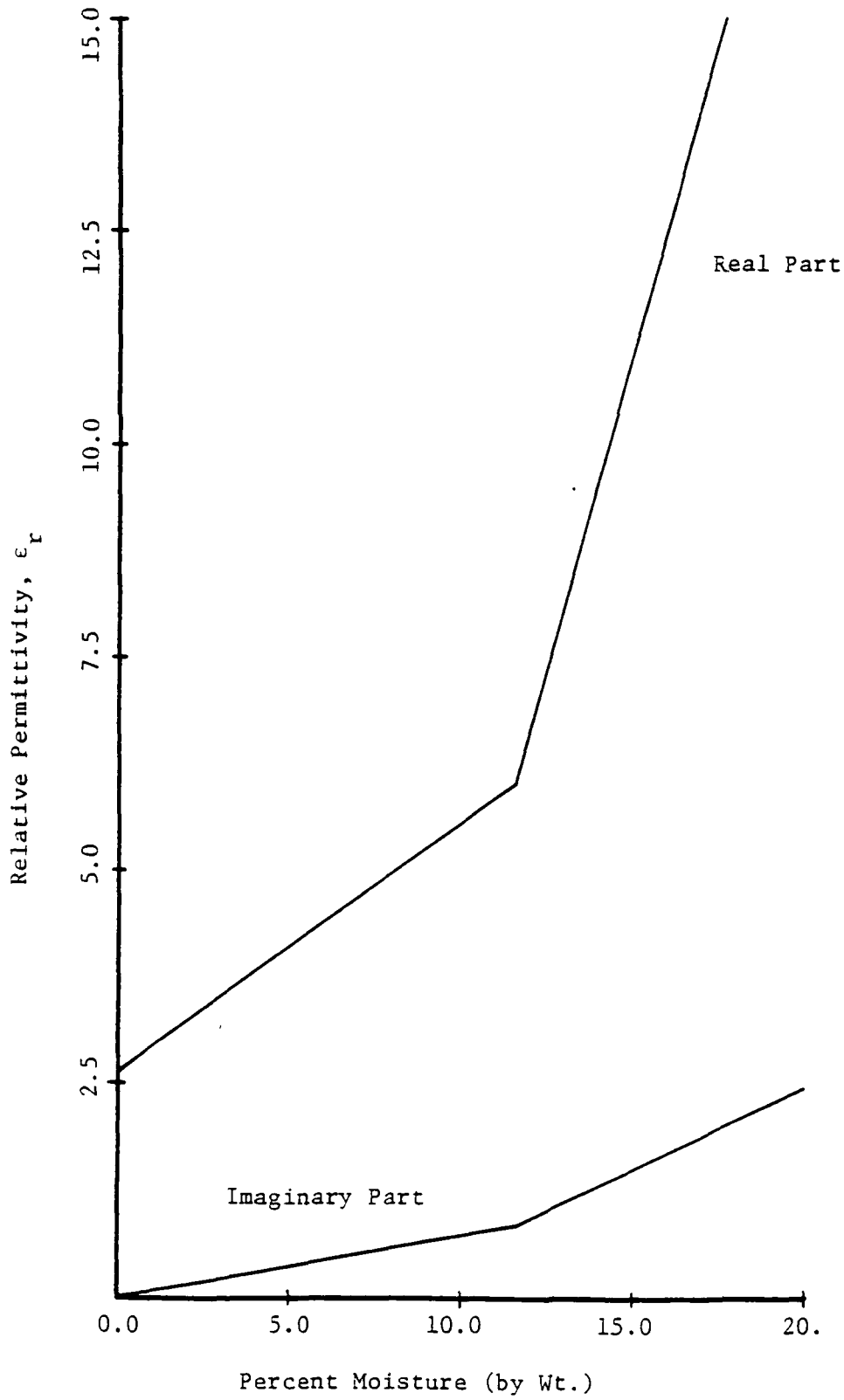
Figure 4.3 Soil permittivity as a function of moisture
(Lundien, 1971).
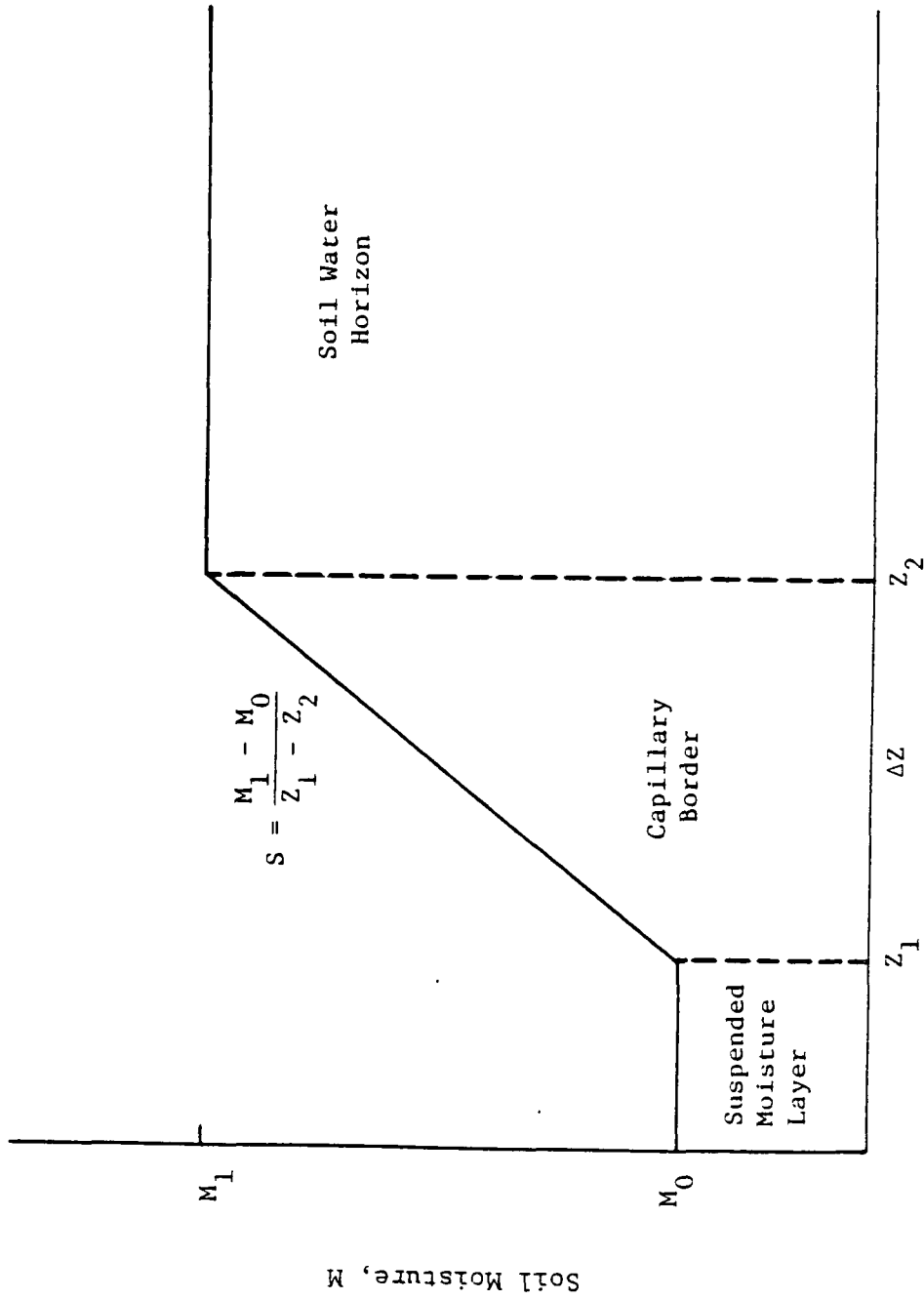
Figure 4.4   Linear approximation of soil moisture profile used in reflectivity model.

The condition used to determine the quarter-wavelength depth is
that the subsurface reflection be 180° out of phase with the reflected
surface component. This requires

$$e^{-2j \sum_{m=0}^{i} \beta_{B,m} d_{B,m}} = -1$$

or
$$2 \sum_{m=0}^{i} \beta_{B,m} d_{B,m} = \pi$$

where $d_{B,n}$ is the distance traveled in layer B of layer set m.

Following are results from this model for various values of wetness
in the suspended moisture layer and soil water horizon as well as different
depths and slopes of the capillary border. Figure 4.5 through 4.16
are the modeled reflectivity curves for frequencies from 1 to 8 GHz
for m_0 = 2.2% and m_1 = 19.1%. Figures 4.5 through 4.12 are reflectivity
curves for a particular depth of the suspended moisture layer as the
slope of the capillary border is decreased. In other words the depth
of the suspended moisture layer is kept constant as the depth to the
soil water horizon is increased. As a contrast Figures 4.13 through
4.16 are reflectivity curves with a capillary border of constant moisture
slope but with the depth to the suspended moisture layer increased
incrementally.

The slope for each curve is a constant given by

$$S = \frac{m_1 - m_0}{Z_2 - Z_1} \qquad \% / cm$$

where m_0 and m_1 are the percent moisture of the crusting layer and
soil moisture horizon respectively, Z_1 is the depth of the crusting
layer, and Z_2 is the depth of the capillary border. The equation
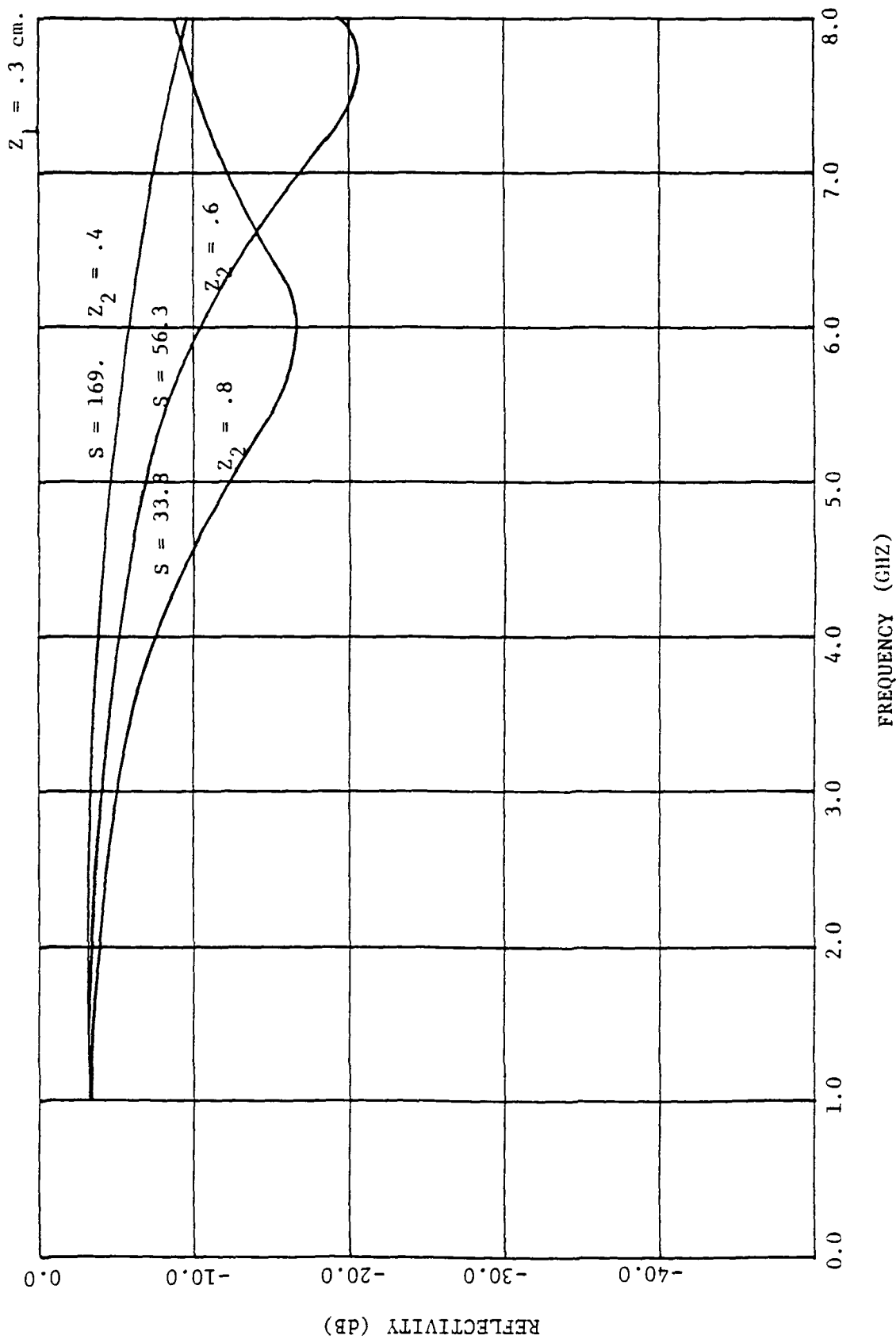
Figure 4.5 Varying capillary moisture slope, S(%/cm), for a .3 cm. suspended moisture layer and soil moisture set (2.2%, 19.1%)

41
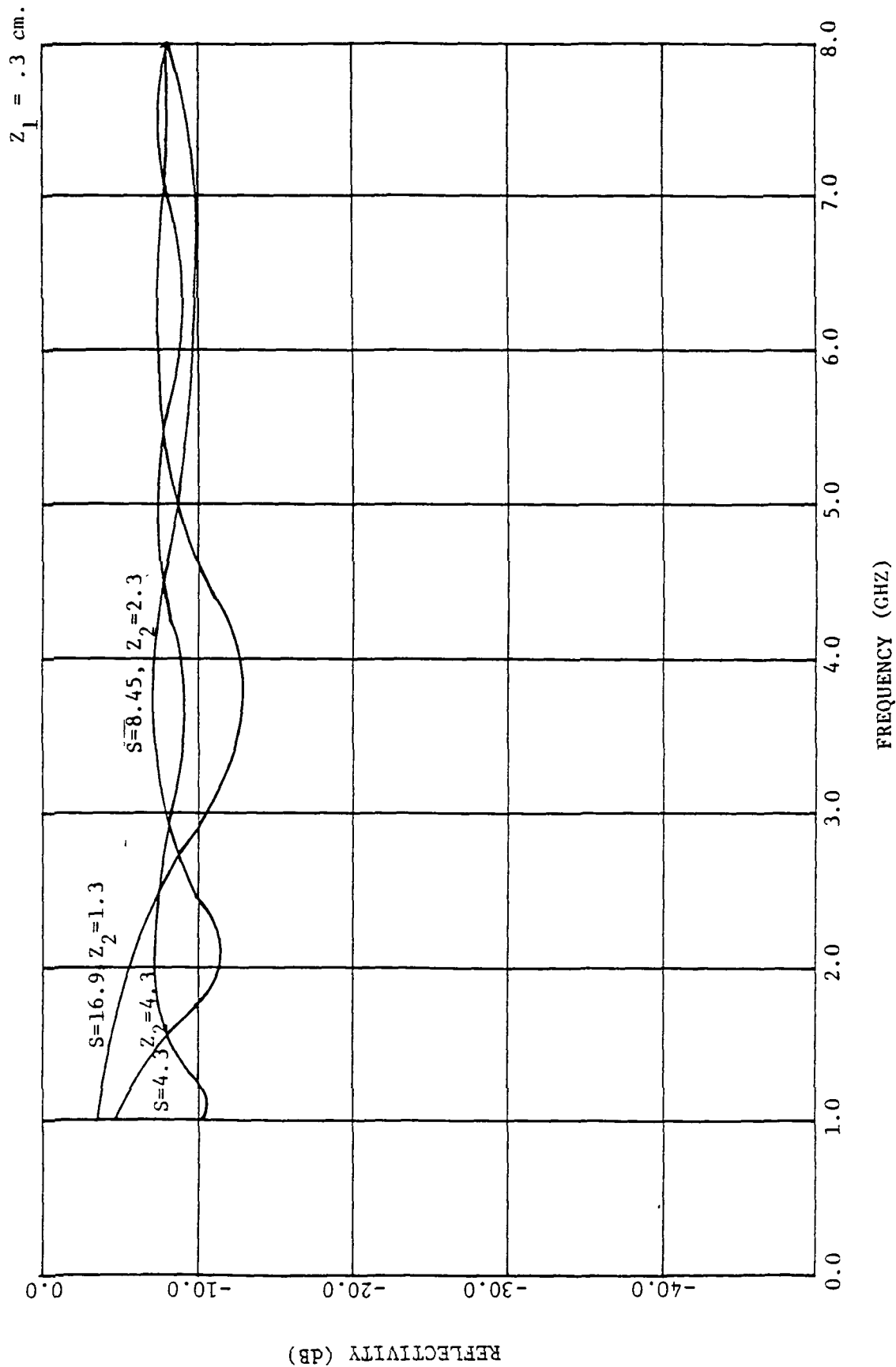
Figure 4.6   Varying capillary moisture slopes, S(%/cm), for a .3 cm. suspended moisture layer and soil moisture set (2.2%, 19.1%).
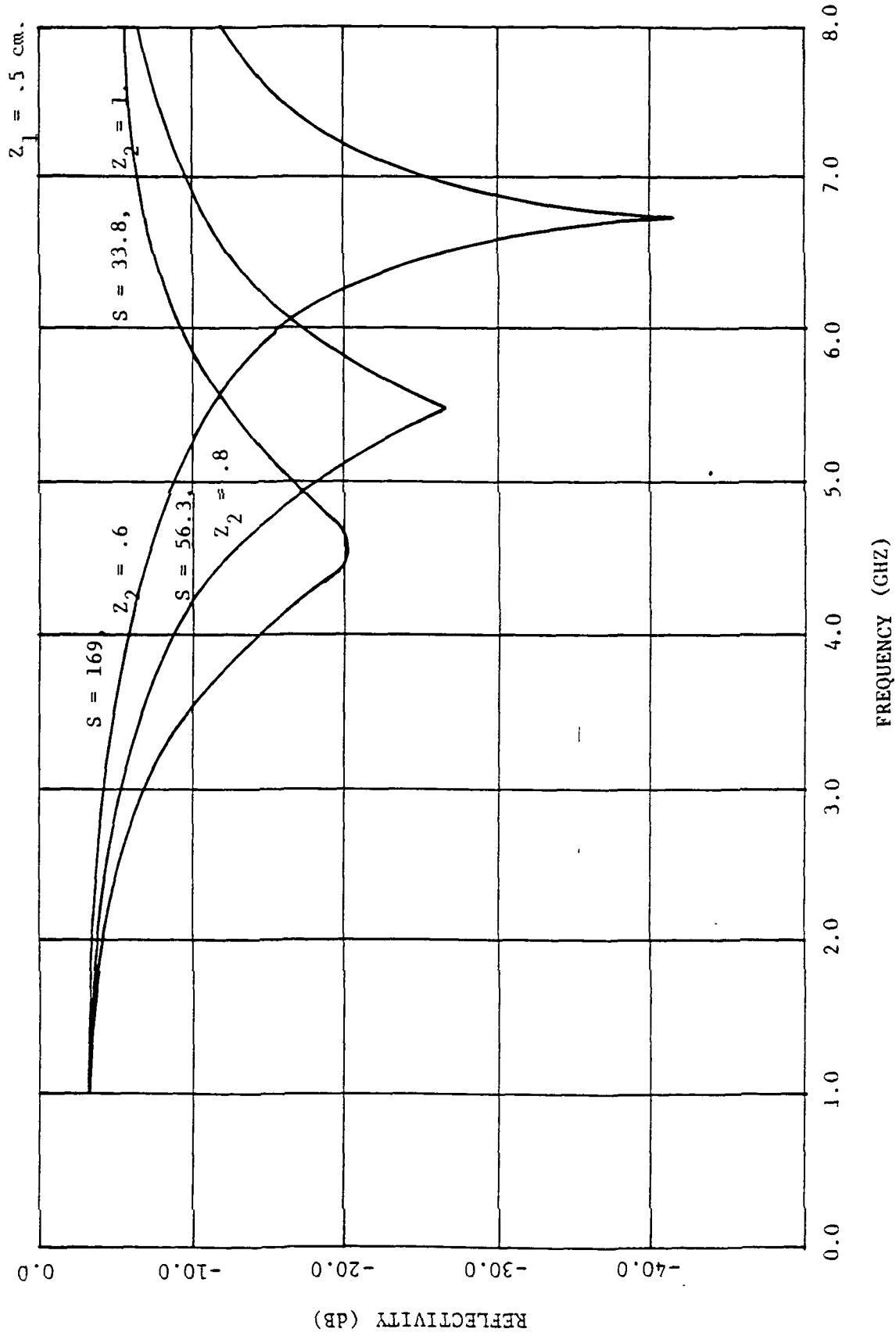
Figure 4.7 Varying capillary moisture slopes, $S(\%/cm)$, for a .5 cm. suspended moisture layer and soil moisture set (2.2%, 19.1%).

43
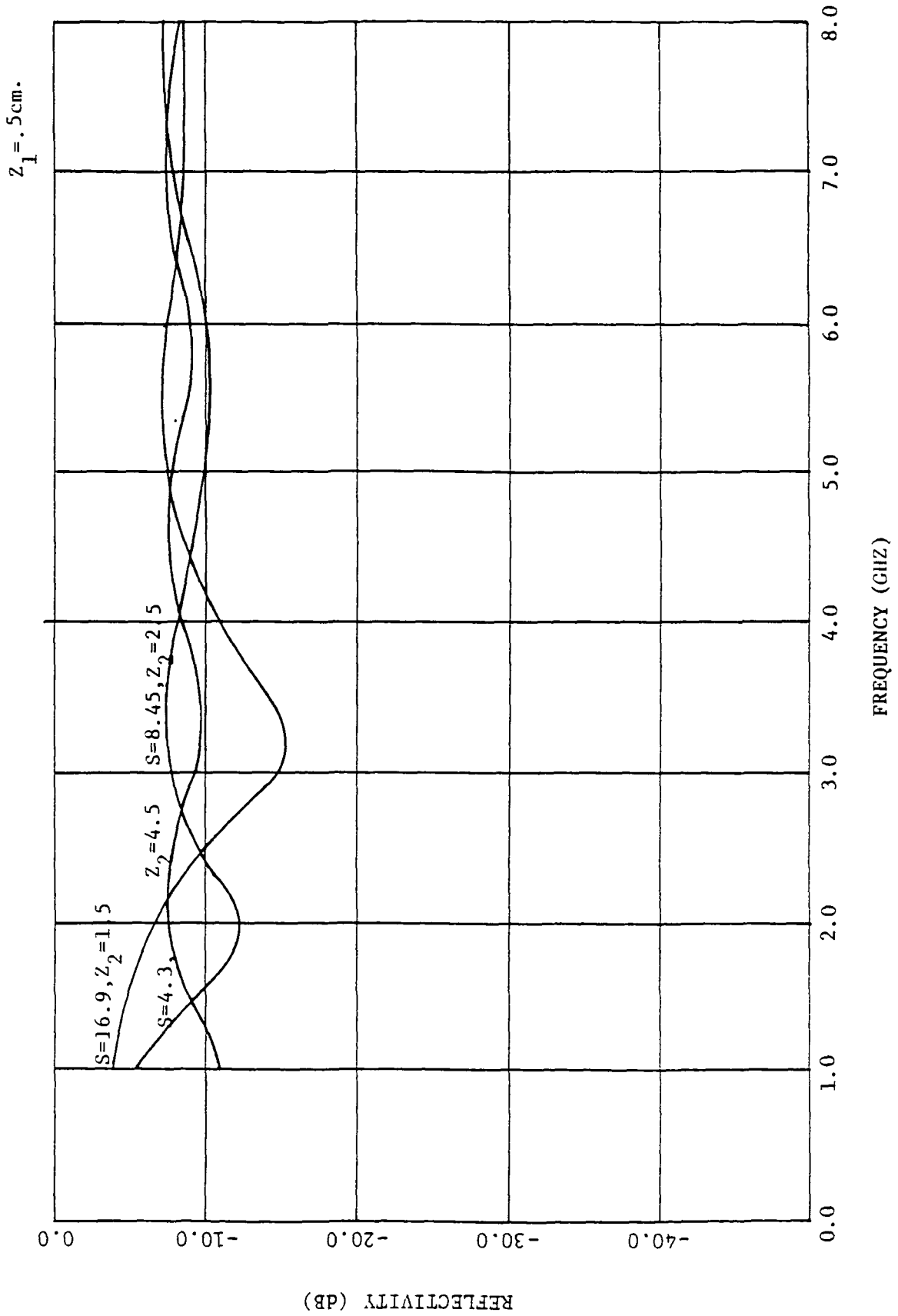
Figure 4.8   Varying capillary moisture slope, S(%/cm), for a .5cm. suspended moisture layer and soil moisture set (2.2%, 19.1%).
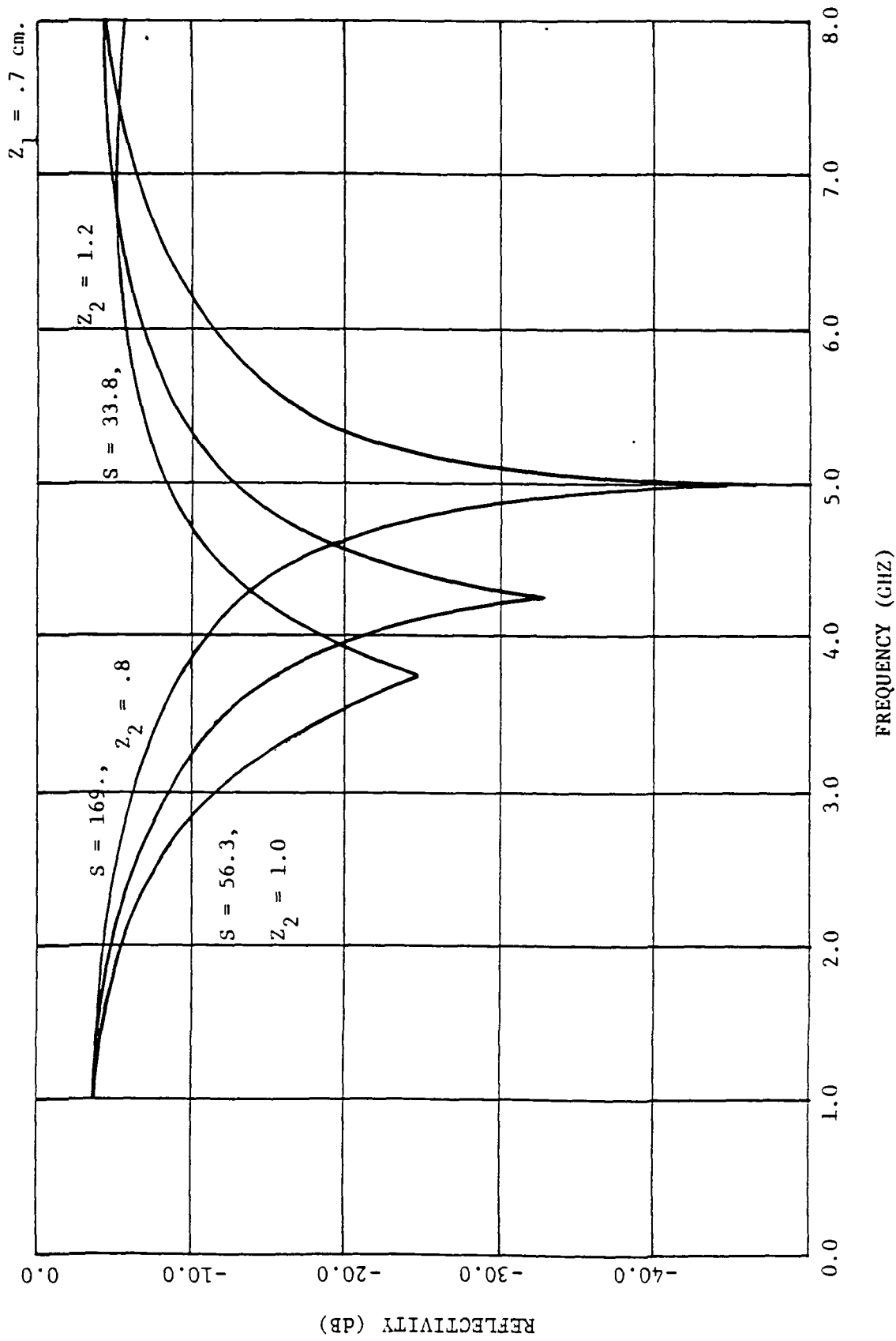
Figure 4.9   Varying capillary moisture slopes, S(%/cm), for a .7 cm suspended moisture layer and soil moisture set (2.2%, 19.1%).
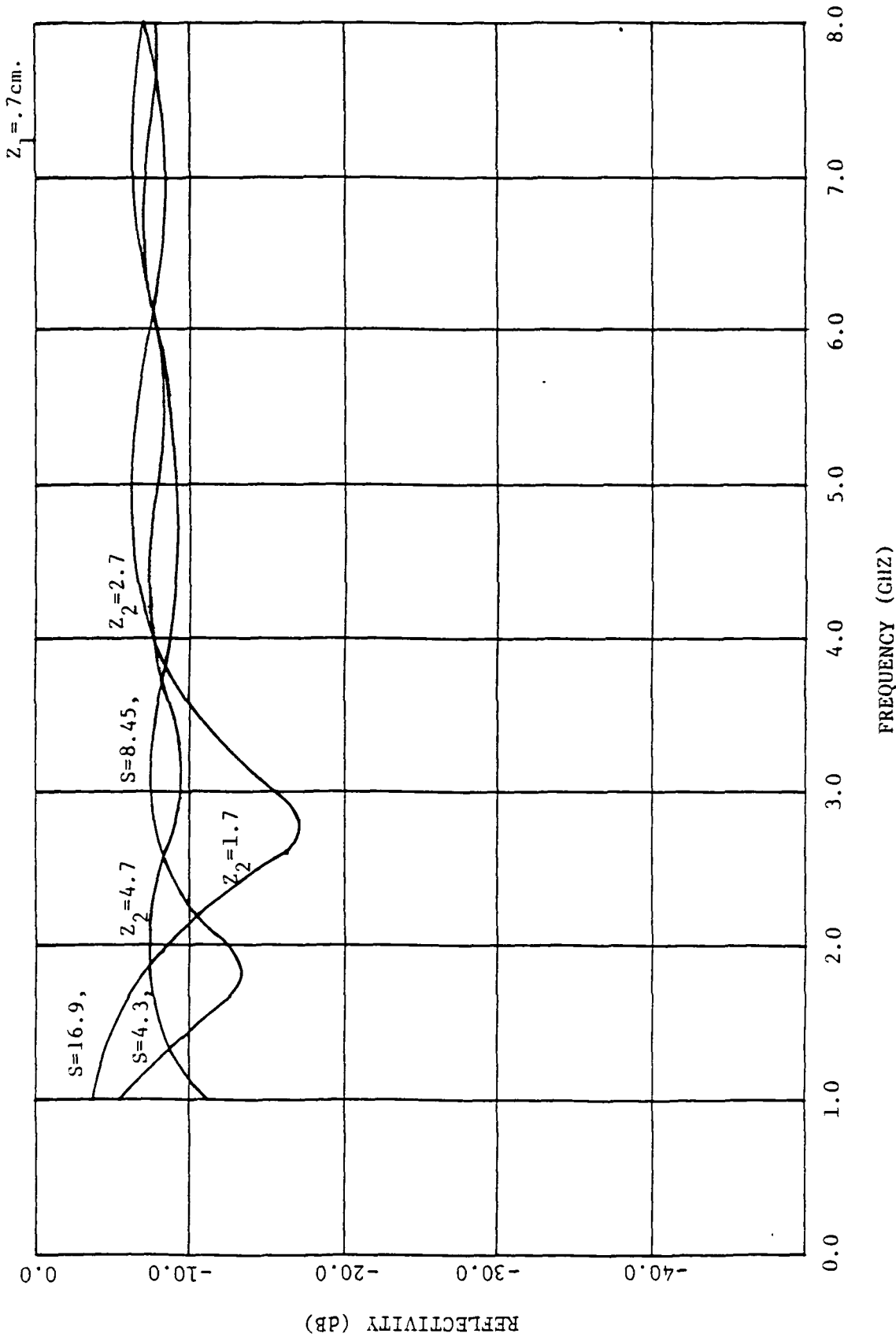
Figure 4.10   Varying capillary moisture slope, $S(\%/cm)$, for a $.7cm$ suspended moisture layer and soil moisture set (2.2%, 19.1%).

46
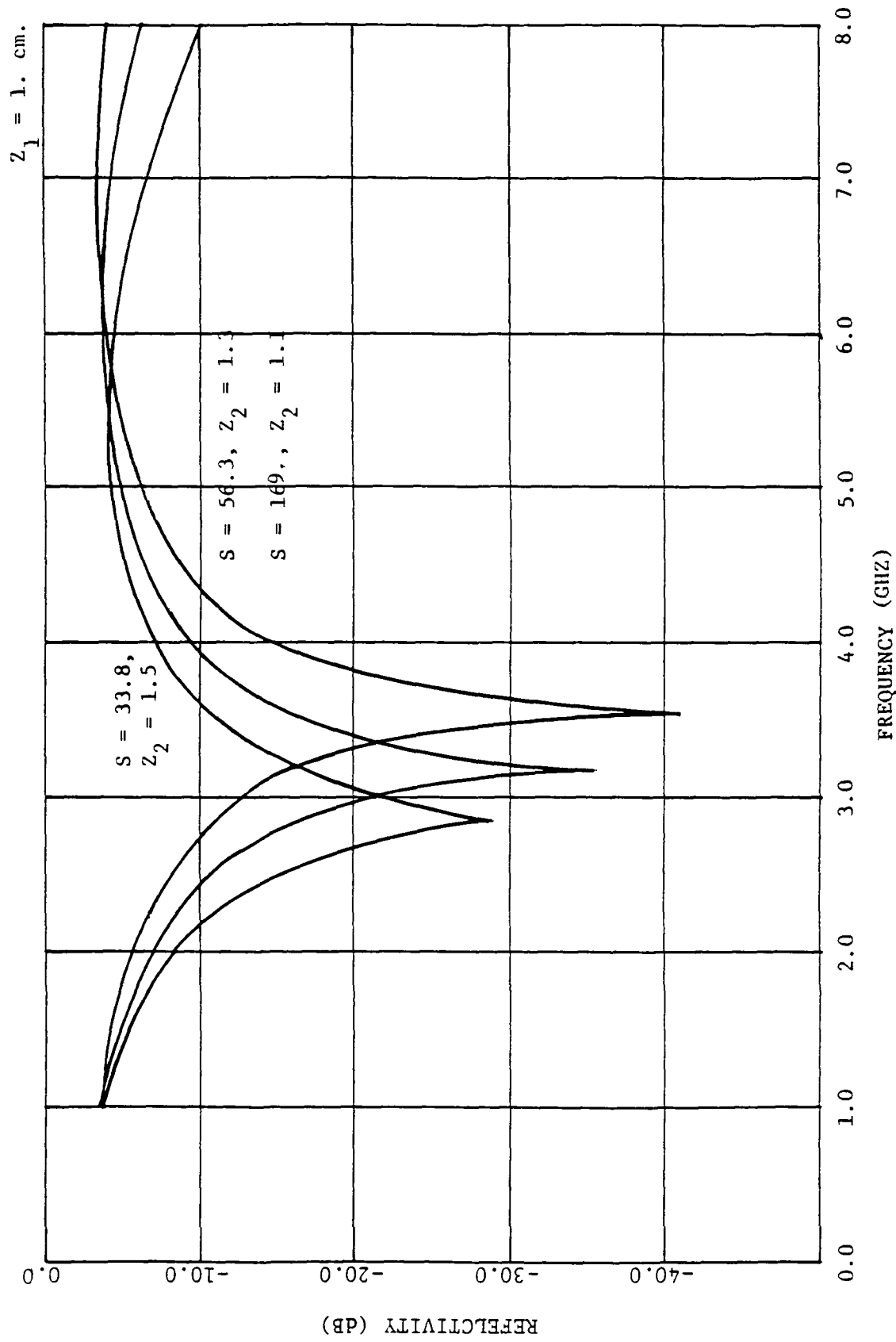
Figure 4.11   Varying capillary moisture slope, S (%/cm), for a 1. cm suspended moisture layer and soil moisture set (2.2%, 19.1%).

47
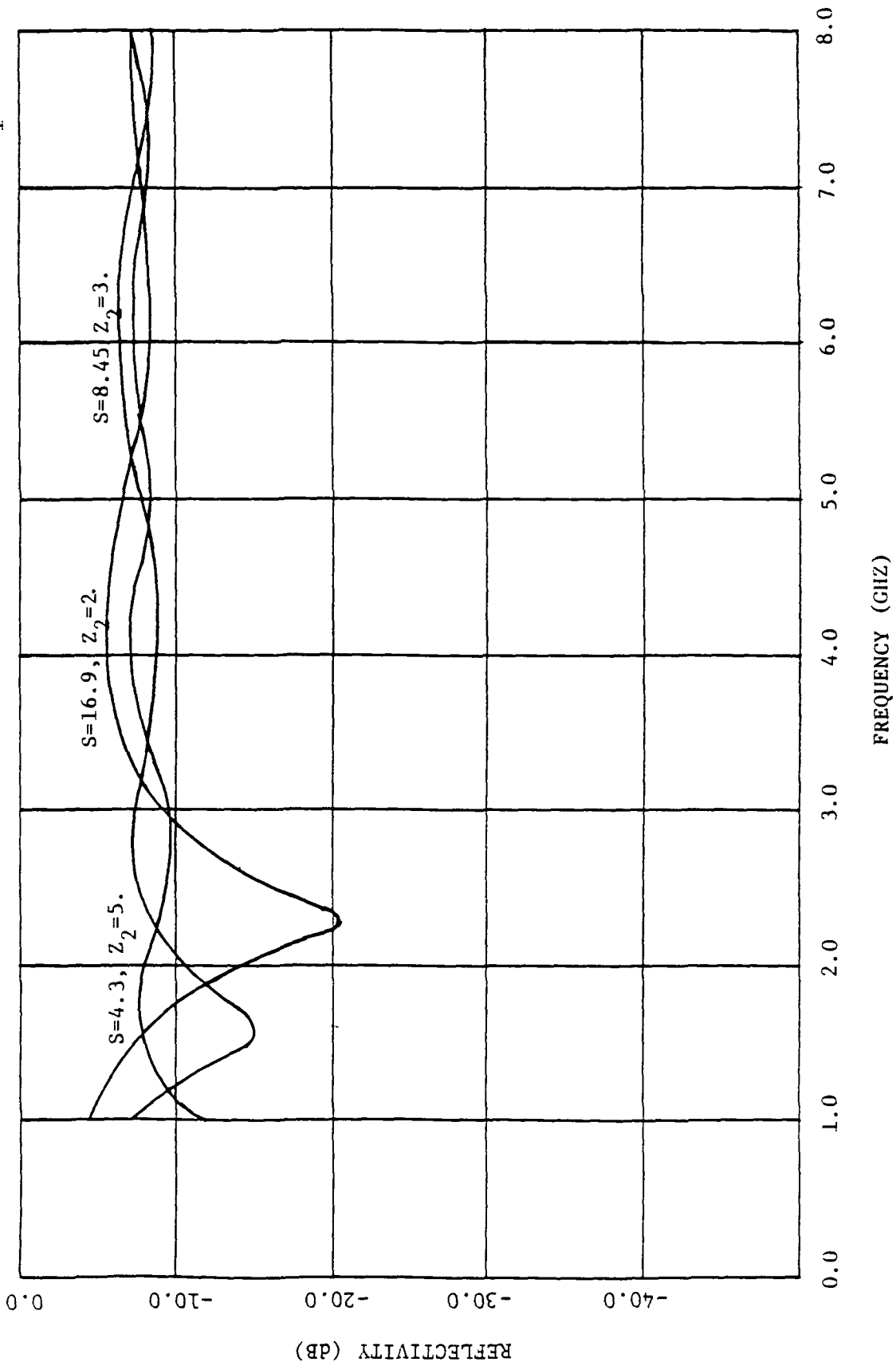
Figure 4.12   Varying capillary moisture slope, S (%/cm), for 1. cm. suspended moisture layer and soil moisture set (2.2%, 19.1%).

48

4.10 gives the soil moisture as a function of depth. These moistures
are then mapped into soil permittivity using the curve of Figure 4.3.
Soil moisture profiles of ground truth data indicate that a uniform
moisture slope is a good initial approximation lending itself to quantitative
analysis.

Figures 4.5 and 4.6 are the calculated reflectivities for a suspended
moisture layer of 0.3 centimeters and a capillary border moisture slope
varying from 169.0 to 4.3 (percent moisture by weight per centimeter).
There are distinct minima in each curve although the curve corresponding
to a slope of 169.0 has its minimum outside the frequency range of
interest at approximately 10.7 GHz. The frequency at which the minima
occur decreases as the moisture slope of the capillary border decreases.
These curves clearly show that the surface component of the reflectivity
is dominant over the subsurface contribution. The reflectivity minima
are due to the interaction of the reflections from the capillary
border and the surface layer. At the frequency of the minimum the
subsurface reflection caused by the changing subsurface permittivity
is in phase opposition to the surface reflection and the subsurface
reflection appears to originate from a point a quarter-wavelength into
the soil volume. The quarter-wavelength depth is increased as the
slope of the subsurface moisture is decreased, and the frequency at
which the minima occurs is decreased since frequency is inversely propor-
tional to wavelength. In Figure 4.6 the slope of the capillary border
moisture has been reduced to the extent that higher odd multiples of
a quarter-wavelength appear.

Figures 4.7 and 4.8 are calculated reflectivities for a soil volume
with a suspended moisture layer extending to 0.5 centimeters. At this

49

depth all moisture slopes give distinct minima within the frequency range. For the slope of 169.0 the surface and subsurface components are nearly equal as indicated by the depth of the minimum. As in the previous two figures the depth of the minima decrease with decreasing frequency and with decreasing moisture slope indicating that the subsurface portion of the reflectivity is becoming smaller and the quarter-wavelength depth is increasing.

Figure 4.9 and 4.10 are the calculated reflectivities for a suspended moisture layer depth of 0.7 centimeters; while, Figures 4.11 and 4.12 are for a suspended moisture layer of 1.0 centimeter. Each of these figures exhibit features similar to the previous figures with the reflectivity minima appearing at lower frequencies as the depth of the suspended moisture layer is increased.

A re-examination of Figures 4.5 through 4.12 shows that the minima in reflectivity are occurring at an ever decreasing frequency and that the frequency span between the minima of individual figures is compressing as the layer depth increases. Increasing the slope of the moisture gradient in the capillary border while maintaining constant moisture in the suspended layer and moisture horizon simply increases the total electrical length of the transitional permittivity region requiring a longer wavelength (lower frequency) to achieve a minimum. The reason that the frequency span is diminishing between the reflectivity minima is due to the inverse relationship between frequency and wavelength. Although there is a decrease in the frequency span between reflectivity minima, this is no change in the incremental wavelength between the minima. The change in wavelength between the first and last reflectivity minimum is approximately 2.1 centimeters for each figure.

Figures 4.13 through 4.16 are reflectivity curves for a fixed capillary border moisture slope parameterized by a varying depth of the suspended moisture layer. The moisture slopes for these four figures are 169.0., 56.3, 33.8, and 16.9 (percent moisture by weight per centimeter), respectively. In each figure there is a reflectivity versus frequency curve for a suspended moisture layer depth of 0.3, 0.5, 0.7 and 1.0 centimeter. In essence what is being depicted by these figures is the effect on soil reflectivity as a capillary border of equal and constant slope moves downward into the soil volume.

As previously stated the reflectivities of Figure 14.13 are for a soil volume with a capillary border of moisture of 169.0. As the suspended moisture layer is increased from 0.5 to 1.0 centimeter, the frequency at which the reflectivity minima occur decreases. The very distinct minima indicate that the surface and subsurface components of the reflectivity are approximately equal for these three curves. The curve for the surface layer depth of 0.3 centimeters has a minimum outside of the frequency range shown at approximately 10.7 GHz.

The minima continue to occur at lower frequencies with a decrease in the moisture slope. However, the deep minima of Figure 4.13 are not present for the curves with lesser slope and particularly for layer depths of 0.3 and 0.5 centimeters. Most notably the reflectivity curve of Figure 4.14 corresponding to a layer depth of 0.3 centimeters has a minimum that is locally smooth with a reflectivity greater than the other three minima. As the dry layer depth is further increased not only does the frequency at which the reflectivity minima occur decrease but the relative magnitude of the reflectivity at the minimum increases, becoming deeper and sharper. For the reflectivities of Figure 4.14 the surface component is dominant. As the capillary border moves deeper
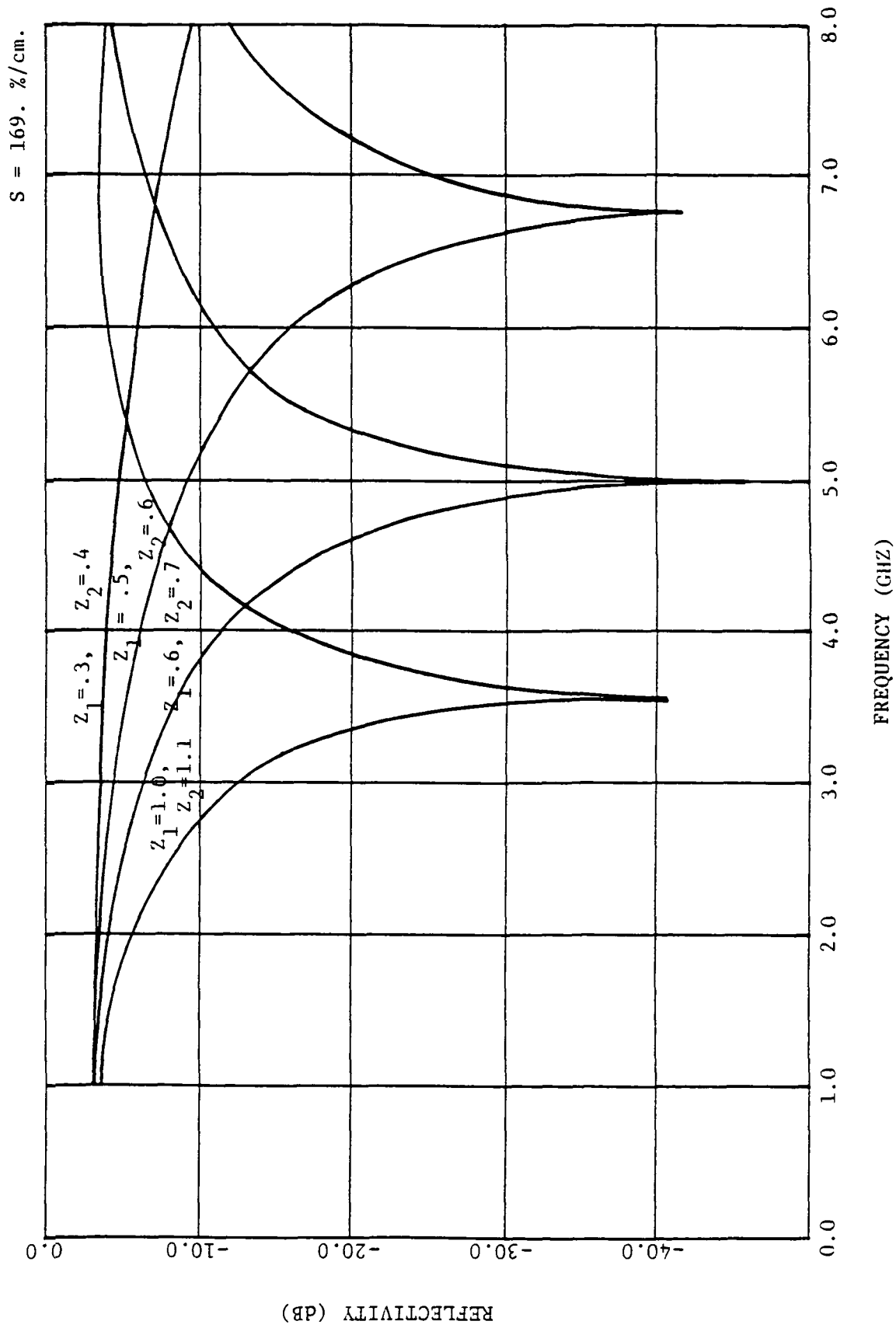
Figure 4.13   Varying suspended moisture layer depth for a 169. %/cm. capillary moisture slope and soil moisture set (2.2%, 19.1%).
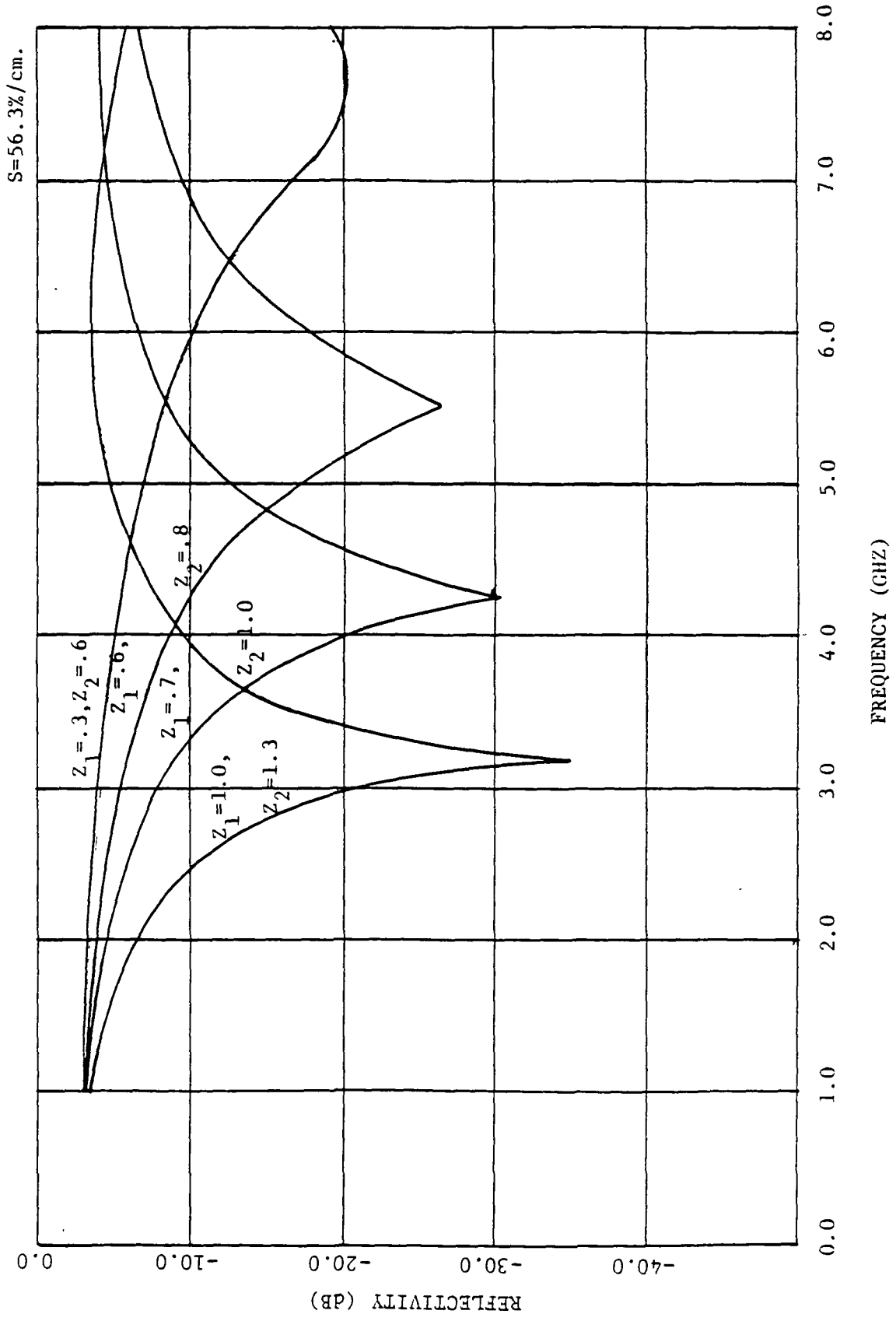
Figure 4.14   Varying suspended moisture layer depth for a 56.3%/cm capillary moisture slope and soil moisture set (2.2%, 19.1%).

53
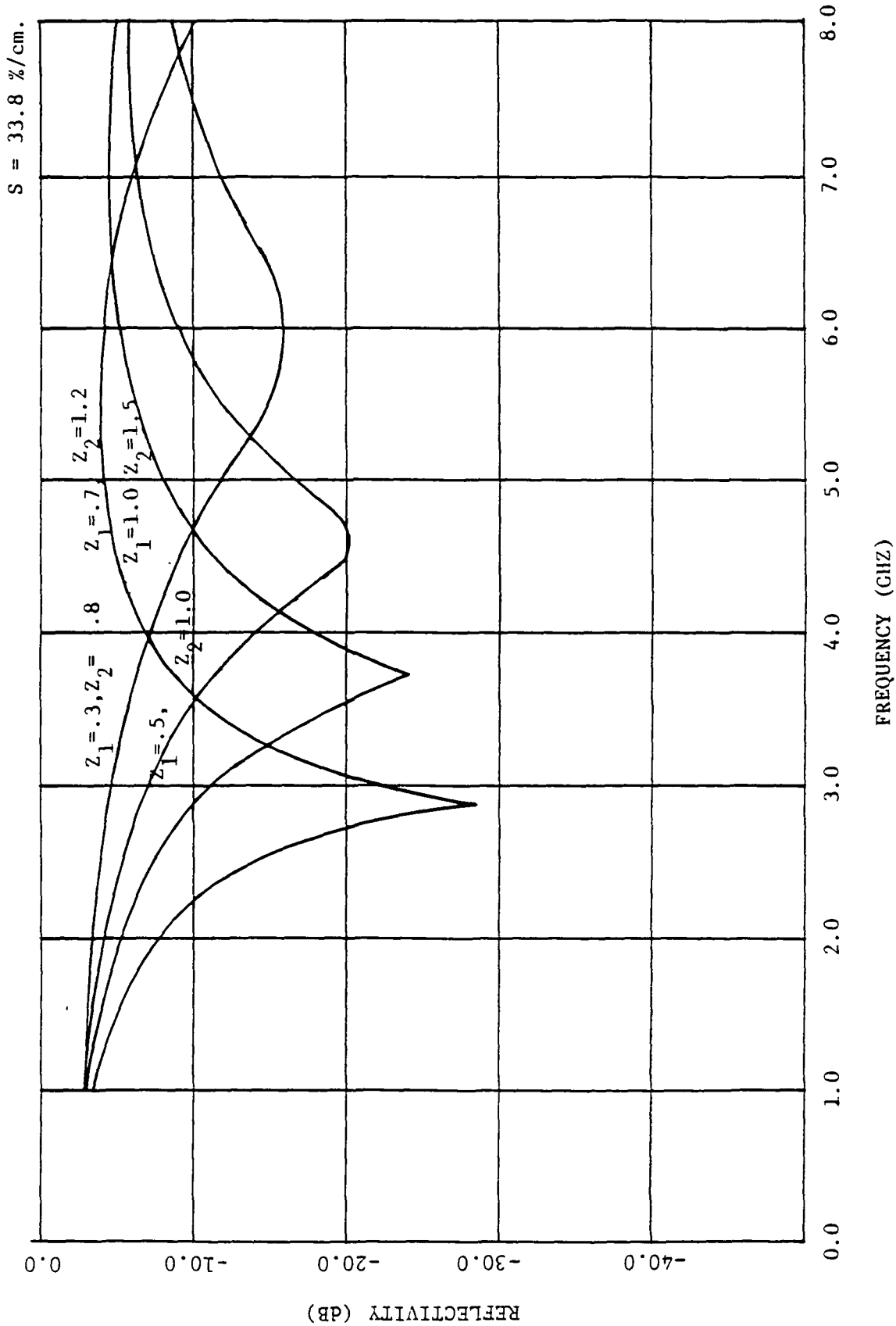
Figure 4.15 Varying suspended moisture layer depth for a 33.8%/cm capillary moisture slope and soil moisture set (2.2%, 19.1%).

54
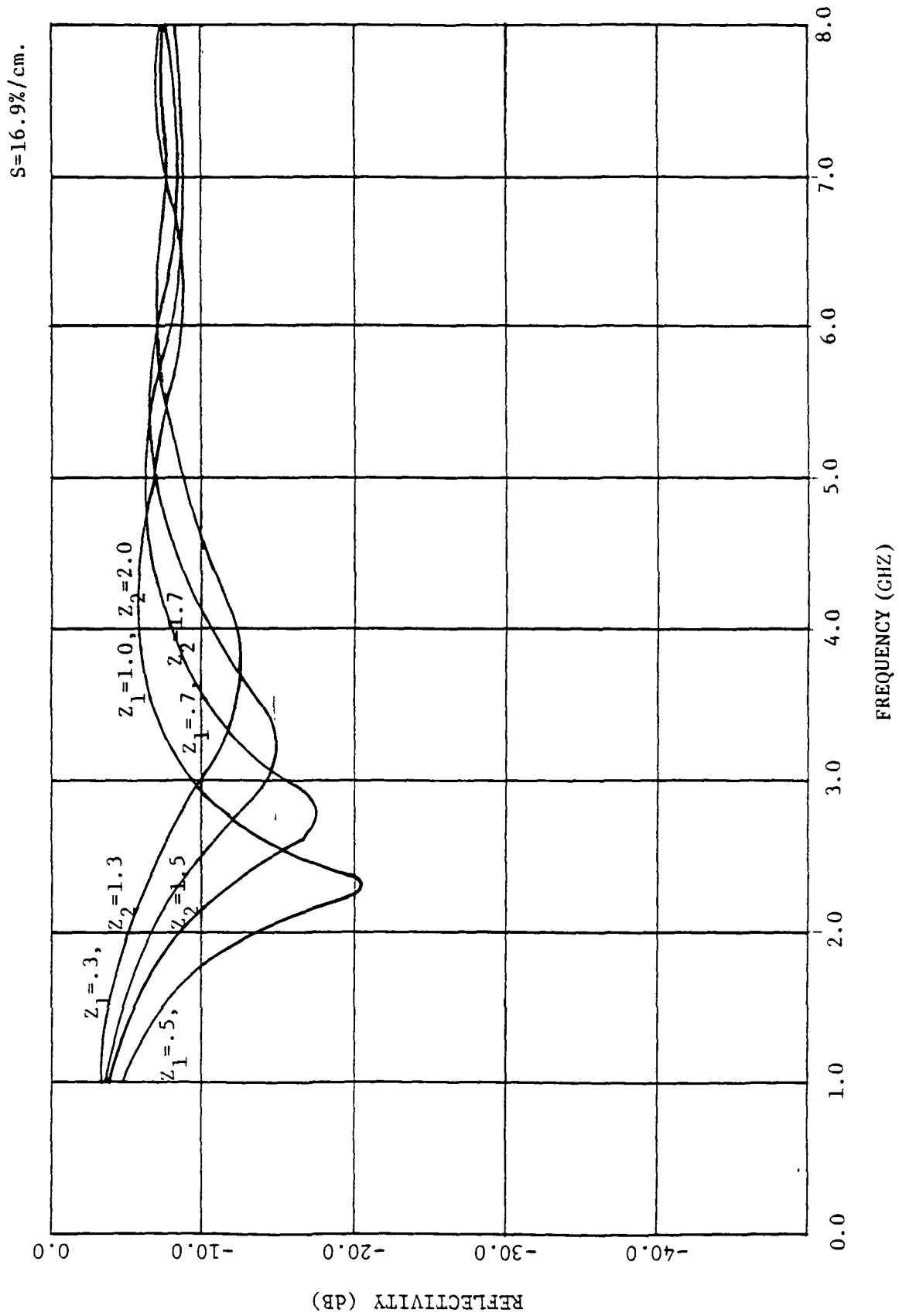
Figure 4.16   Varying suspended moisture layer depth for a 16.9%/cm capillary moisture slope and soil set (2.2%, 19.1%).

55

into the soil volume, the minima occur at longer wavelengths and the relative width of the capillary border with respect to wavelength, $\Delta Z/$, becomes less. This causes the phase change due to the varying permittivity of this region to become smaller. This in turn causes the reflected component due to the subsurface to become larger creating deeper minima. This is further verified by the reflectivities of Figures 4.15 and 4.16 which have subsurface moisture slopes of 33.8 and 16.9 %/cm, respectively. In both figures the surface reflection is larger but the subsurface component increases as the wavelength at the reflectivity minimum becomes larger due to the increase of the suspended moisture layer depth.

The moisture slope of the capillary border and the depth of the suspended moisture layer acting together determine the point of minimum reflectivity and the corresponding quarter-wavelength depth. The quarter-wavelength depth for minimum reflectivity will be greater than the depth of the suspended moisture layer for any slope of the capillary border unless the slope is infinite. The infinite slope condition reduces the model to that of the two-layer model previously considered. The quarter-wavelength depth for the reflectivity minima of all curves was within 0.55 + .02 of the width of the capillary border. The moisture contents at this depth were all within a range of 11.8 ± .5%.

The next set of figures is presented to give insight into the effect of a change in the moisture content of the suspended moisture layer and soil water horizon. For Figures 4.17 through 4.24 the assumed moisture content of the suspended moisture layer and soil water horizon are 4.2% and 21.1%, respectively. These two choices of moisture content give moisture slopes and capillary border widths corresponding to those used in the previous figures.

In each of Figures 4.17 through 4.20 are four reflectivity curves for a particular suspended moisture layer of constant depth. Each reflectivity curve corresponds to a different soil moisture slope and width of the capillary border. The four moisture slopes are 169.0, 56.3, 33.8, and 16.9 (percent moisture by weight per centimeter), respectivel;.

The suspended moisture layer of Figure 4.17 has a depth of 0.3 centimeters. A comparison of this figure with curves of equal moisture slope in Figures 4.5 and 4.6 indicates that the reflectivities of similar slopes have two distinct differences. The reflectivity minima of Figure 4.17 are not as deep as·those of Figure 4.5 and 4.6 and these minima form at different frequencies. The change in the assumed moisture content of the upper layer increases the permittivity which increases βd, the electrical length of the layer, requiring a longer wavelength to achieve the reflectivity minimum.

The differences between the reflectivity minima can be explained in the following manner. A small increase in the permittivity of the suspended moisture layer requires a larger increase in the subsurface permittivity in order to keep the reflectivity at the same value. This is due to the non-linear relationship between the permittivities in the model for reflectivity. This can be more clearly seen by assuming that the width of the transitional permittivity region is much smaller than the wavelength at which the minimum occurs. Under this assumption the problem reduces to a two-layer model. Further stipulating that the electric field has normal incidence and that losses are neglected, the total reflection coefficient at the frequency of the minimum will be given by

$$\Gamma_{TOTAL, min} = \frac{\sqrt{\epsilon_c} - \epsilon_B}{\sqrt{\epsilon_c} - \epsilon_B}$$

Figure 4.17   Varying capillary moisture slope, S (%/cm), for a .3 cm. suspended moisture layer and soil moisture set (4.2%, 21.1%).

58

$Z_1 = .5$ cm.

REFLECTIVITY (dB)

FREQUENCY (GHZ)

Figure 4.18 Varying capillary moisture slope, S (%/cm), for a .5 cm. suspended moisture layer and soil moisture set (4.2%, 21.1%).

59

Figure 4.19 Varying capillary moisture slope, S (%/cm), for a .7 cm suspended moisture layer and soil moisture set (4.2%, 19.1%).

Figure 4.20   Varying capillary moisture slope, S(%/cm), for a 1. cm suspended moisture layer and soil moisture set (4.2%, 21.1%).

S = 16.9, Z_2 = 2.0
S = 33.8, Z_2 = 1.5
S = 56.3, Z_2 = 1.3
S = 169., Z_2 = 1.1

FREQUENCY (GHZ)

REFLECTIVITY (Ghz)

61

where ε_B is the permittivity of the surface and ε_C is permittivity of the subsurface. If permittivity is increased by some multiple k, then the subsurface permittivity must be increased by the square of the same multiple to keep the reflectivities equal at the minimum. For non zero angles of incidence and lossy materials the increase in the subsurface permittivity must be even greater to achieve equality.

comparison of Figures 4.18 through 4.24 with the corresponding reflectivities of similar surface layer depths and moisture slopes from Figures 4.8 through 4.16 indicates that the surface reflection is dominating at the minima in a manner consistent with the observations made for Figure 4.17. For these figures the quarter-wavelength depth occurs within 0.55 $\pm$ .03 of the capillary border width corresponding to approximately 13.4 $\pm$ .42% moisture.

The next set of figures, Figures 4.25 thorough 4.32, are the reflectivic for moisture contents of 0.2% and 17.1% in the suspended moisture layer and soil water horizon, respectively. Although a moisture content of 0.2% may seem artificial, this value of soil moisture was obtained by considering the surface layer to be an uncompacted aggregated soil mass with large interaggregate pores containing no free water and modeling this upper soil layer as an air-soil mixture. Assuming the surface soil aggregates to have a moisture content of 3%, a worse case porosity of 0.3 (Hillel, 1971), and using the mixing formula,

$$\varepsilon_{eff} = (1 - \rho) \varepsilon_{soil} + \rho \varepsilon_{air}$$

where ρ is the porosity of the soil, ε_{soil} is the permittivity of the soil, and ε_{air} is the permittivity of the air, gives an effective relative permittivity, ε_{eff}, of 2.6. This relates to a moisture content of 0.2% using the permittivity curves of Figure 4.3.

Figure 4.21   Varying suspended moisture layer depth for a 169. %/cm capillary moisture slope and slope moisture set (4.2%, 21.1%).

63

Figure 4.22 Varying suspended moisture layer depth for a 56.3%/cm capillary moisture slope and soil moisture set (4.2%, 21.1%).
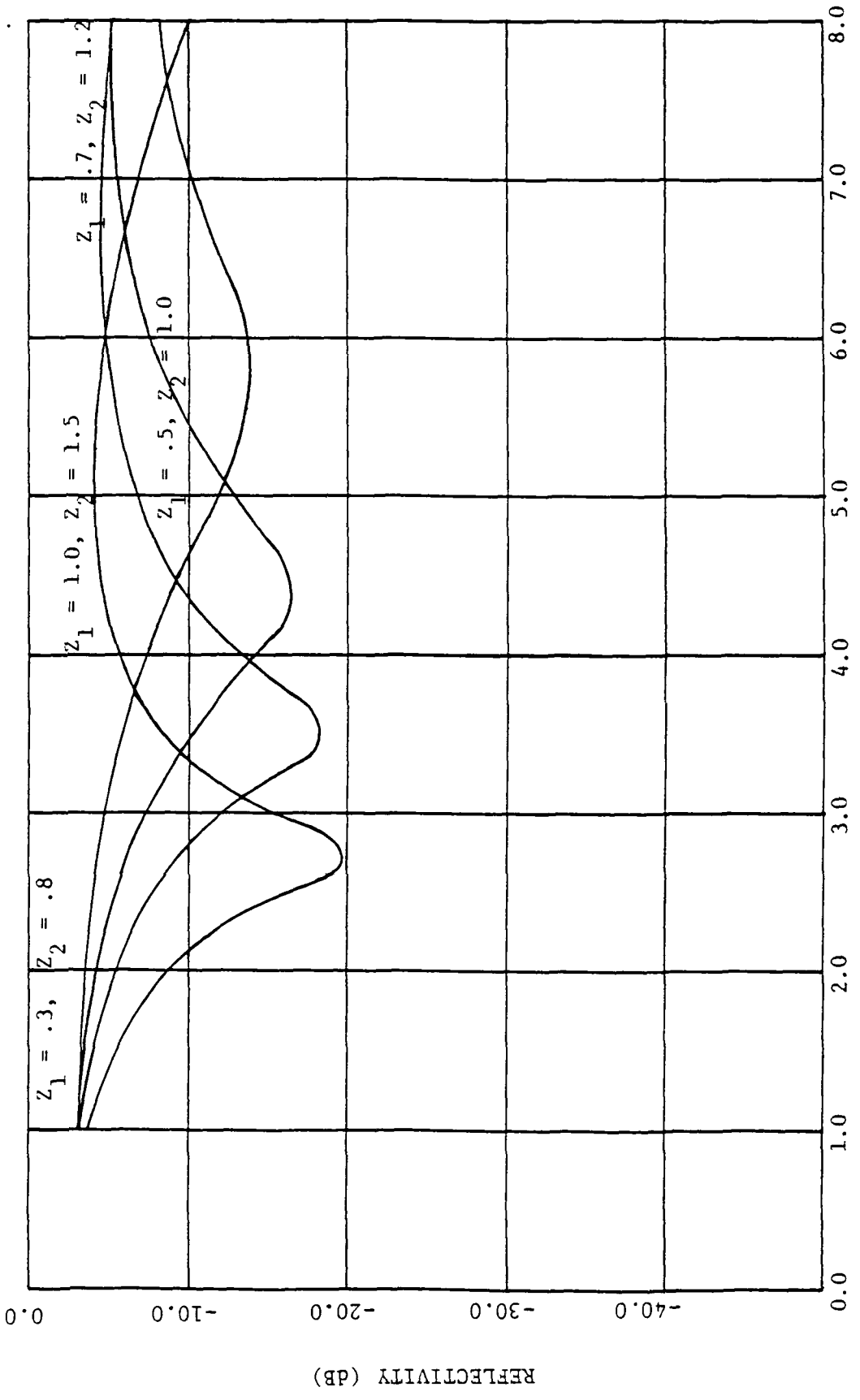
Figure 4.23   Varying suspended moisture layer depth for a 33.8%/cm. capillary moisture slope and soil moisture set (4.2%, 21.1%).

65
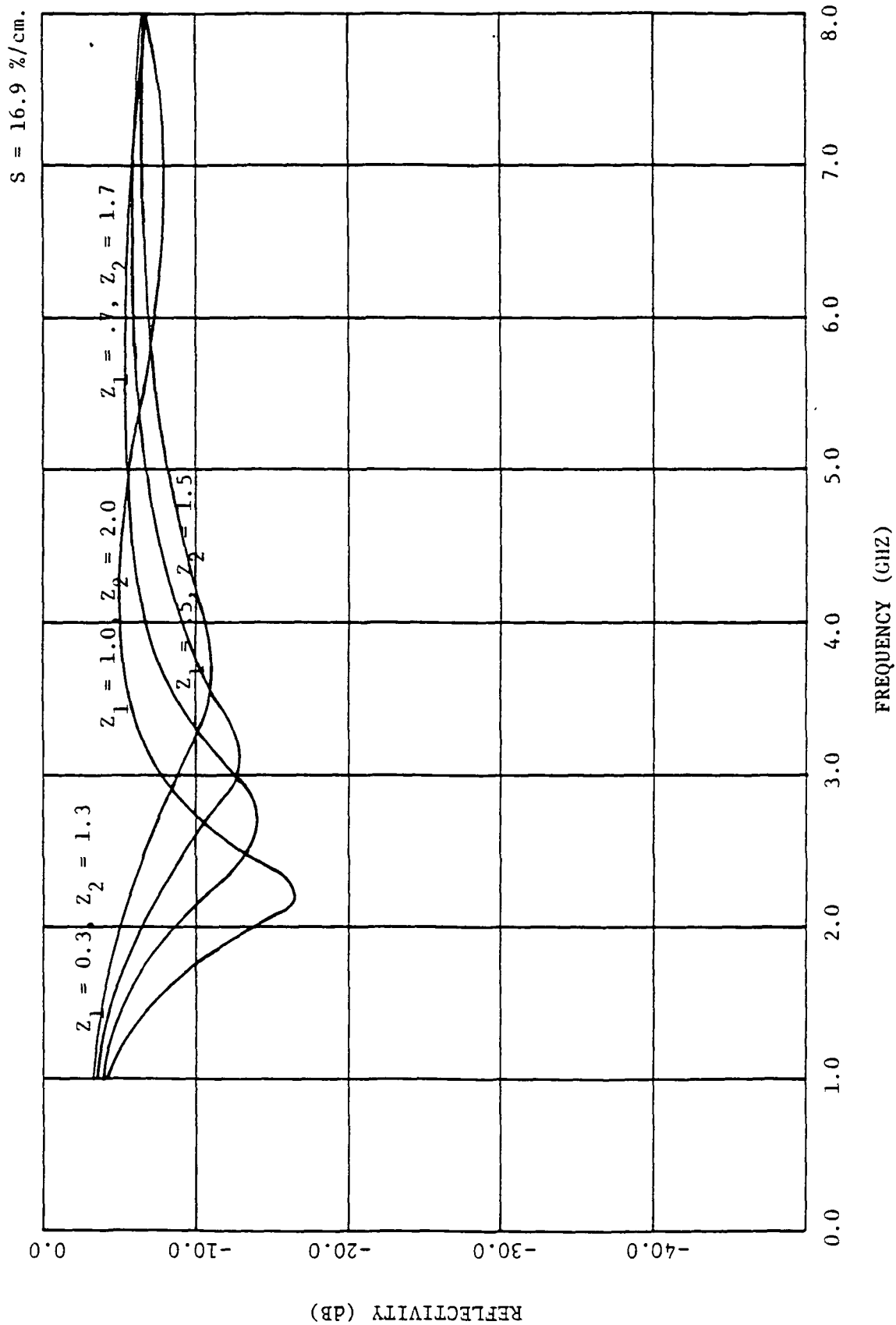
Figure 4.24 Varying suspended moisture layer depth for a 16.9 %/cm. capillary moisture slope and soil moisture set (4.2%, 21.1%).

66

As in the previous sets of figures, Figures 4.25 through 4.28 are the reflectivity curves for a surface layer of 0.3, 0.5, 0.7, and 1.0 centimeters, respectively. The reflectivities of each figure are parameterized by soil moisture slopes of 169.0, 56.3, 33.8, and 16.9 (percent moisture by weight per centimeter).

A comparison of the appropriate reflectivities of Figures 4.5 and 4.6 with those of Figure 4.25 shows the overall magnitude of the reflectivities of the latter figure to be less and the frequency at the reflectivity minima greater. Both of these effects are due to the differences in permittivity as a result of using decreased moisture content for the reflectivity curves of Figure 4.25.

Figure 4.26 shows that, unlike the reflectivities of equivalent moisture slope in Figures 4.7 and 4.8, the relative minima decrease as frequency and moisture slope increase until the slope equals 56.3. The next increase in slope (169.0) causes an increase in the relative minimum. For the curves of lowest slope, the surface reflection is the dominant component of the total reflectivity. As the moisture slope increases the frequency of the reflectivity minimum increases. The relative width of the capillary border with respect to wavelength, $\Delta Z/\lambda$, continues to decrease, thus the reflections from the transitional region of permittivity are more nearly in phase and therefore larger. As the slope is increased from 33.8 to 56.3, the reflections from the subsurface become sufficiently large to dominate the reflectivity and cause the minima to again increase.

An examination of Figures 4.27 and 4.28 illustrates the same pattern shown in Figure 4.26 except that the exchange from surface reflection dominance to subsurface dominance occurs at lower frequencies due to the greater depth of the suspended moisture layer.

67
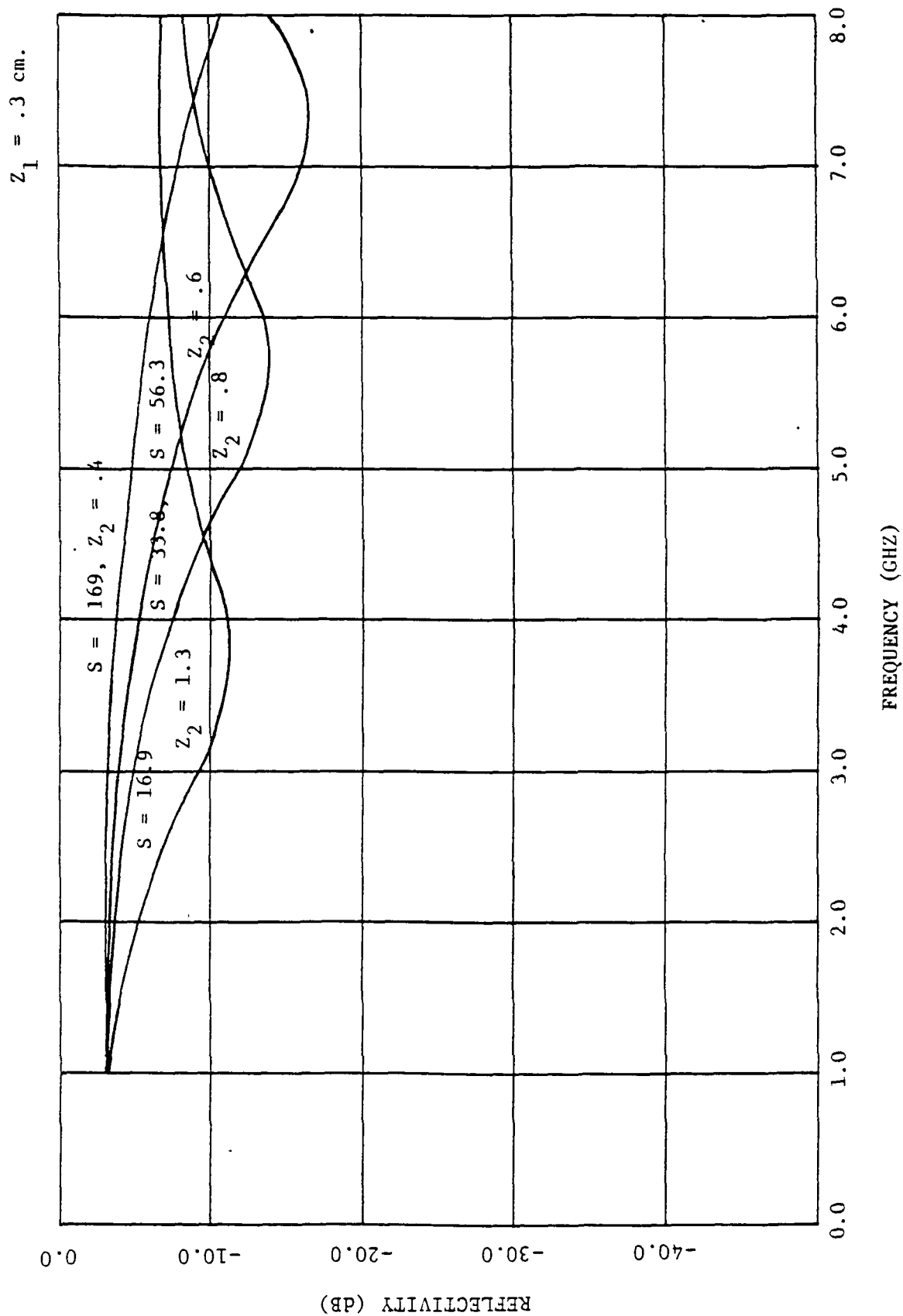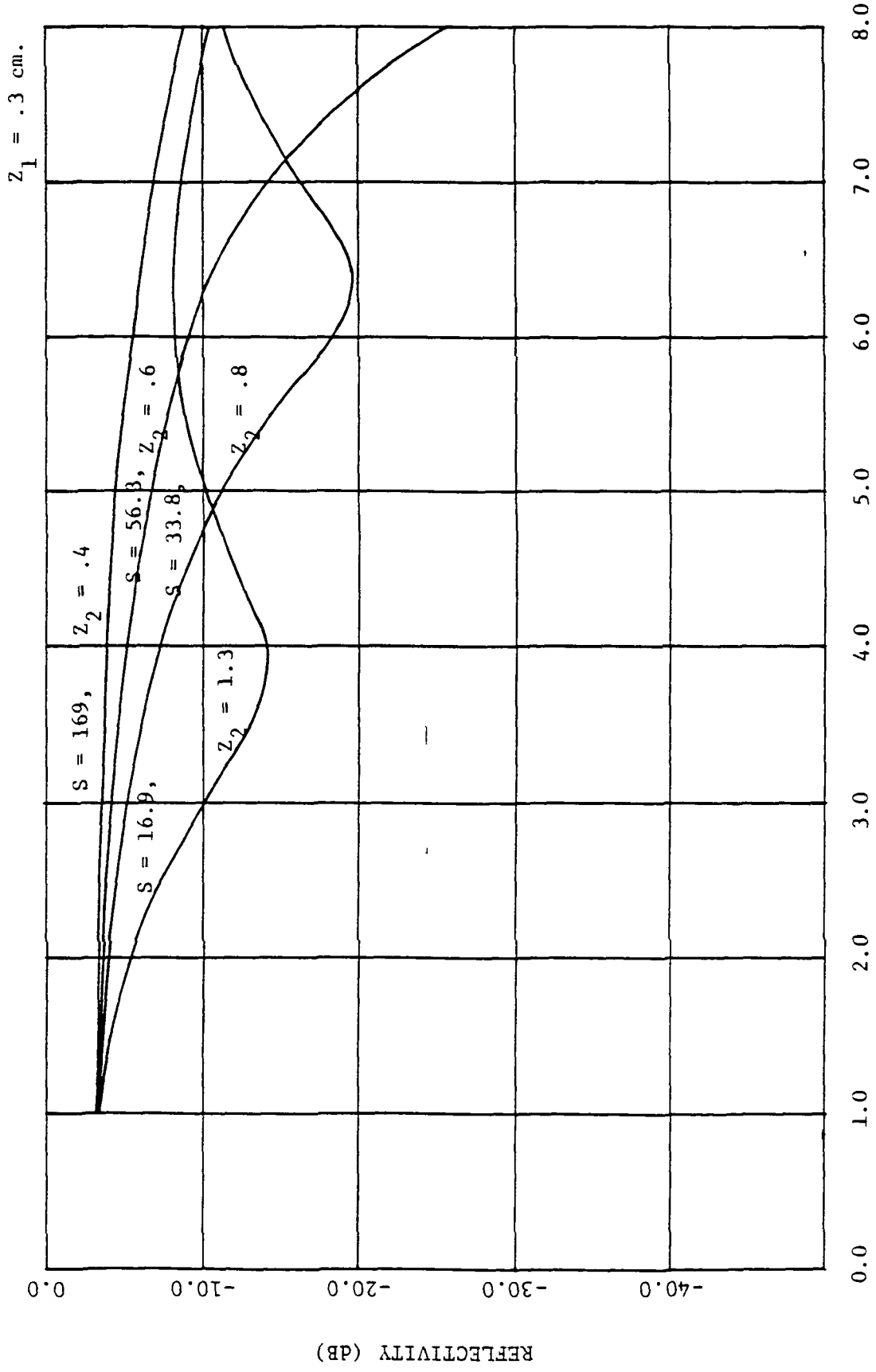
Figure 4.25 Varying capillary moisture slope, S (%/cm), for a .3 cm suspended moisture layer and soil moisture set (0.2%, 17.1%).
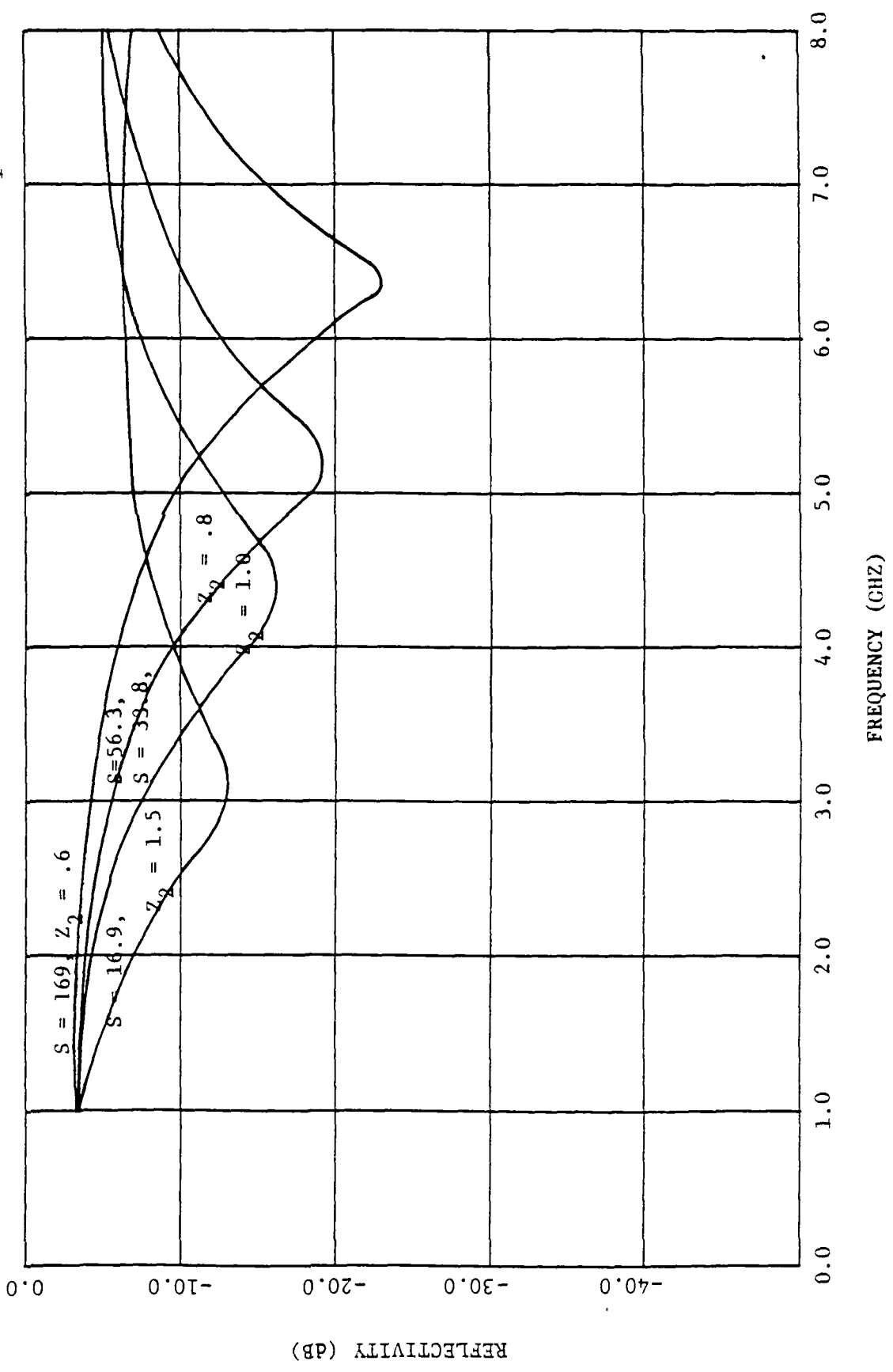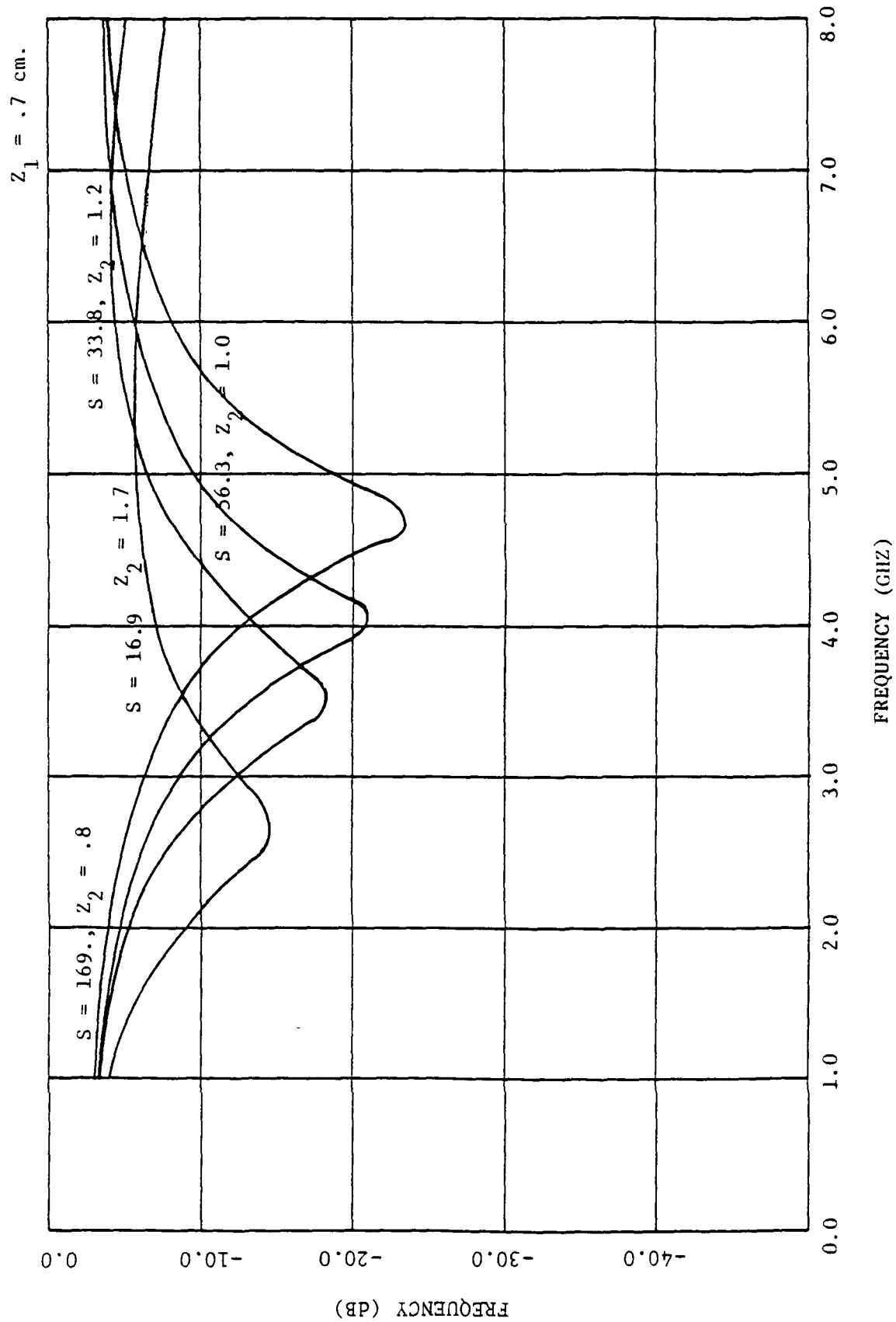
68
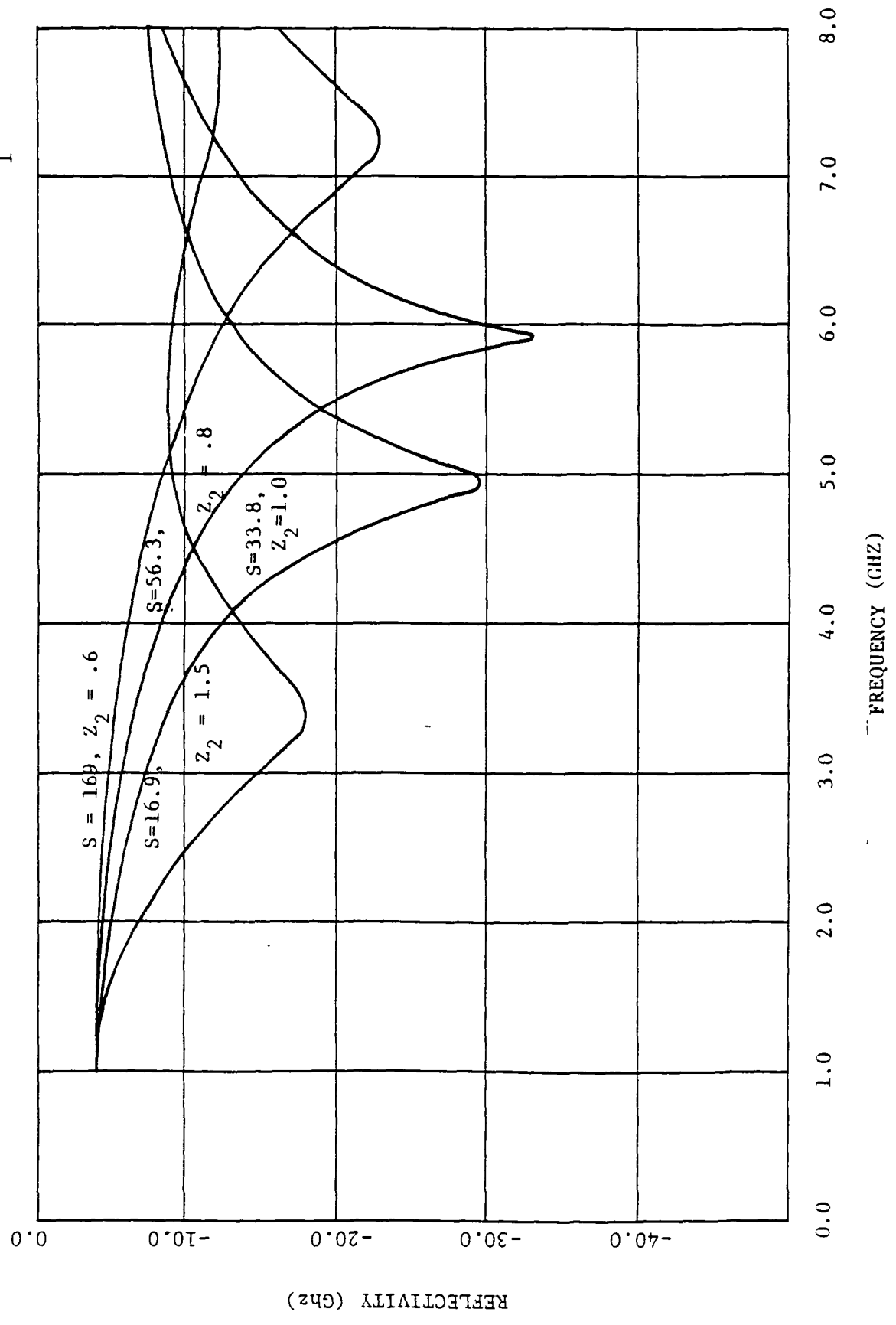
Figure 4.26 Varying capillary moisture slope, S(%/cm), for a .5 cm suspended moisture layer and soil moisture set (0.2%, 17.1%).
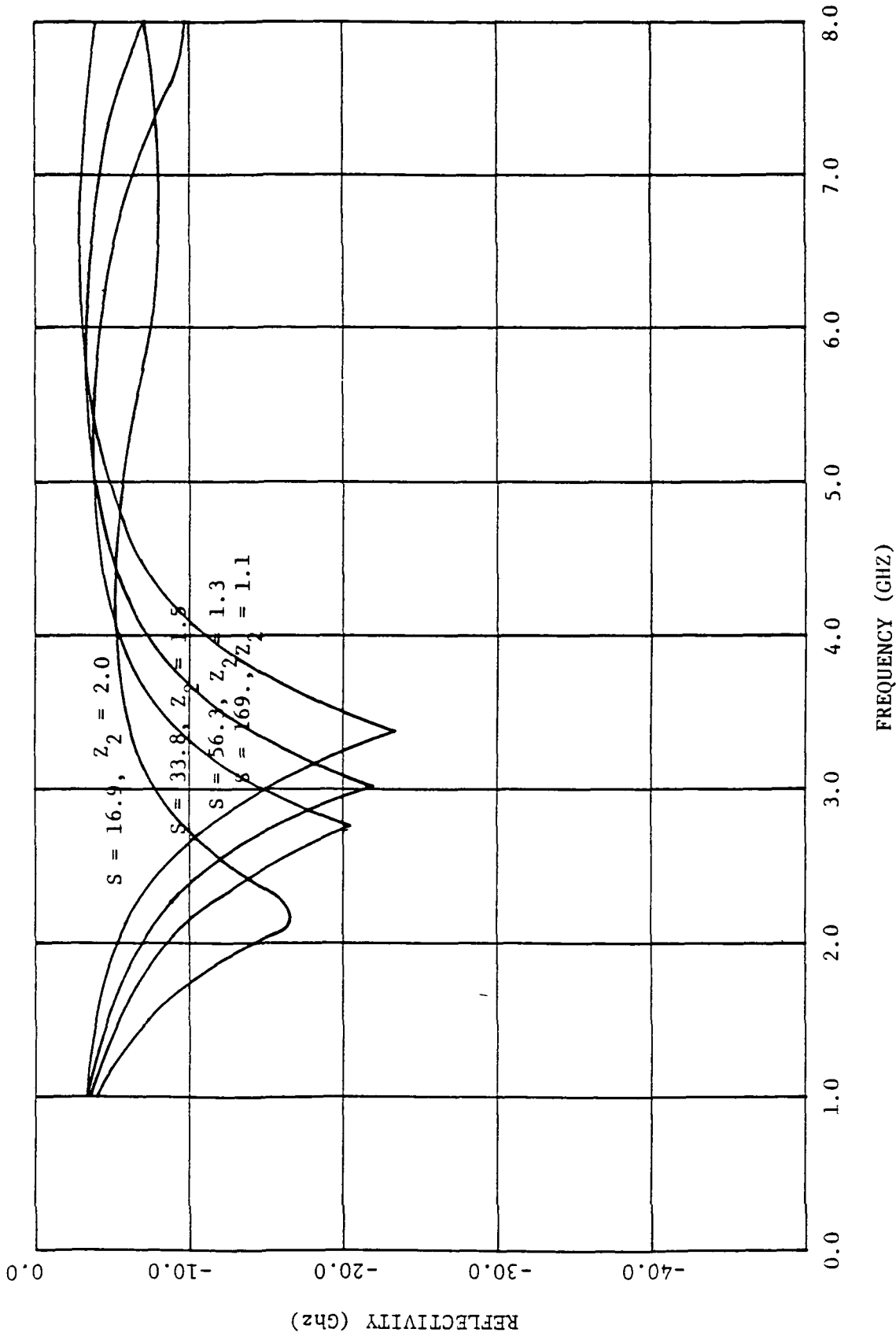
69
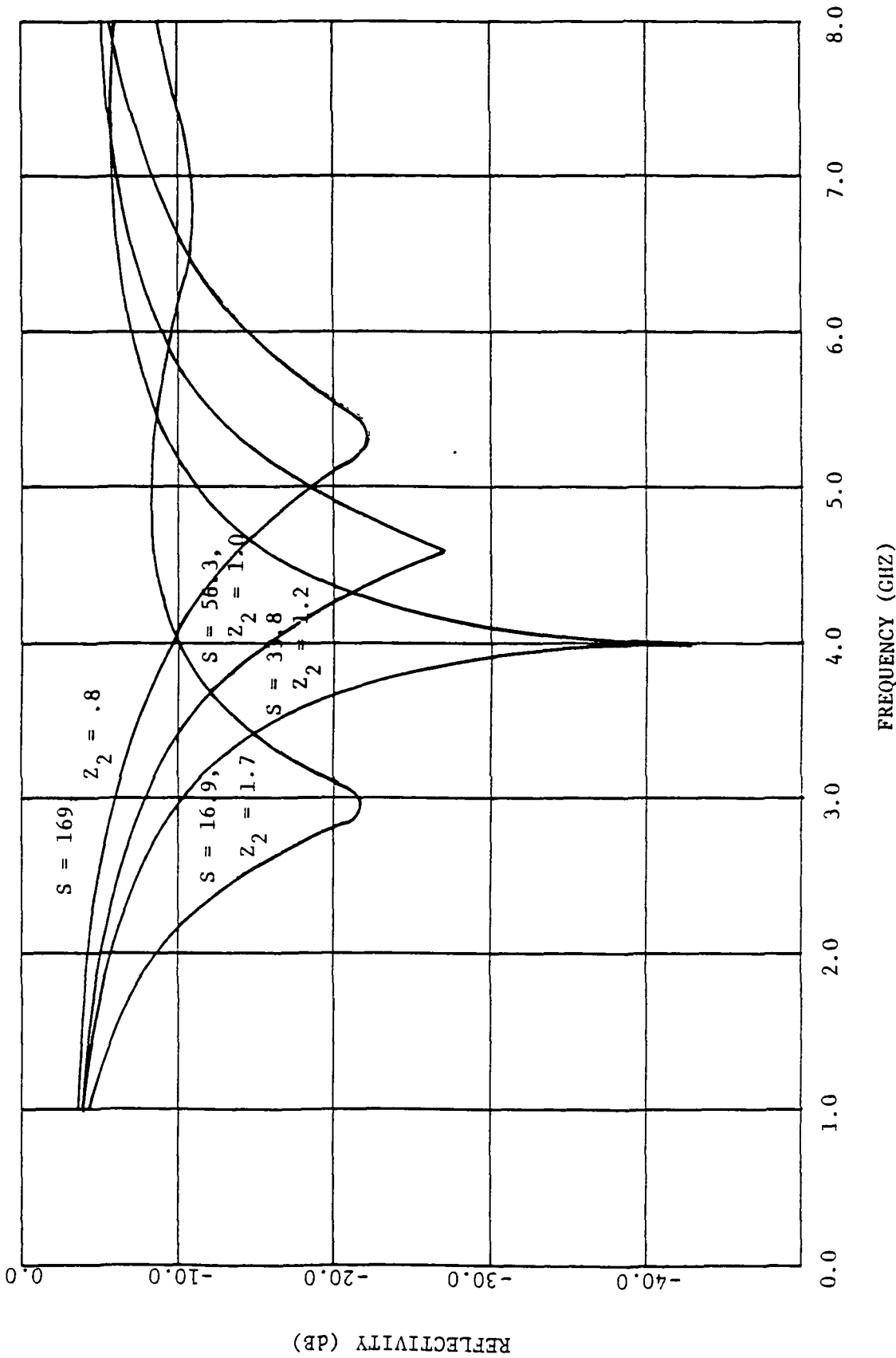
Figure 4.27 Varying capillary moisture slope, S(%/cm), for a .7 cm. suspended moisture layer and soil moisture set (0.2%, 17.1%).

70
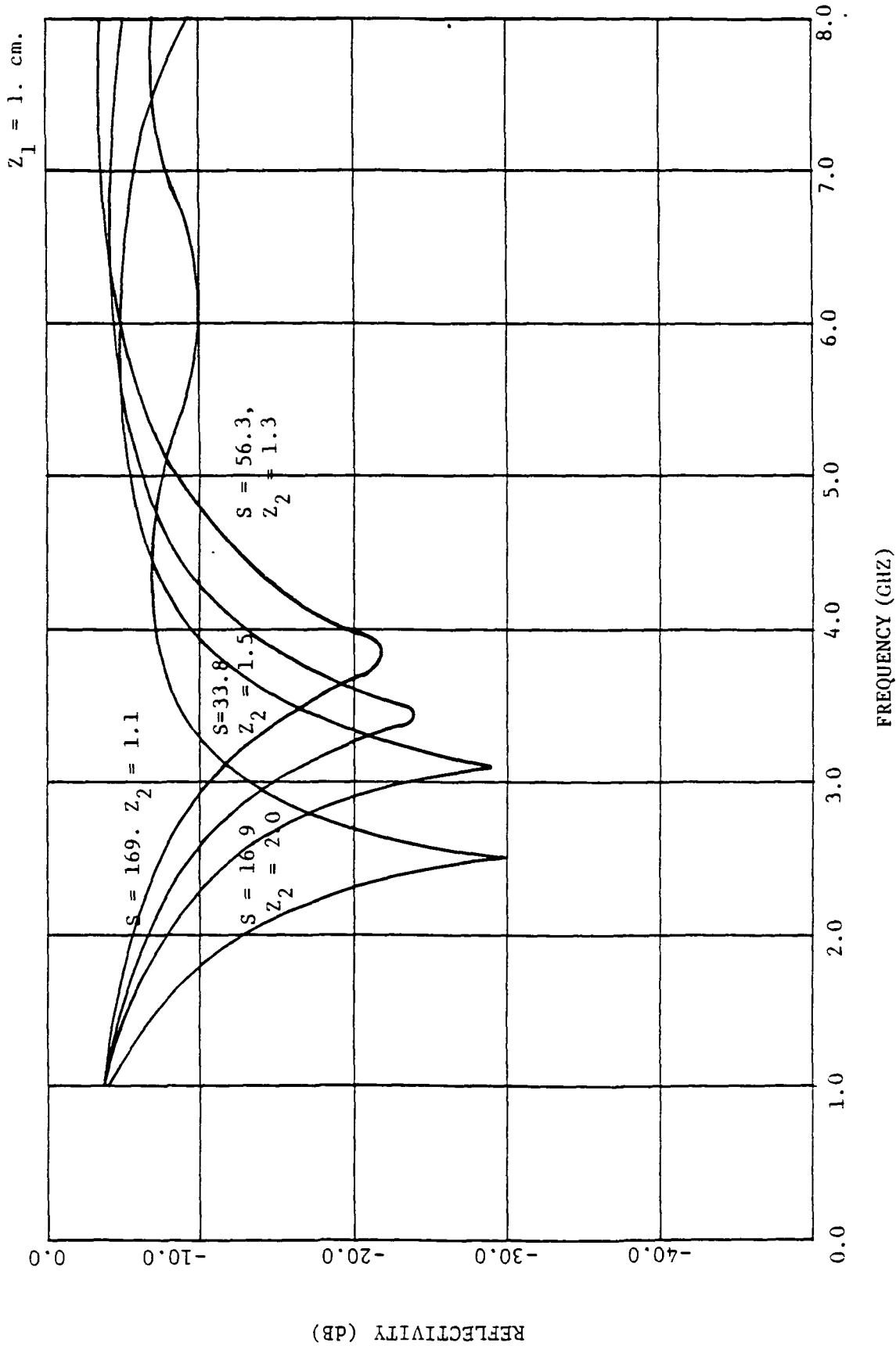
Figure 4.28 Varying capillary moisture slope, $S(\%/cm)$, for 1. cm. suspended moisture layer and soil moisture set (0.2%, 17.1%).

Figures 4.29 through 4.32 show the reflectivity of a particular moisture slope parameterized by the depth of the suspended moisture layer. These four figures are equivalent in moisture slope to Figures 4.13 through 4.16, but differ in assumed surface and subsurface moisture content.

The reflectivity curves of Figures 4.29 and 4.30 indicate that the subsurface component increases with the depth of the suspended moisture layer for moisture slopes of 169.0 and 56.3. The decrease in the relative minima as the region of transitional permittivity moves deeper into the soil volume is due to the relative width of that region becoming smaller with respect to wavelength causing the total subsurface reflection to increase. Note that this effect overcomes the increased attenuation suffered by the subsurface component.

Figures 4.31 and 4.32 show in greater detail the effects of the relative width of the capillary border with respect to wavelength. The moisture slope of Figure 4.31 is 33.8 and as the upper soil layer is increased by moving the capillary border deeper into the volume, the relative reflectivity minima decrease showing that the surface reflection is larger than the subsurface component. When the depth of the suspended moisture layer is 0.7 centimeters the subsurface and surface reflections are nearly equal giving the very deep minimum. The subsurface component becomes larger as the upper surface layer depth is increased to 1.0 centimeter causing the relative reflectivity minimum to again increase in value. Figure 4.32 shows a similar effect except that the subsurface component does not clearly dominate even to a surface layer of 1.0 centimeter.
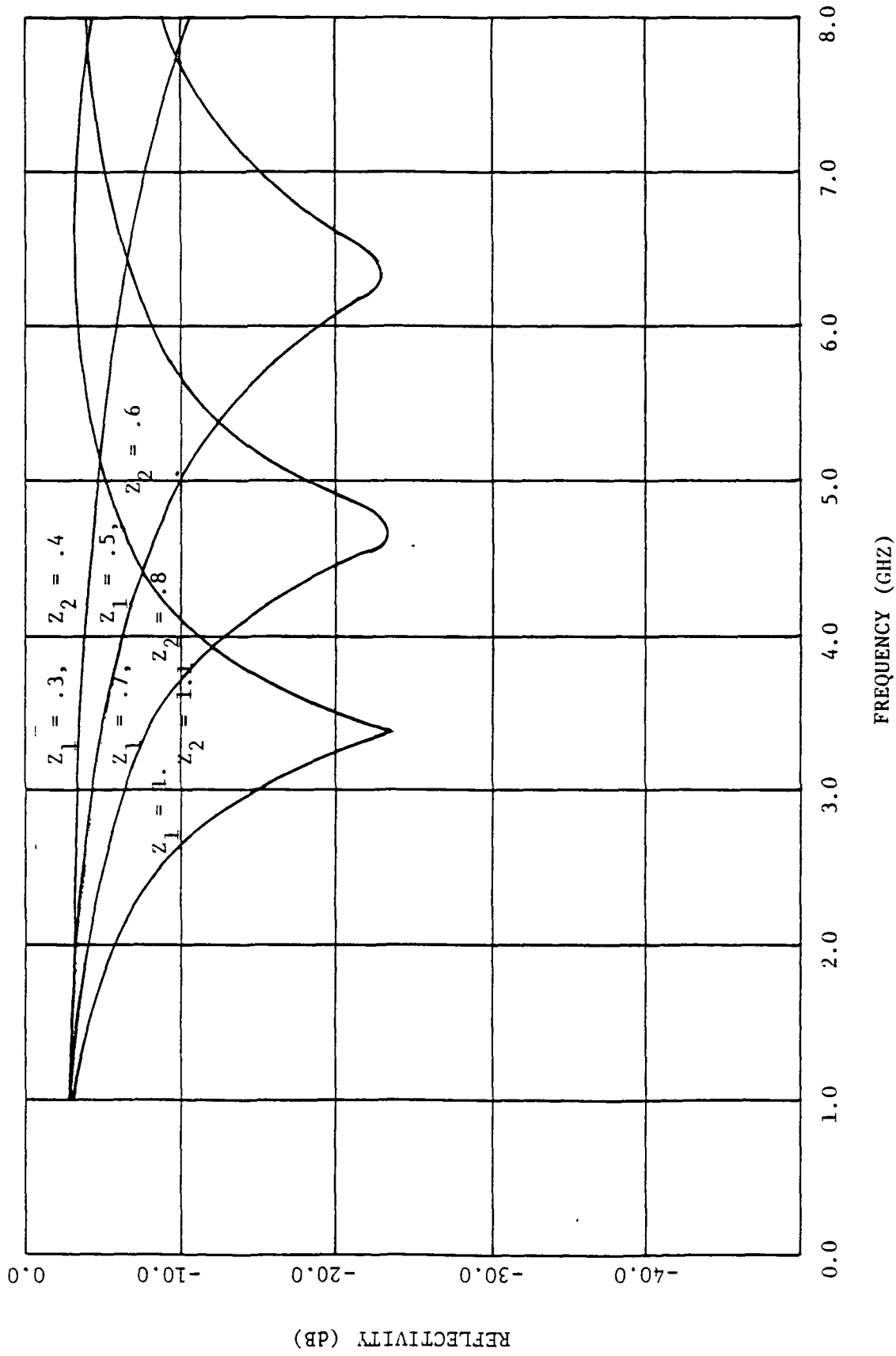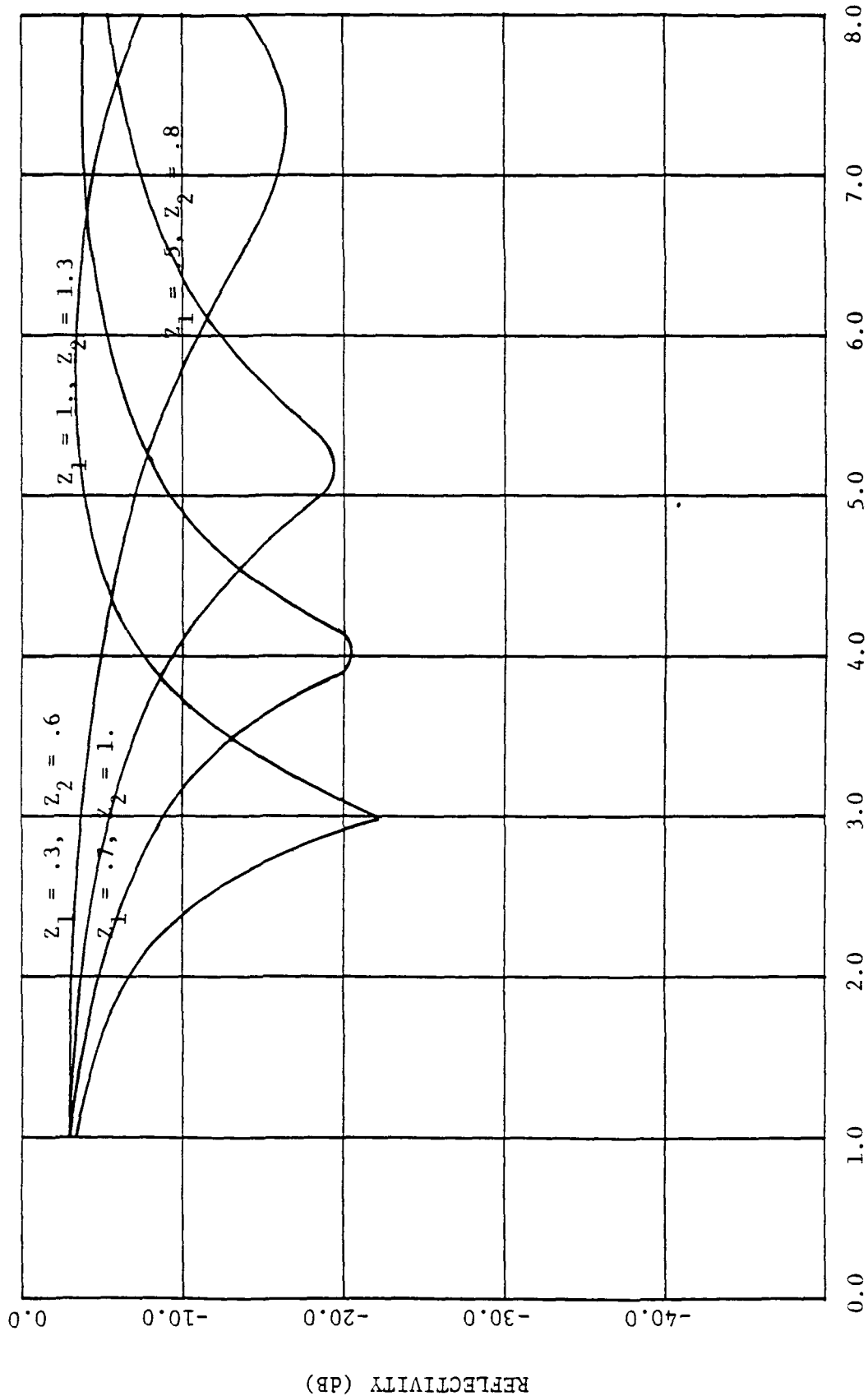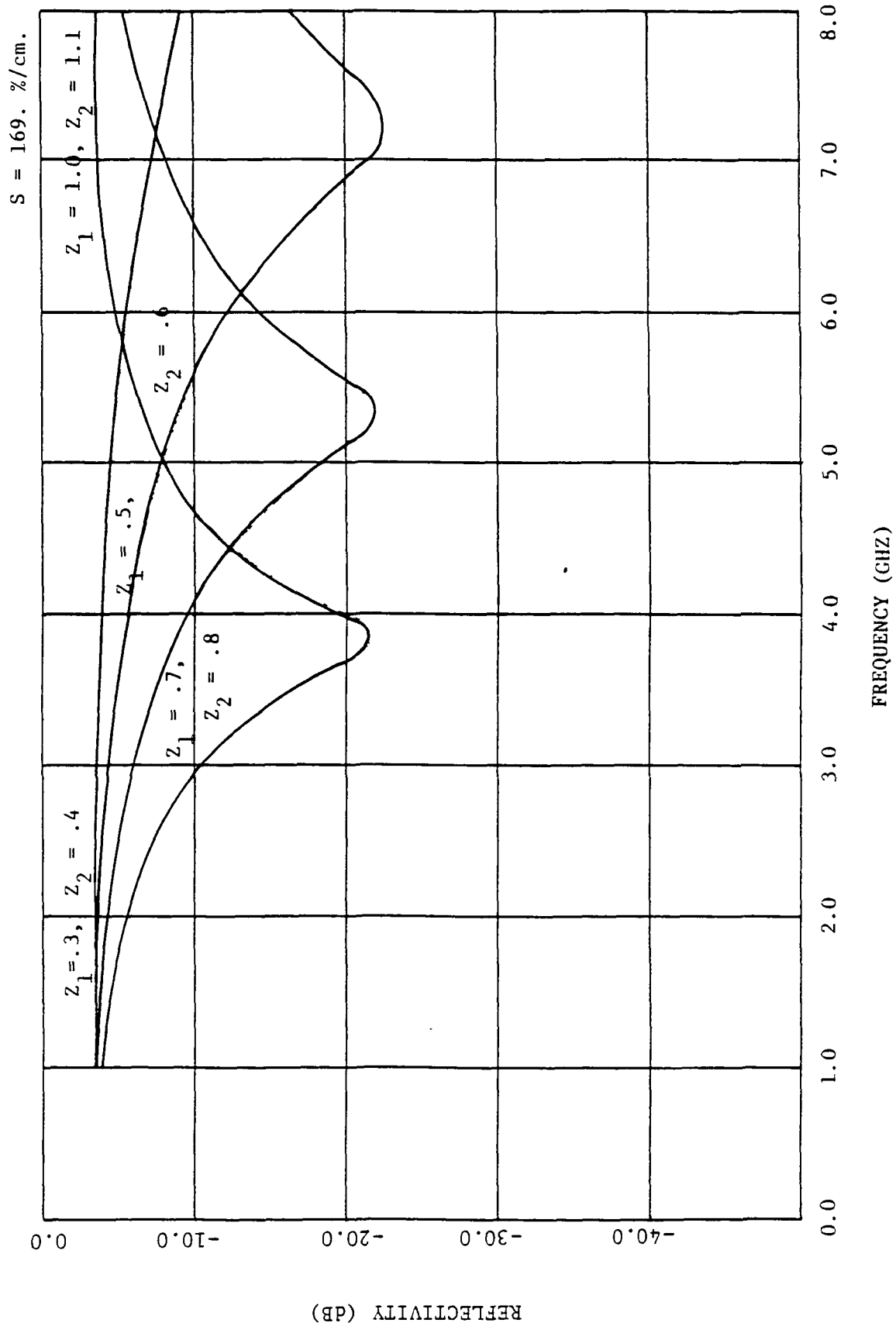
Figure 4.29 Varying suspended moisture layer depth for a 169. %/cm. capillary moisture slope and a soil moisture set (0.2%, 17.1%).

73

S = 56.3 %/cm.

$z_2 = 1.3$

$z_1 = 1.0$,

$z_1 = .3$, $z_2 = .6$

$z_1 = .5$, $z_2 = .8$

$z_1 = .7$, $z_2 = 1.0$

FREQUENCY

REFLECTIVITY (dB)

0.0   -10.0   -20.0   -30.0   -40.0

0.0   1.0   2.0   3.0   4.0   5.0   6.0   7.0   8.0
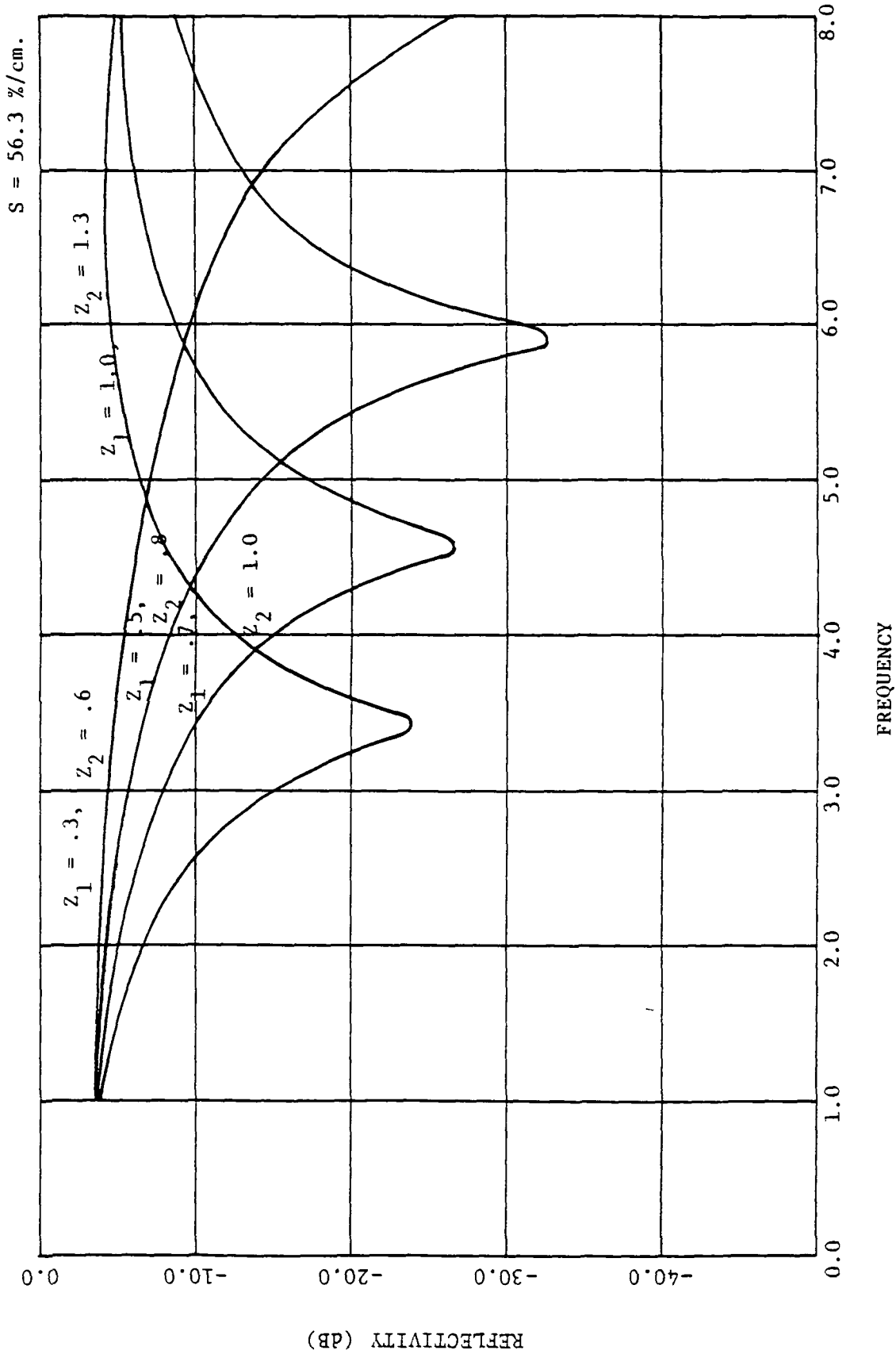
Figure 4.30   Varying suspended moisture layer depth for a 56.3 %/cm. capillary moisture slope and a soil moisture set (0.2%, 17.1%).

S = 33.8 %/cm.

z_1 = 1., z_2 = 1.5

z_1 = .7, z_2 = 1.2

z_1 = .5, z_2 = 1.0

z_1 = .3, z_2 = .8

FREQUENCY (GHz)

REFLECTIVITY (dB)
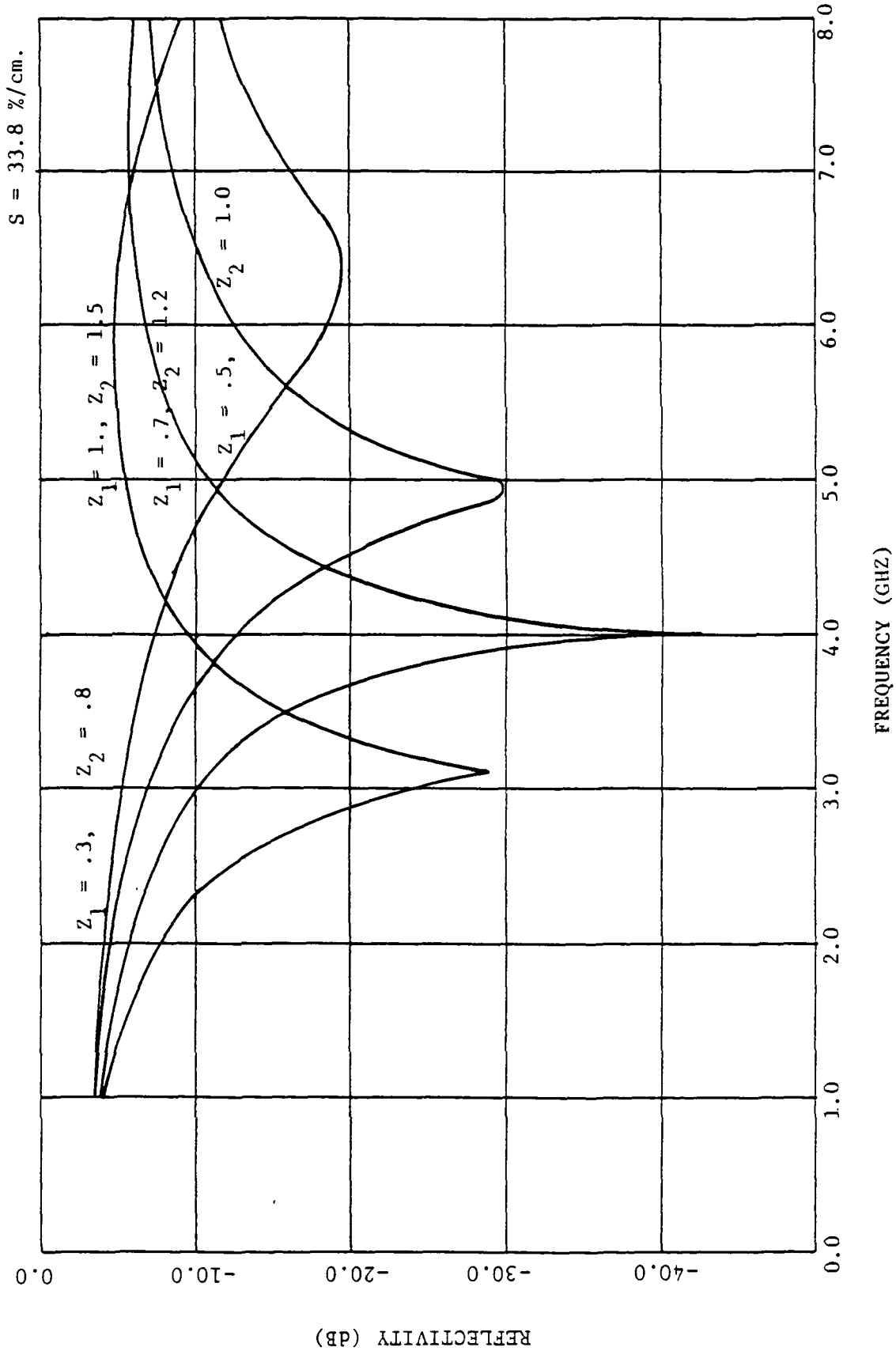
Figure 4.31 Varying suspended moisture layer depth for a 33.8%/cm capillary moisture slope and a soil moisture set (0.2%, 17.1%).

75
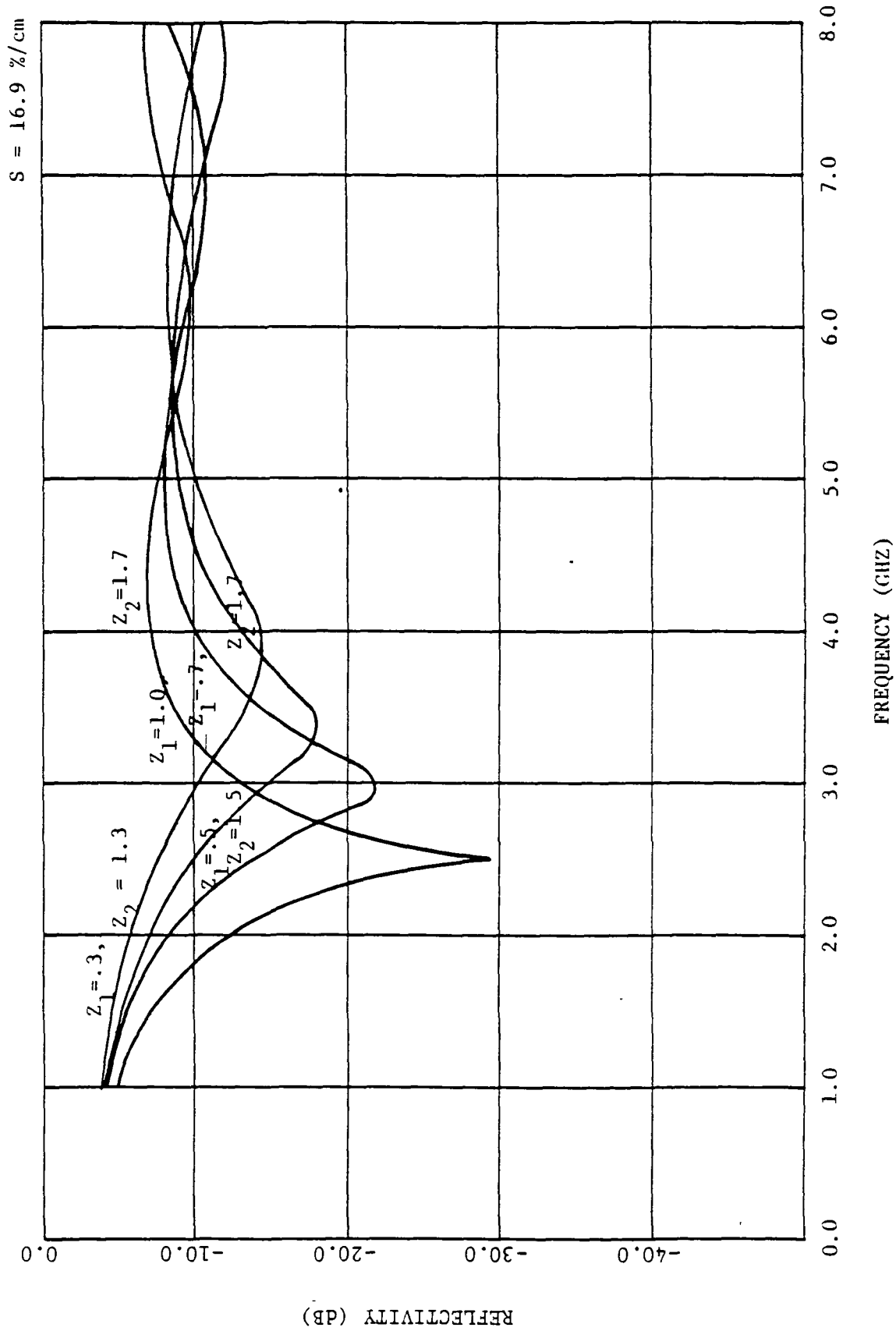
Figure 4.32 Varying suspended moisture layer depth for a 16.9%/cm. capillary moisture slope and soil moisture set (0.2%, 17.1%).

76

The quarter-wavelength depth estimate for these moisture contents

(0.2%, 17.1%) is 0.56 $\pm$ .06 of the capillary border width, which corresponds

to a moisture content range of 9.7 $\pm$ .2%. The quarter-wavelength depth

for the moisture content set (2.2%, 19.1%) was 0.55 $\pm$ .02 of the capillary

border width with a moisture content range of 11.8 $\pm$ .5%. The quarter-

wavelength depth for the moisture content set (4.2%, 19.1%) was 0.55

+ .03 of the capillary border width corresponding to a 13.4 $\pm$ .4% moisture

content. Comparison of the quarter-wavelength depth on a fractional

basis indicates that the point of occurence is essentially the same

for each moisture set. This is also verified by the moisture content

at the quarter-wavelength depth, since the difference is approximately

the same as the difference between each moisture content set (2%).

One purpose in presenting these three sets of figures of the same

moisture slope but different moisture contents, was to show that relatively

small changes in the depth of the suspended moisture layer, the width

of the capillary border, and the moisture content in each region may

cause significant changes in the reflectivity. Another purpose was

to demonstrate the non-linear relationship of the permittivities in

the reflectivity calculations. The figure set, Figures 4.25 through

4.32, using the smallest moistures contents (0.2%, 17.1%) had, depending

on the depth of the surface layer and the moisture slope, reflectivities

dominated by either the subsurface or the surface components. The

figure set, Figures 4.17 through 4.24, using the highest moisture contents

(4.2% 21.1%) had reflectivities that were never dominated by the subsurface

reflection regardless of the moisture slope of the capillary border

and the depth of the suspended moisture layer. This non-linear relationship

becomes more dramatic by comparing the real part of the relative

permittivities of the two different moisture content sets. The lowest
moisture content set (0.2%, 17.1%) maps into the relative real permittivity
set (2.6, 13.8), while the highest moisture content set (4.2%, 21.1%)
maps into the relative real permittivity set (3.9, 19.5). A comparison
of the permittivity values of these sets and the reflectivity curves
generated from them using the multi-layer model illustrates the importance
of the upper surface of the volume on the total reflectivity.

4.3 Field Measurements of Continuous Moisture Profiles

4.3.1 Description of Field Experiment

The field experiment was conducted at the University of Arkansas,
Agricultural Experimental Station #1. The choice of this site permitted
good accessibility and provided soils of a common texture, a silt loam.
The duration of the experiment spanned the period from July 9 to October
19, 1979. This period was divided into five separate time intervals
marking different test plot cycles. Of primary interest are the measurements
of plot cycles 3 and 4 as the plot was established to simulate tilled
fields during these intervals.

Measurements taken coincident with the soil reflectivity included
soil moisture profile, bulk density profile, soil moisture potential
profile, soil temperature profile, and air temperature. The measurements
dealt with here are those of the microwave reflectivity and soil ground
truth. The ground truth data of the experiment will be used as a basis
for the multi-layer model developed in the previous section of this chapter,
and the results of this model shall be compared to the field measured
soil reflectivities.

78

Figure 4.33 shows the layout of the test plot, the approximate positioning of the sensors, and the sampling areas.

4.3.1.1 Test Plot Preparation - Initial plot preparation consisted of tilling and boxing a portion of the area with a 4.57 by 4.57 meter wooden frame. This wooden frame was constructed of 2.5 by 30 cm. pine boards. The boards of the frame were placed into the soil to a depth of approximately 20 centimeters leaving 10 centimeters of the board above the soil surface. Framing the plot in this manner clearly desig- nated the plot area, aided in plot irrigation and levelling, and confined the soil moisture redistribution to a specific area.

Final plot preparation included irrigation, retilling, and levelling as required by the objectives of the experiment for a particular initial soil moisture content and density. The goal of the experiment for test plot cycles 3 and 4 was to achieve a loose upper soil horizon of at least 15 centimeters in depth. This objective stemmed from the desire to simulate freshly cultivated fields as an initial condition.

The method used to obtain the desired initial condition was to till and level the test plot, irrigate using a sprinkler system, allow the moisture to redistribute for an appropriate period of time, then retill and level. The final tilling loosened the soil, gave a uniform initial soil content in the tilled horizon, and re-established the soil surface roughness structure. Plot cycle 4 was given a higher initial moisture content than plot cycle 3 by increasing the amount of irrigation and decreasing the time allowed for moisture redistribution before retilling.

NORTH

REFLECTOMETER
RECEIVER PLATFORM

DATA LOGGER

W

E

REFLECTOMETER
TRANSMITTER PLATFORM

——————— TENSIOMETER BANKS
— — — — — THERMOCOUPLE BANKS
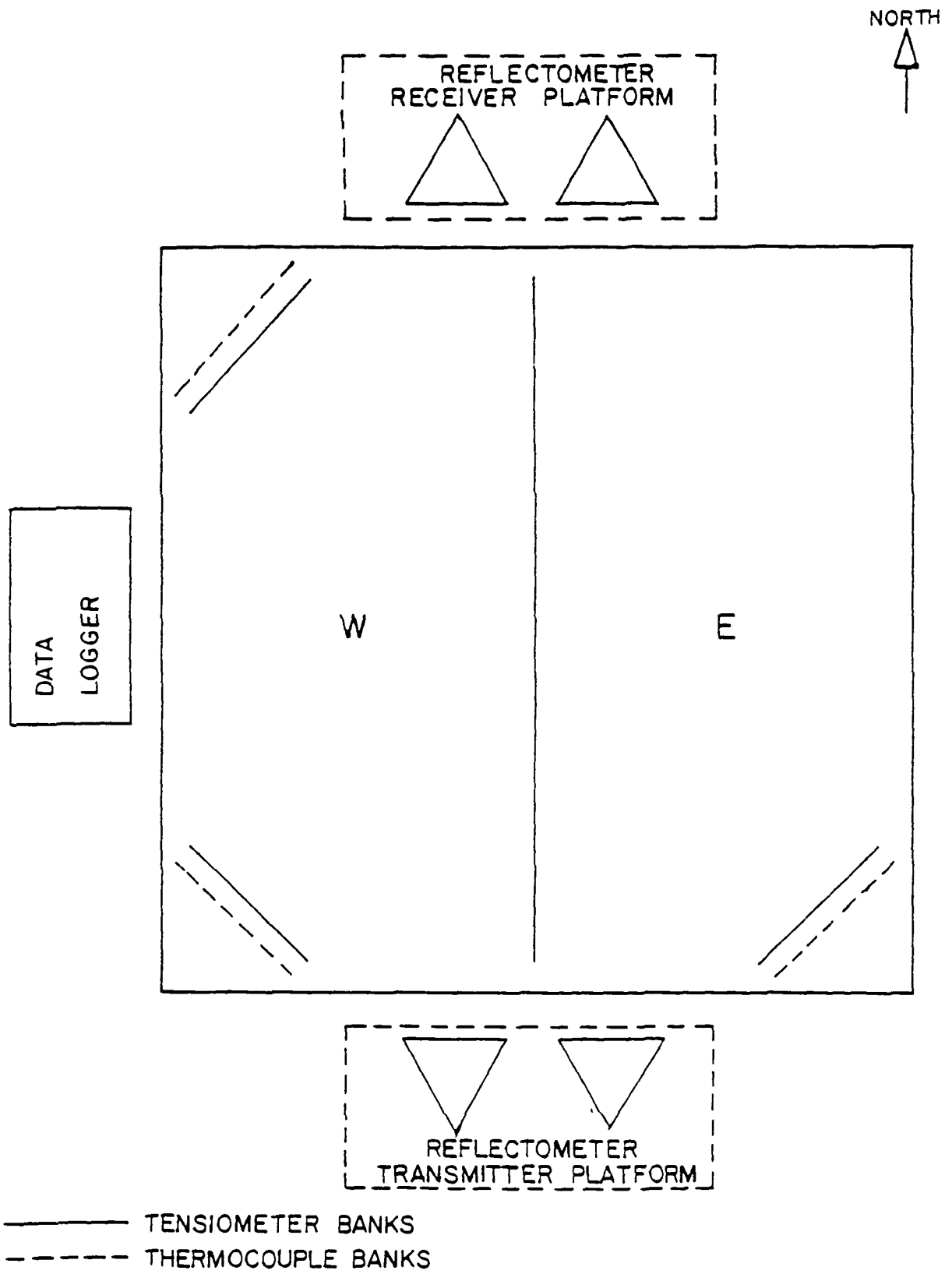
Figure 4.33 Test plot and sensor arrangement.

4.3.1.3 Reflectometer System - The reflectivity data was obtained utilizing

a bistatic reflectometer system measuring at the specular angle of 45°.

This reflectometer system featured separate antenna support platforms

of the same construction for both the transmit and receive portions of

the device. The system also featured dual mounted standard gain horn

antennas for the bandwidths of 1 to 2 GHz and 4 to 8 GHz. A 1 to 2 GHz

and a 4 to 8 GHz antenna were positioned on each support platform in

a parallel side by side arrangement. The transmitter portion of the

system consisted of a microwave sweep oscillator mainframe with individual

sweep plug-ins for the 1 to 2 and 4 to 8 GHz bandwidths. Receiver implemen-

tation was accomplished by using a network analyzer with storage normalizer

as a ratio meter and an X-Y plotter to furnish a record of the data.

Table 4.1 gives a listing of the reflectometer parameters used in the

system, and Figure 4.34 shows a block diagram of the system with cable

interconnects.

System calibration was external and employed a thin sheet of aluminum.

The calibration procedure involved placing the aluminum sheet over the

soil area to be illuminated and making a swept frequency measurement

of the power reflected from the aluminum sheet. The aluminum calibration

sheet was removed and a swept frequency measurement of the reflected

power from the bare soil was made. The ratio of these two swept frequency

measurements gives the reflectivity of the bare soil. A more detailed

description of a bistatic reflectometer using this calibration procedure

is given in Waite, et. al., 1973.

4.3.1.3 Reflectivity Data - In order to meet the measurement

objectives for diurnal and long term time periods, the measurement frequency

had the following schedule. At the start of plot cycle 3 and after a
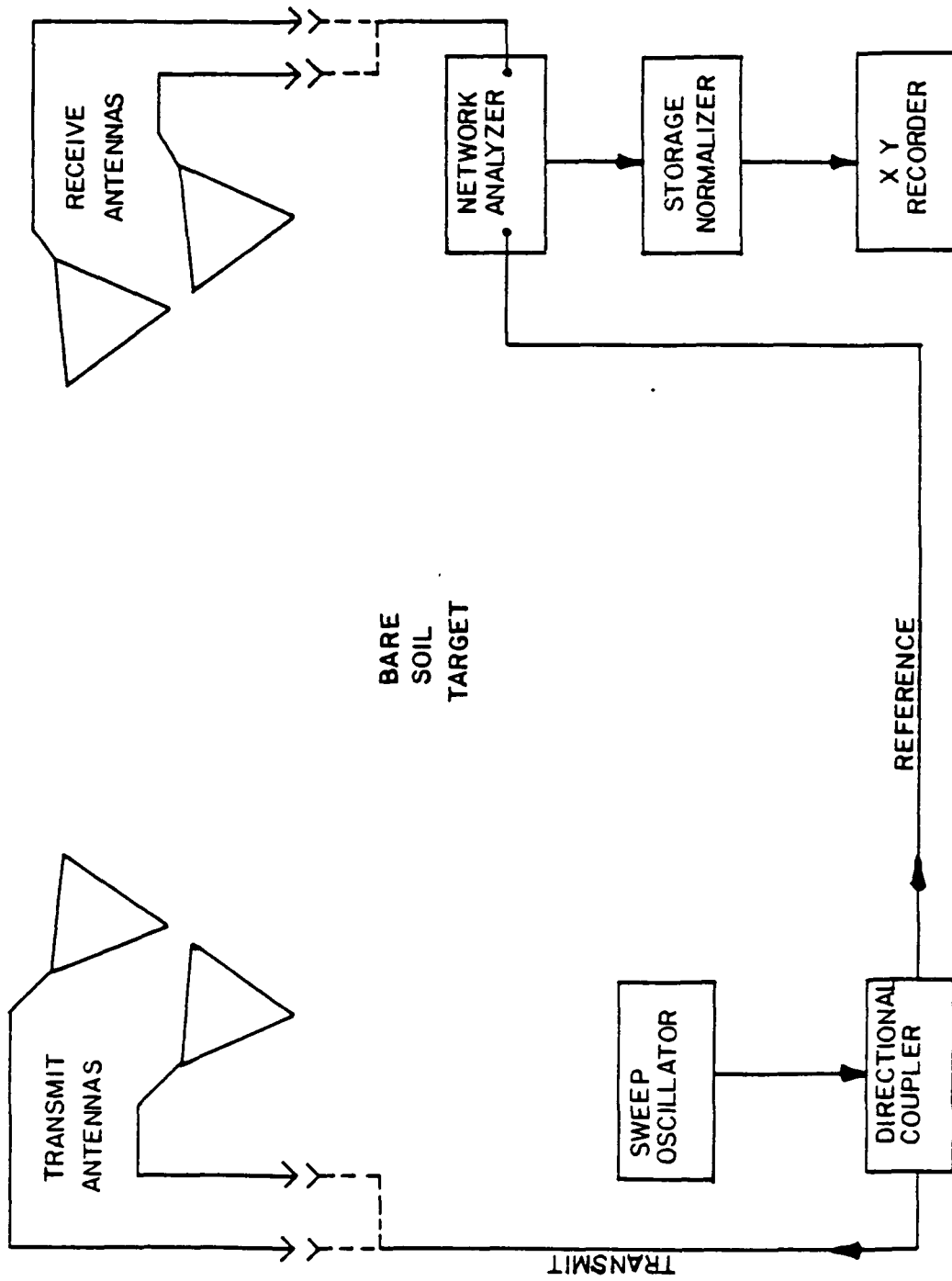
4.34 Block diagram of field bistatic reflectometer instrumentation.

rain event the rate of measurement was three per day: morning, solar noon, and afternoon. As the soil moisture redistributed, the solar noon measurement was eliminated. The rate was further reduced to the afternoon measurement alone as the test plot moved into a long term measurement interval. The regime for plot cycle 4 was to initially make at least one afternoon measurement a day, accomplish a diurnal experiment, and then reduce measurements to one every other day.

4.3.1.4 Soil Moisture and Bulk Density Data - Soil moisture sampling was conducted immediately after each reflectivity measurement. The soil sampling intervals for cycles 3 and 4 were 0. - .5 cm., .5 - 1. cm., 0. - 1. cm., 1. - 2., 2. - 5. cm., 5. - 9. cm., and 9. - 15. cm. Note that the first centimeter of the soil volume was sampled in half-centimeter intervals in addition to a 0 - 1 cm. measurement. Due to the finite area of the test plot, it was impractical to separately conduct frequent soil moisture and bulk density sampling. This problem was overcome by using a simple plastic cylinder to make soil samples of known volume at the various soil depth intervals. This method allowed the soil sample to serve for both the soil moisture and bulk density measurement. All soil samples were immediately weighted after sampling and oven dried at 105° C for a period of twenty-four hours.

4.3.2. Results of Field Experiment

The following figures are representative reflectivity data from the 1979 bare soil experiment. A corresponding soil moisture profile is presented with each reflectivity curve, and each reflectivity curve is explained in terms of the multi-layer model for a smooth surface. The initial data presented are taken from cycle 3 of the experiment, which began August 21, 1979. In order to show diurnal effects, consecutive measurement results are presented beginning with the afternoon measurement of August 21, followed by the morning, midday, and afternoon measurements of the succeeding day. The visual appearance of the plot surface during this time interval was dry with the dominate soil structure being peds resembling pea gravel in size and shape.

Figure 4.35 shows the soil moisture profile taken during the afternoon of August 21, 1979 at 1615 hours. An examination of this moisture profile, and subsequent soil moisture profiles, indicates that the modeled reflectivity using the soil moisutre set (2.2%, 19.1%) should provide a suitable comparison for the field reflectivity data. In this figure and following figures depicting soil moisture profiles, the solid lines represent the field moisture data over the sampling depths 0. - .5, .5-1., 1.-2., and 2.-5. centimeters, while the dashed lines represent the approximate soil moisture profile used for model calculations

The reflectivity curve taken August 21, 1979 at 1615 hours is shown in Figure 4.36. In this figure, and succeeding figures showing reflectivity, the solid curves are the reflectivities calculated from the multi-layer model using the soil moisture set (2.2%, 19.1%) for the surface and deep subsurface moisture contents, while the dashed curve is the measured soil reflectivity.
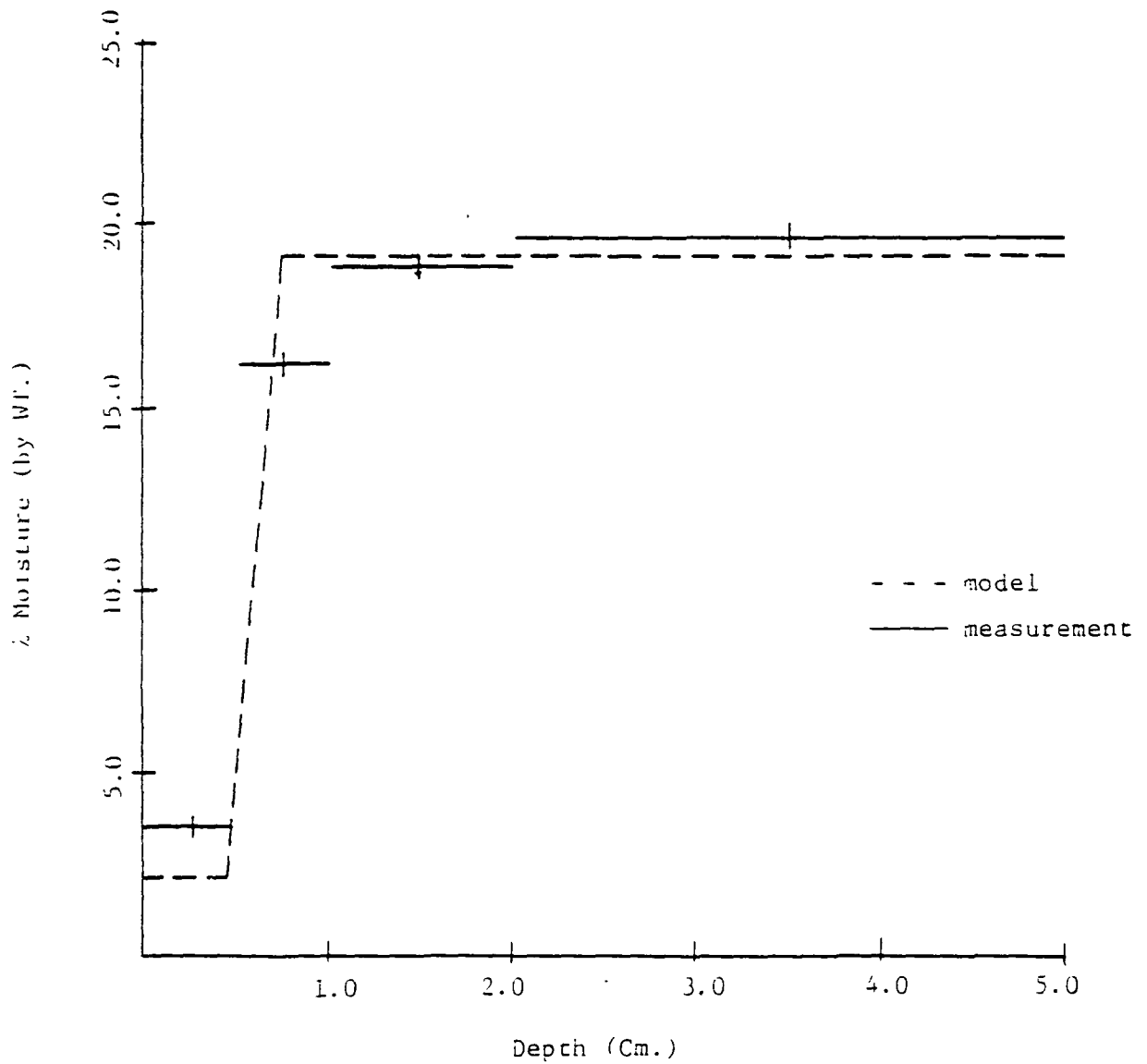
Figure 4.35 Measured and approximate soil moisture profiles for August 21, 1979 at 1615 hours.
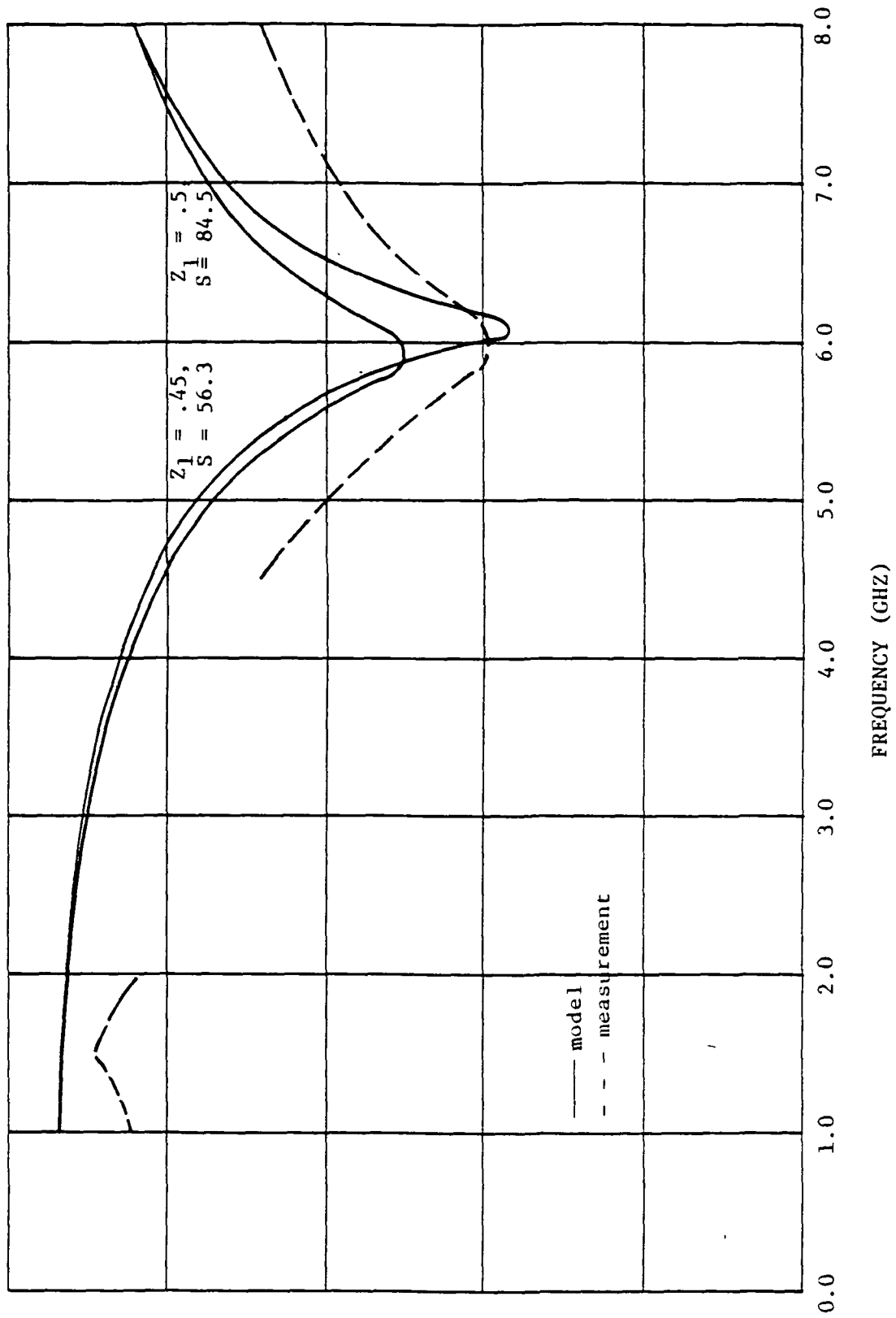
Figure 4.36 Measured and model reflectivity for August 21, 1979 at 1615 hours.

REFLECTIVITY (dB)

FREQUENCY (GHZ)

The solid reflectivity curves of Figure 4.36 were obtained using the soil moisture set (2.2%, 19.1%) and varying the depths of the suspended moisture layer and the soil water horizon. One curve corresponds to a suspended moisture layer depth of .5 centimeters and a soil water horizon at .7 centimeters giving a constant moisture slope of 84.5%/cm. for the capillary border, while the other curve has a suspended moisture layer of .45 centimeters and a soil water horizon depth at .75 centimeters resulting in a capillary border moisture slope of 56.3 %/cm. These fractional changes in the depth of the various components of the model soil moisture profile produce significant differences in the magnitude of the minima yet produce minima near the same frequency as shown in Figure 4.36. The measured reflectivity and the modeled reflectivity of moisture slope 84.5%/cm. agree in magnitude for those frequencies about their minima, but the difference in magnitude increases at frequencies away from the minima. The modeled reflectivity of moisture slope 56.3%/cm. gives the best comparison with regard to the shape of the measured re-flectivity, but a comparison in magnitude over the frequency interval of 4.5 to 8.0 Ghz shows an offset of approximately 5dB.

The magnitude of the model reflectivities for both assumed moisture profiles is essentially the same in the 1.0 to 2.0 GHz frequency interval. A comparison of the modeled and measured reflectivities over the frequency range of 1.0 to 2.0 GHz shows reasonable agreement with the differences being a slight offset and a greater sensitivity to frequency for the measured curve. The frequency sensistivity over this interval is found to some degree in all of the measured reflectivities. There are two possibilities for this trait: one, a characteristic resonance of the reflectometer measurement system, or two, a deep layer produced by the

tilling of the upper 15 centimeters of the plot soil volume. The possibility of a deep layer due to a loose, uncompacted surface layer over a compacted soil volume remains to be shown.

The model soil moisture profile of Figure 4.35 is for a suspended moisture layer of .45 centimeters and a capillary border moisture slope of 56.3%/cm. which places the depth of the soil water horizon at .75 centimeters. This moisture profile yields the modeled reflectivity curve with the same overall shape as the measured reflectivity curve in Figure 4.36. The comparison between the modeled and measured moisture profile is good with the major discrepancy a difference in the measured moisture content of the 0.-.5 centimeter interval and the assumed moisture content of the suspended moisture layer. It should also be noted in the comparison of the modeled and measured moisture profiles that the depth of the suspended moisture layer is .45 centimeters which is slightly less than the initial soil sampling interval of .5 centimeters. This points to the possiblity that a sampling interval of .5 centimeters may not be small enough to determine the moisture content of the soil crust since the soil sample may include a portion of the moisture from the capillary border leading to an erroneously higher moisture content. This possibility is more distinctly indicated in the next data set.

The next experimental measurement was made the following morning, August 22, 1979 at 0915 hours. The reflectivity curve for this measurement is shown in Figure 4.37. Although the measured reflectivity has a minimum, it should be noted that the minimum is not nearly as distinct as the minimum in the curve of the previous afternoon. The two modeled reflectivity curves were generated from the same moisture content set (2.2%, 19.1%) for the surface and deep subsurface with the differences being in the depth of the suspended moisture layer and soil water horizon of the

Figure 4.37 Measured and model reflectivity for August 22, 1979 at 0915 hours.
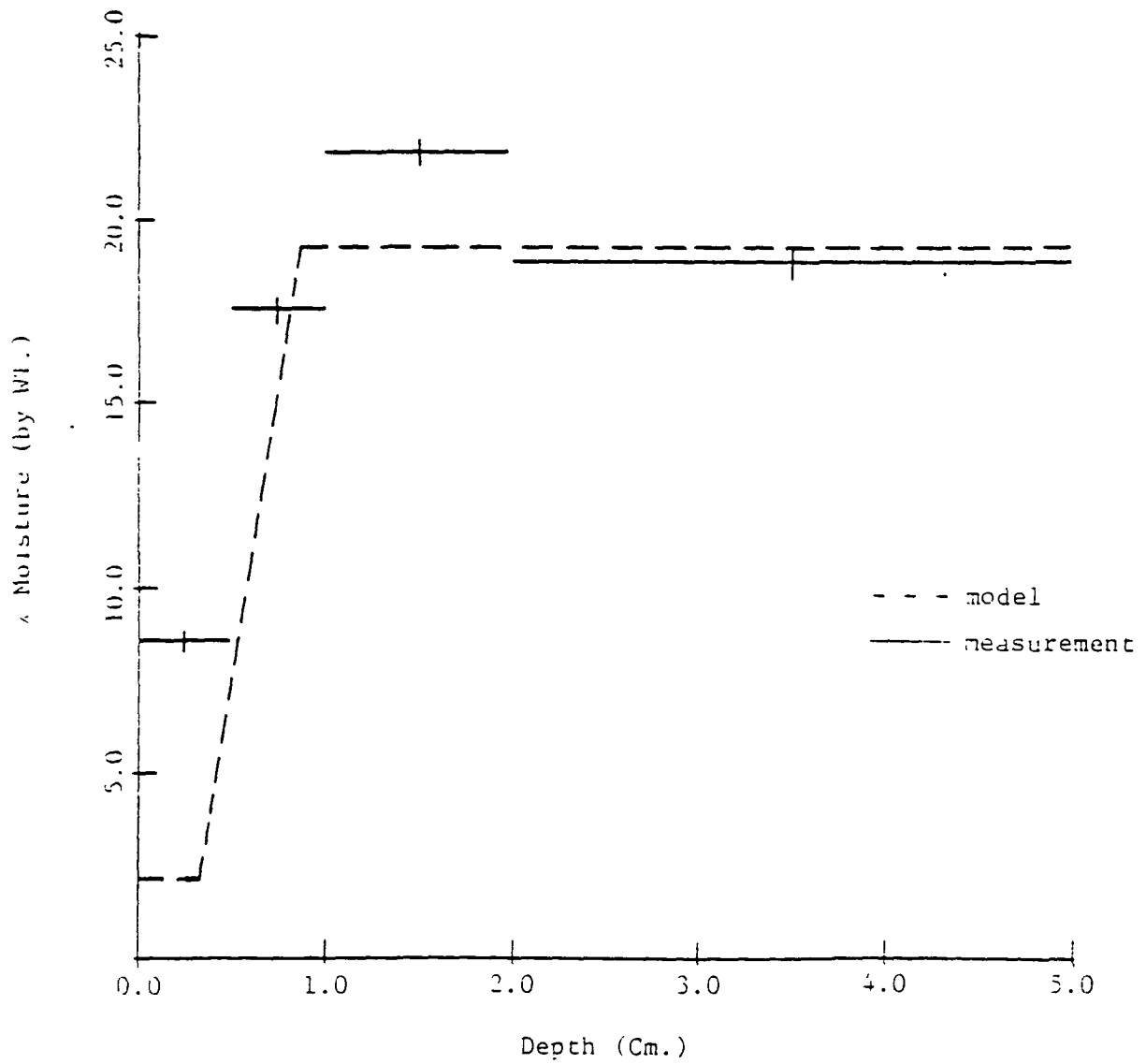
Figure 4.38 Measured and approximate soil moisture profiles
for August 22, 1979 at 0915 hours.

assumed soil moisture profile. One modeled moisture profile has a suspended moisture layer depth of .35 centimeters and a soil water horizon depth of .85 centimeters giving a capillary border moisture slope of 33.8%/cm. The other moisture profile has a suspended moisture layer extending to .4 centimeters, a soil water horizon beginning at .8 centimeters, and a capillary border moisture slope of 42.3%/cm. These small changes in the surface layer and the soil moisture slope give modeled reflectivity curves of different characteristics as seen in Figure 4.37.

A comparison of the model and measured reflectivity over the frequency span of 1.0 to 2.0 GHz shows relatively good agreement except the measured reflectivity again displays the frequency sensitivity noted in Figure 4.36. From 4.5 to 5.35 GHz the best agreement is with the modeled reflectivity of the soil moisture profile with a capillary border slope of 33.8%/cm. Over the frequency span 5.35 to 6.25 GHz both modeled reflectivities achieve clearly definable minima while the measured reflectivity has a broad, relatively flat minimum. In the interval 6.25 to 8.0 GHz the modeled reflectivity increases at a faster rate than that of the measurement.

The most probable cause for the measured reflectivity having no distinct minimum in the frequency range of 5.35 to 6.25 GHz is spatial variability in the soil crusting depth. In other words, the suspended moisture layer is not a smooth horizontal layer within the soil volume, but is tilted due to the soil plot not being level. Also there may be local variability as a consequence of the heterogenous nature of the soil. Any spatial variability of the suspended moisture layer need only be a few fractions of a millimeter to give an effect similar to the superpositioning of several reflections with relative minima near the same frequency. This would result in a total reflectivity having

91

a relative minima with a magnitude less than that from a surface layer of uniform depth and similiar in appearance to the measured reflectivity of Figure 4.37.

The corresponding soil moisture profiles for the reflectivities of Figure 4.37 are shown in Figure 4.38. The modeled soil moisture profile is for a suspended moisture layer depth of .35 centimeters and a capillary border moisture slope of 33.8%/cm. which places the soil water horizon at a depth of .85 centimeters. A comparison of the modeled and measured soil moisture profiles discloses two major differences: a high value in the 0.-.5 cm. sampling interval and another high value in the 1. to 2. cm. sampling interval. Comparison of the measured soil moistures for the sampling interval of 1. to 2. cm. for all measurements conducted during the diurnal cycle indicates that the high moisture content is most probably an anomaly caused by the handling and weighing of the soil material. The high moisture content of the 0. to .5 cm. sampling interval could also be an anomaly, however, it should be noted that the modeled suspended moisture layer only extends to a .35 centimeters depth. Since the predicted dry depth is less than the sampling interval, the cause of the high moisture content is probably due to sampling into the higher moisture of the capillary border.

The midday measurement of August 22, 1979 was made at 1315 hours, CDT. The reflectivity curve from this measurement is shown in Figure 4.39. The two model reflectivities shown for comparison were calculated using suspended moisture layer depths of .55 and .5 cm. with capillary border moisture slopes of 84.5 and 56.3%/cm., respectively.

Over the 1.0 to 2.0 GHz frequency range the modeled and measured reflectivity curves indicate the same trends as in Figure 4.36 and 4.37.
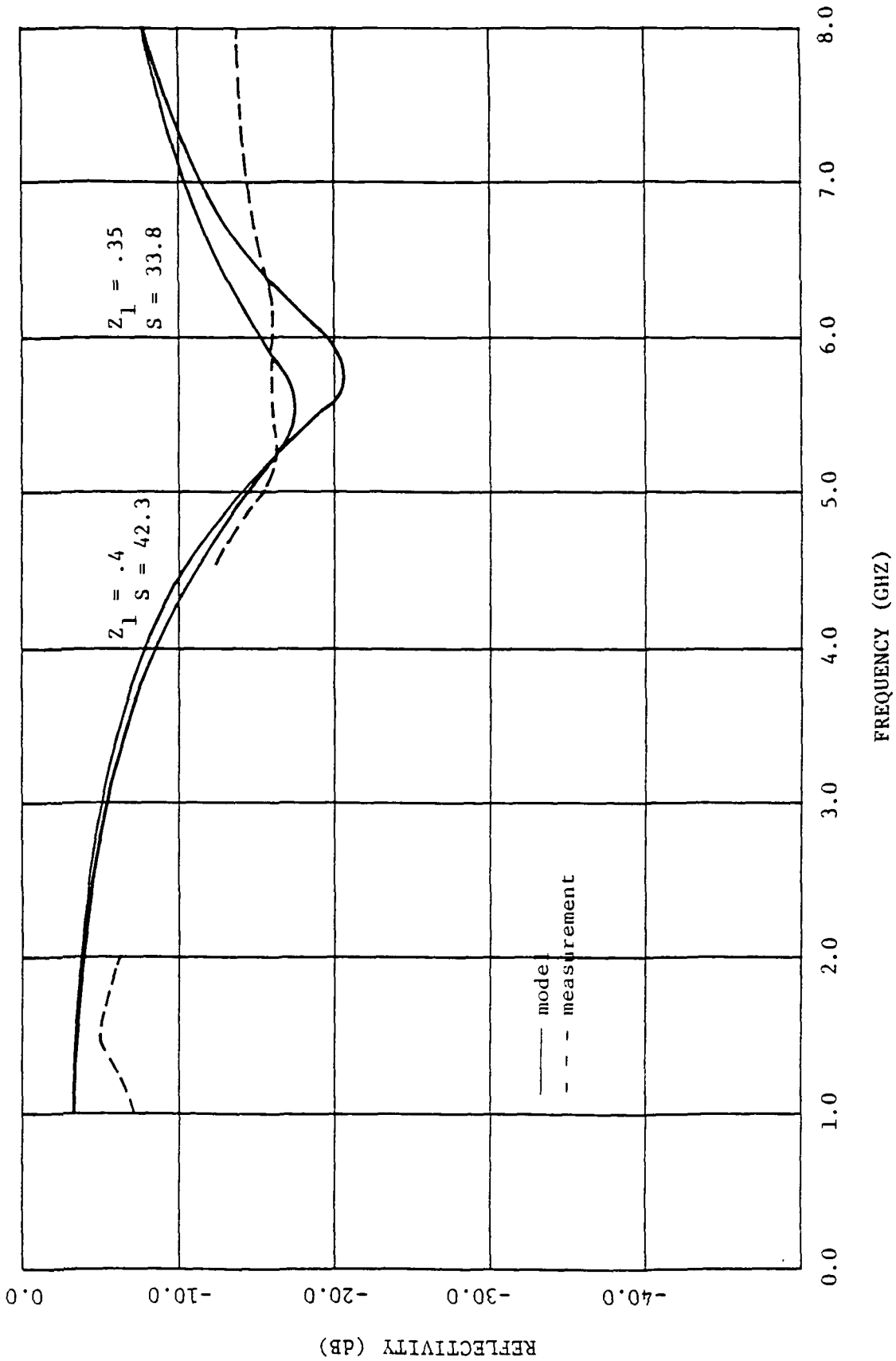
92

Figure 4.39 Measured and model reflectivity for August 22, 1979 at 1315 hours.
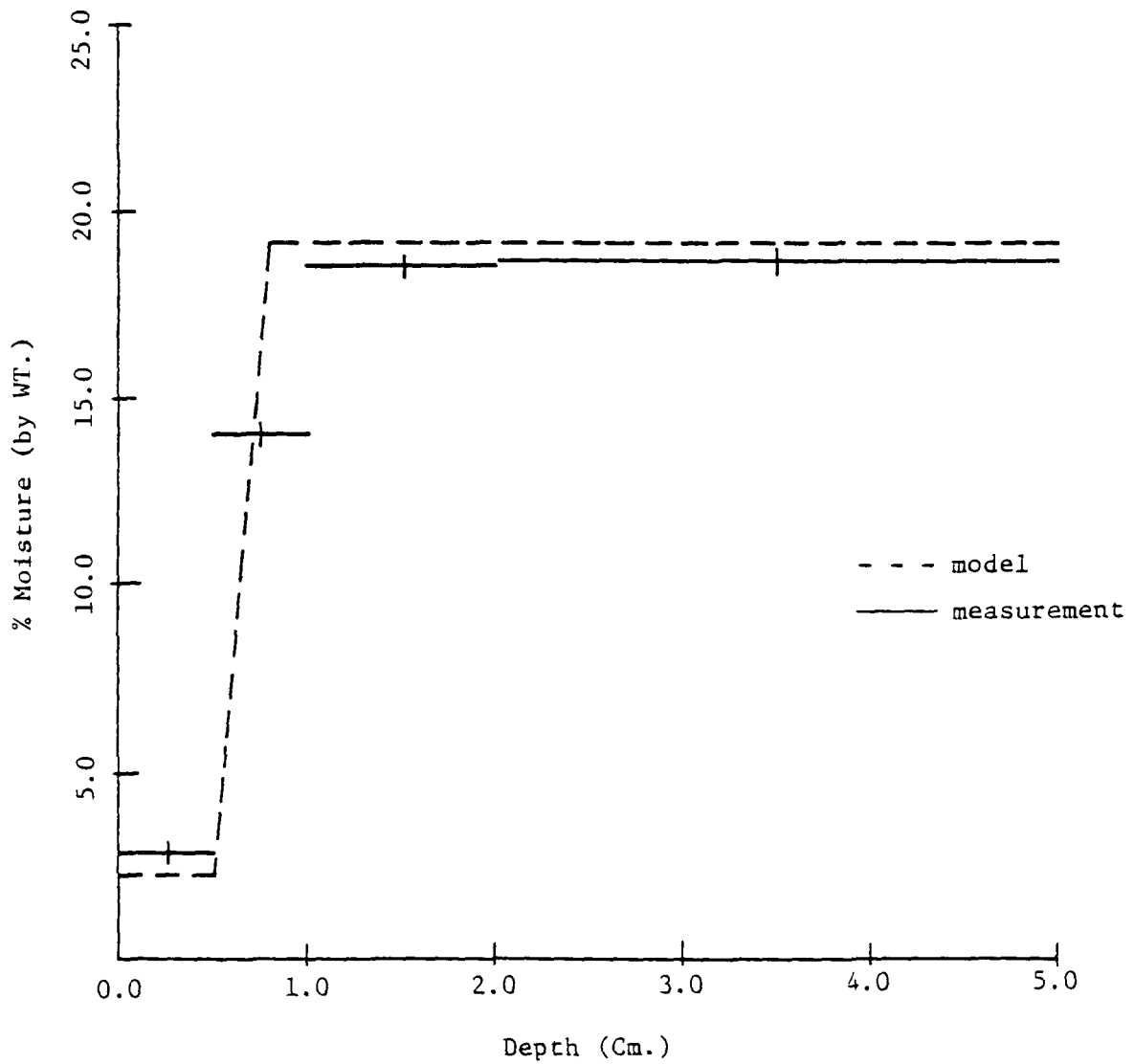
Figure 4.40   Measured and approximate soil moisture profiles
for August 22, 1979 at 1315 hours.

In the 4.5 to 8.0 GHz frequency range the measured reflectivity has a relatively broad minimum similar to that of the measured curve of Figure 4.37. Both the modeled reflectivities agree favorably in shape with the measured curve at frequencies away from the minimum with the model of capillary border moisture slope 84.5 %/cm. giving the best agreement. However, as in the reflectivity comparison of Figure 4.36, there is an offset in magnitude of approximately 5 dB.

The soil moisture profiles of the above measured and modeled reflectivities are shown in Figure 4.40. The model profile shown corresponds to a suspended moisture layer of .55 cm. with a capillary border moisture slope of 84.5%/cm. Comparison of the profiles shows good agreement, indicating that since the morning measurement the suspended moisture layer has extended into the soil volume with an increase in the capillary border moisture slope.

Figure 4.41 shows the modeled and measured reflectivites for the afternoon of August 22, 1979 taken at 1610 hours, CDT. The measured reflectivity in the 1.0 to 2.0 GHz frequency range shows the same characteristic as the previous measurements, but comparison with the model reflectivity shows a greater offset in magnitude. All reflectivities show clear minima in the 4.5 to 8.0 GHz frequency range. Comparison of the modeled and measured reflectivities in this frequency range shows the model reflectivity with a capillary border moisture slope 42.3%/cm. to have the best agreement at the frequency of the minimum. The model reflectivity with capillary border moisture slope 33.8%/cm. gives the best overall comparison in shape, but has an offset in magnitude of approximately 5 dB.
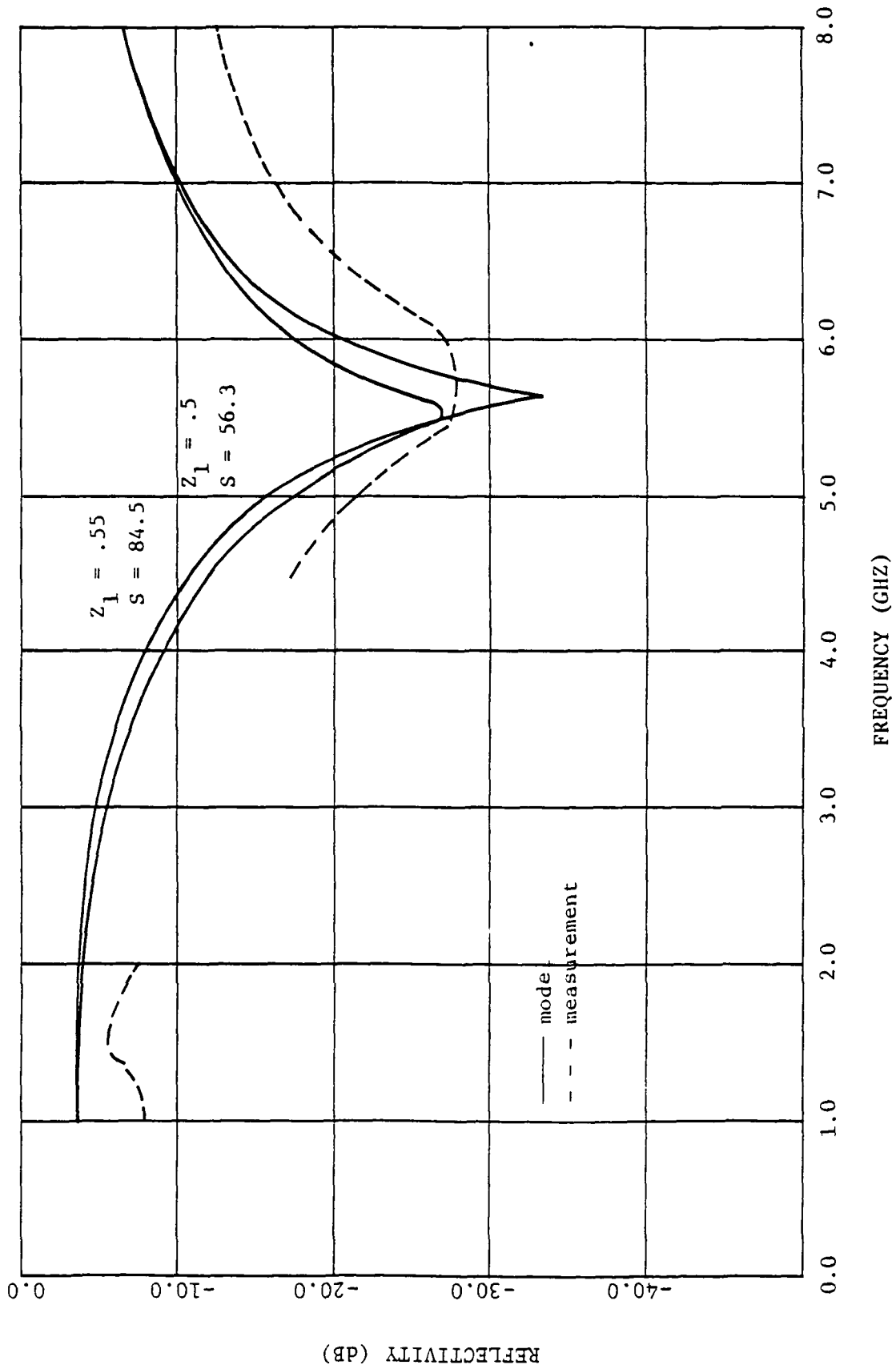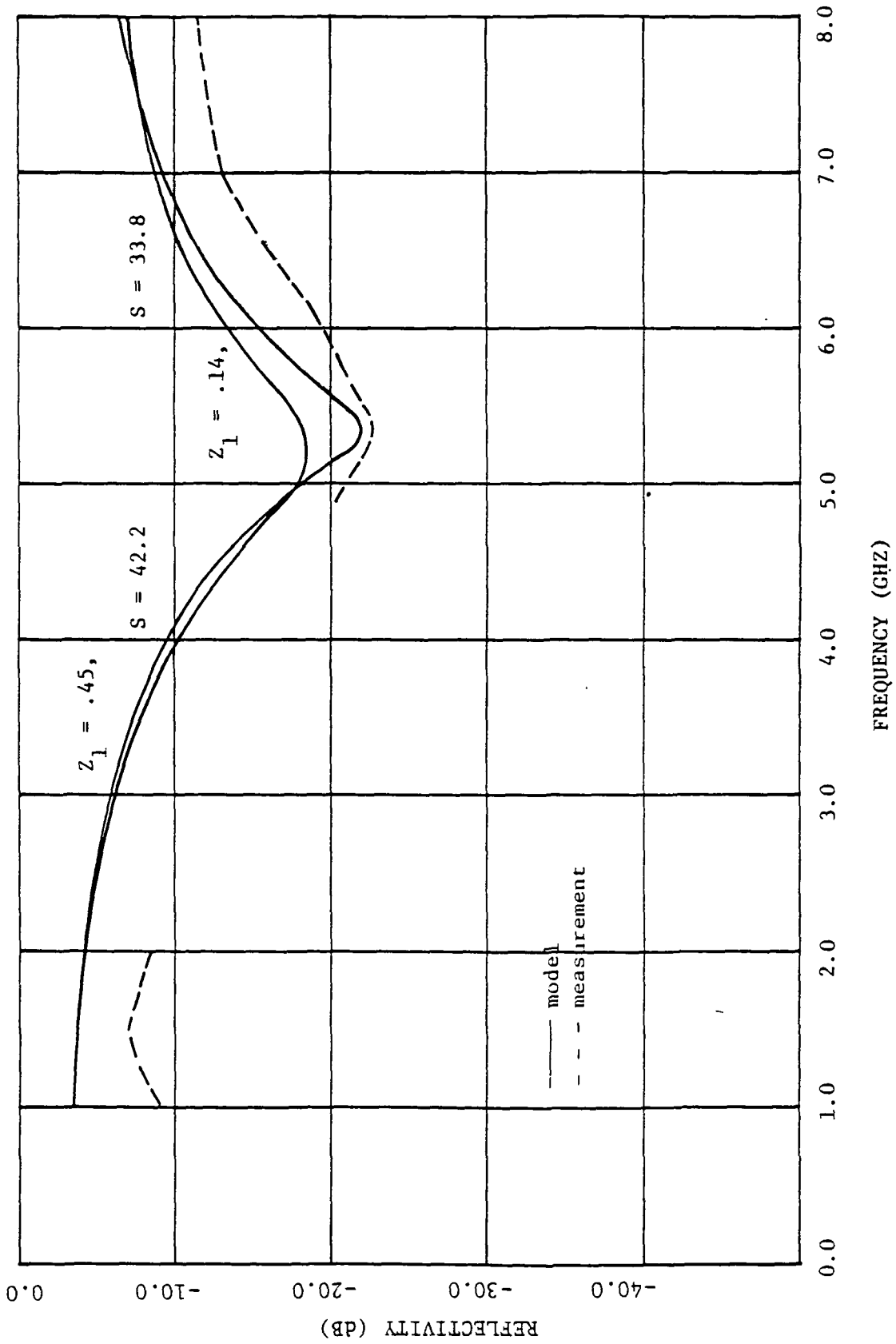
Figure 4.41 Measured and model reflectivity for August 22, 1979 at 1610 hours.

96
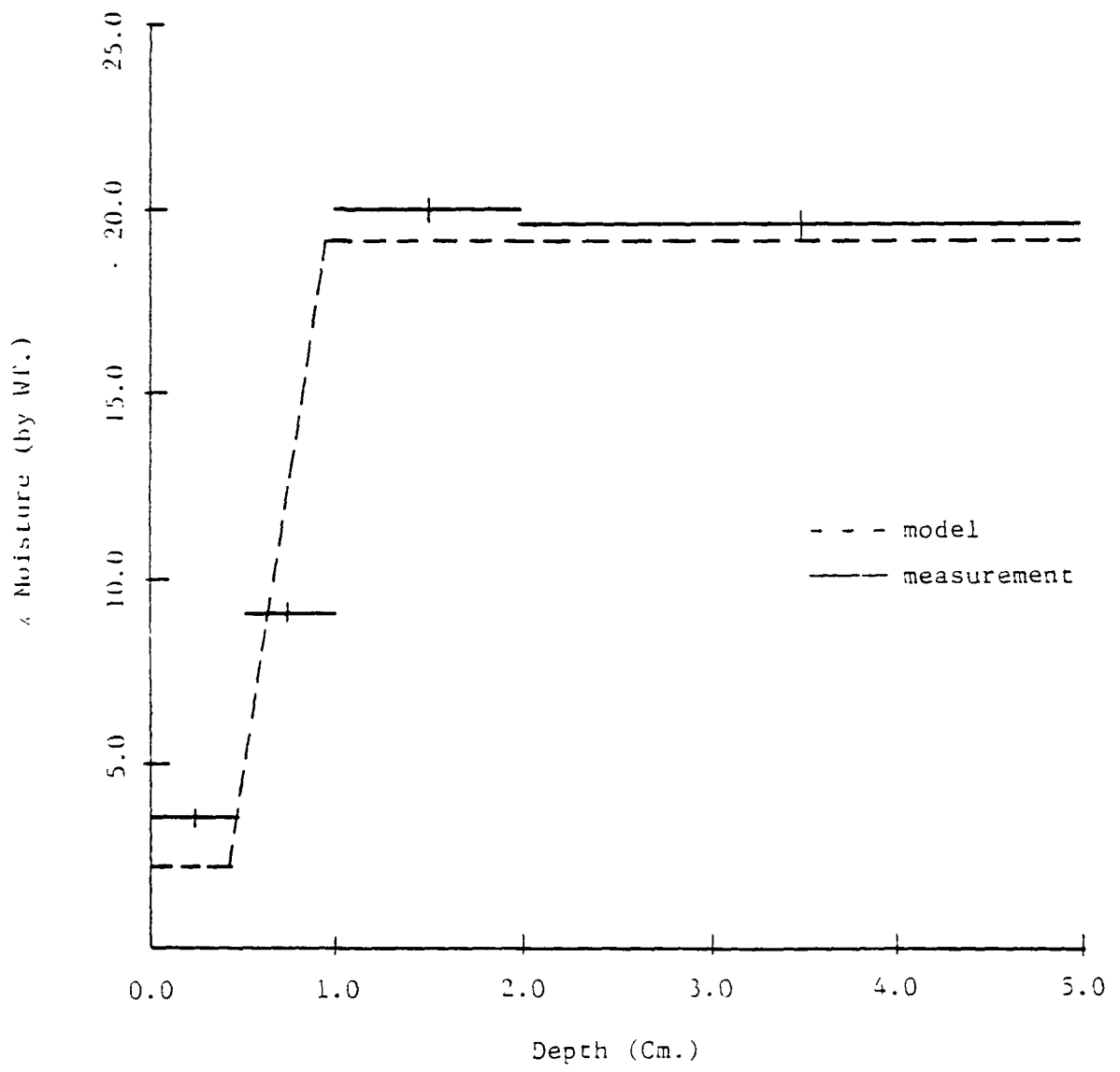
Figure 4.42 Measured and approximate soil moisture profiles for
August 22, 1979 at 1645 hours.

The modeled and measured soil moisture profiles for the afternoon

of August 22 are shown in Figure 4.42. The modeled soil moisture profile

is for a suspended moisture layer depth of .4 cm. and a capillary border

moisture slope of 33.8%/cm. This corresponds to the reflectivity curve

nearest in shape to the measured curve and comparison of the two soil

moisture profiles shows good agreement. The decrease in both the suspended

moisture layer depth and the capillary border moisture from the midday

measurement indicates that the upper surface layer has undergone some

rewetting at the expense of increasing the capillary border width.

Comparison of the measured and modeled reflectivities shown in

Figures 4.36, 4.37, 4.39, and 4.41 gives insight into the diurnal changes

of the soil moisture. The soil moisture profile of the afternoon of

August 22, 1979, shown in Figure 4.35, indicates a relatively deep suspended

moisture layer with a sharp transition from absorbed to free moisture

demonstrated by the steep slope of the capillary border moisture. The

soil moisture profile of the following morning, shown in Figure 4.38

indicates rewetting of the upper surface by the decrease in both the

depth of the suspended moisture layer and the slope of the capillary

border moisture. The midday soil moisture profile of Figure 4.40 points

to drying of the soil surface due to atmospheric demand. This is indicated

by an increase in both the depth of the suspended moisture layer and

slope of the capillary border moisture. The soil moisture profile for

the afternoon of the same day, shown in Figure 4.42 indicates a slight

rewetting of the suspended moisture layer with a depletion of the moisture

in the capillary border. In conclusion these changes in soil moisture

profile are what would be during a diurnal cycle (Jackson, 1973).

The following set of figures are taken from measurements of cycle 4 of the 1979 soil experiment (Hancock, 1980) which began September 7, 1979. Figures 4.43, 4.44, and 4.45 contain the early afternoon measurements of September 7, 8, and 9, respectively. The measurements were taken between approximately 1415 and 1430 hours, CDT. Each curve shows a distinct minimum with the minimum occurring at a lower frequency each succeeding day. The measured reflectivity of Figure 4.43 has a minimum at 7.85 GHz; the reflectivity of Figure 4.44 has a minimum at 7.5 GHz; and the reflectivity minimum of Figure 4.45 occurs at 6.65 GHz. This daily decrease in the frequency of the minimum is due to the drying of the upper soil boundary. This can be more easily seen by comparing the measured reflectivities with those generated from the model (solid curves) using the soil moisture set (2.2%, 19.1%).

The two modeled reflectivities shown for comparison in Figure 4.43 are for suspended moisture layers of .4 and .35 cm. and capillary border moisture slopes of 169.0 and 84.5%/cm., respectively. Both modeled moisture profiles have a soil water horizon beginning at a depth of .5 cm. This change of .05 cm. in the depth of the suspended moisture layer gives calculated reflectivities different in both the magnitude of the minima and the frequency at which the minima occur. The best comparison in overall shape and location of the minimum between modeled and measured reflectivity is the model with a suspended moisture layer of .35 cm. and capillary moisture slope of 84.5%/cm. However, a significant difference in magnitude remains.

The difference in magnitude over the 4.5 to 8.0 GHz frequency range between modeled and measured reflectivities can also be seen in Figures 4.44 and 4.45. In Figure 4.44, the 1430 hour measurement of September 8, 1979, the best model comparison at the minimum is with a .45 cm. suspended
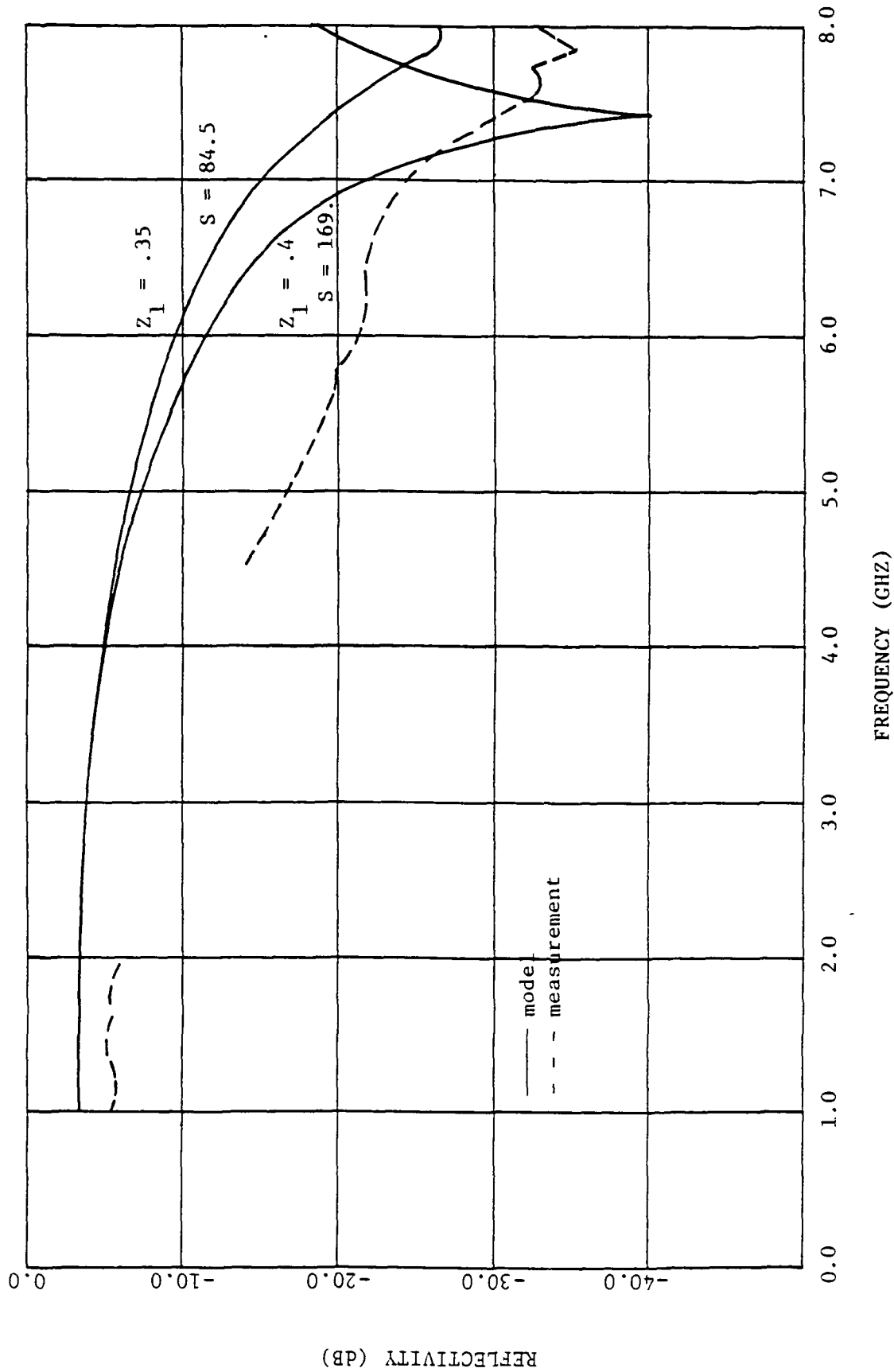
Figure 4.43   Measured and model reflectivity for September 7, 1979 at 1445 hours.
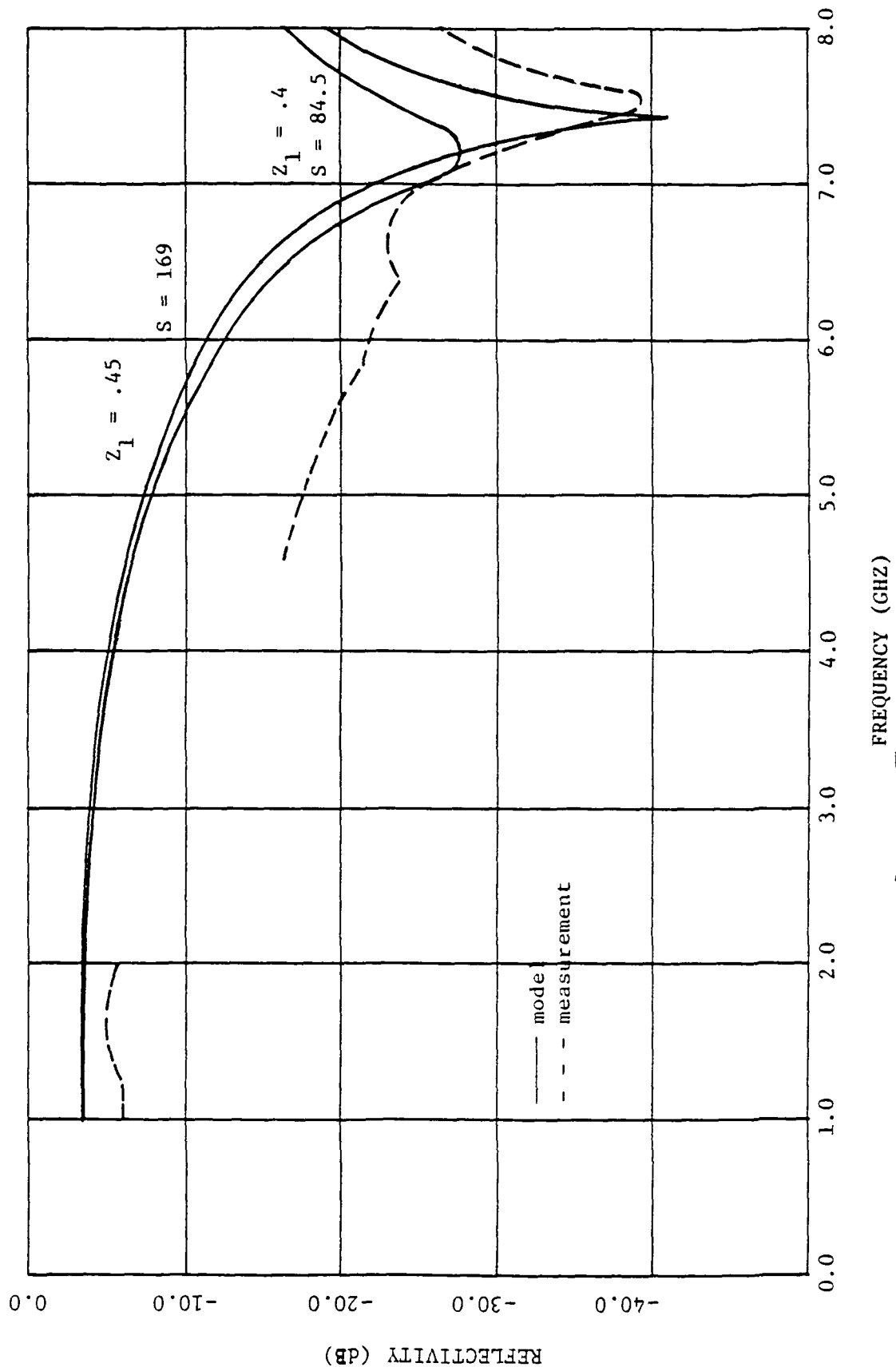
Figure 4.44 Measured and model reflectivity for September 8, 1979 at 1430 hours.

101
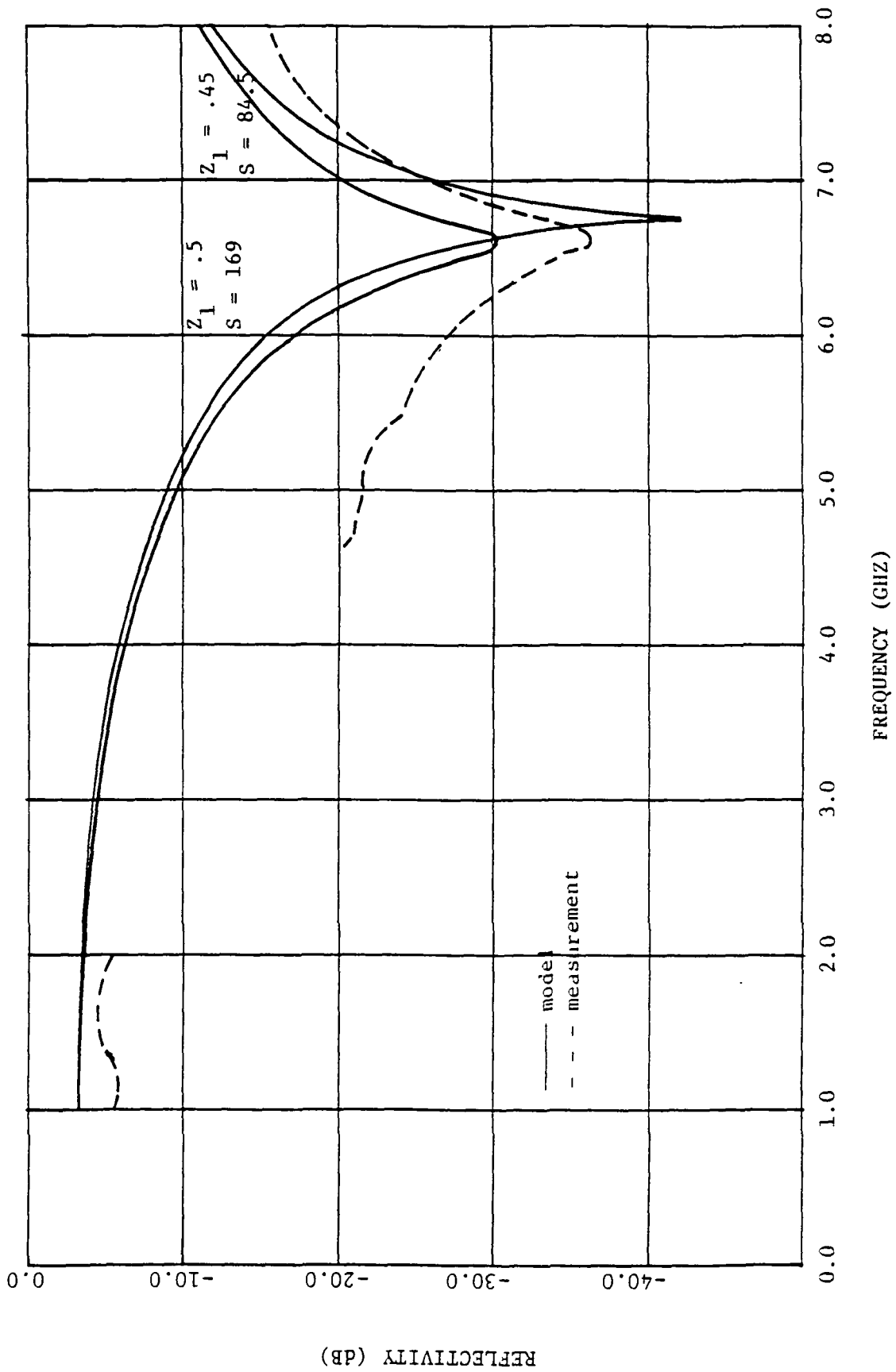
Figure 4.45 Measured and model reflectivity for September 9, 1979 at 1415 hours.

moisture layer and a capillary moisture slope of 169%/cm. Agreement

of this curve with the field reflectivity is good, [considering the slight

difference in frequency], but at frequencies away from the minimum, the

difference in magnitude as again significant. It should also be noted

that the measured reflectivity has a relative minimum at a frequency

of approximately 6.35 GHz. This relative minimum suggests the possibility

of spatial variability in the soil volume with another soil layer effecting

the reflectivity in the frequency interval about the relative minimum.

A comparison of two model reflectivities with that of the measurement

for 1415 hours, September 9, 1979 is shown in Figure 4.45. The model

reflectivity corresponding to a .45 cm. suspended moisture layer and

84.5%/cm. capillary border moisture slope has the best agreement at the

frequency of the minimum. Again, as in the previous two figures, there

are significant differences in the magnitude of the modeled and measured

reflectivities especially in the frequency interval from 4.5 GHz to the

frequency of the minima.

The differences in magnitude of the modeled and measured reflectivities

in the previous figures can be explained to a degree by examining the

corresponding soil moisture profiles. Figures 4.46, 4.47, and 4.48 are

the soil profiles for the early afternoon measurements of September 7,

8, and 9, respectively. With the measured profiles are shown the model

soil moisture profiles giving the best overall reflectivity comparison

with that of the measurement. The model soil moisture profiles for these

three days indicates an increase in the depth of the suspended soil moisture

layer for each succeeding day with a variation in the slope of the capillary

border moisture. The measured soil moistures in the 0. - .5 cm. and

.5 - 1.0 cm sampling interval show a decreasing trend for each succeeding
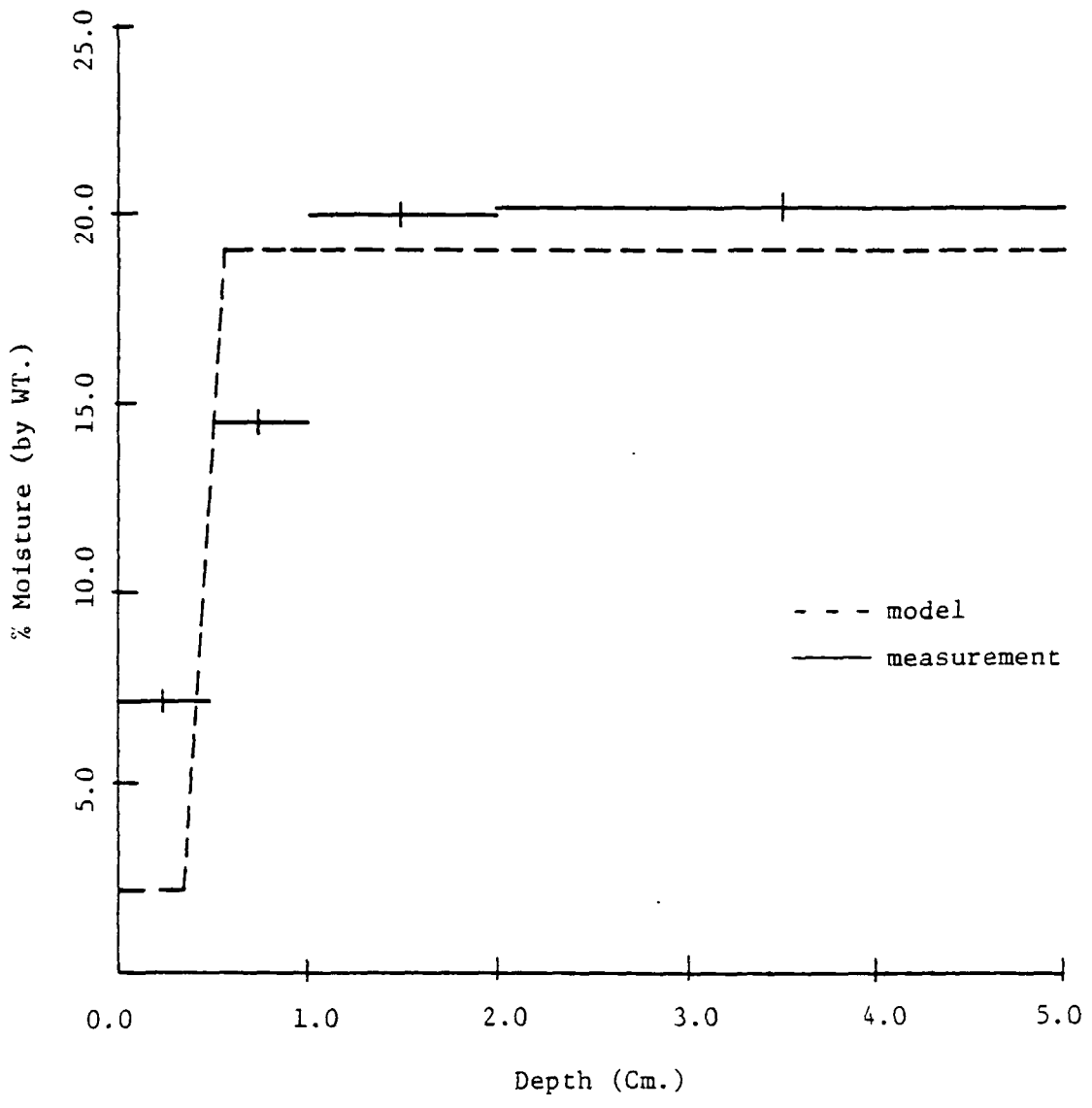
Figure 4.46   Measured and approximate soil moisture profiles for
September 7, 1979 at 1445 hours.
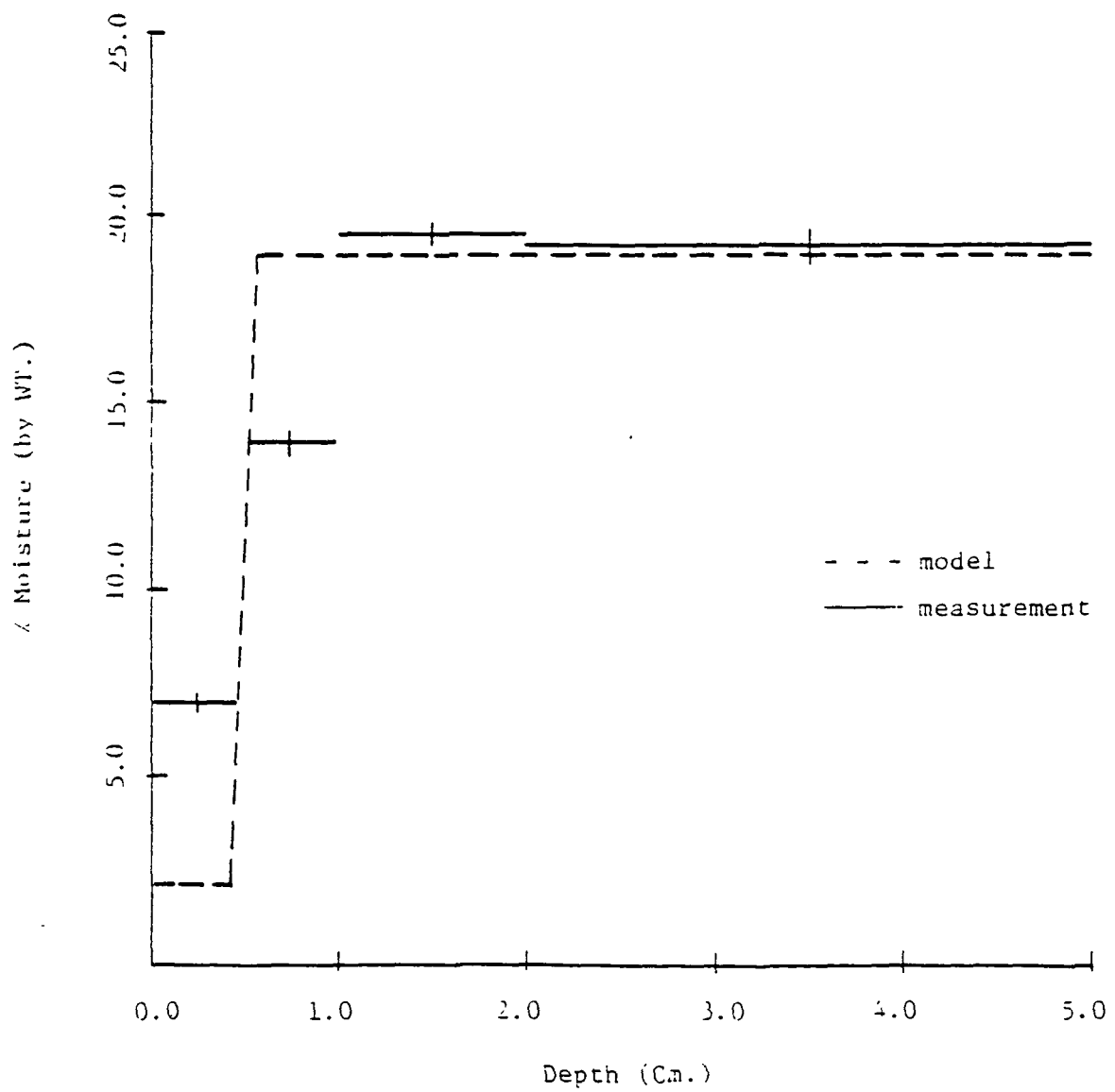
Figure 4.47 Measured and approximate soil moisture profiles for
September 8, 1979 at 1430 hours.
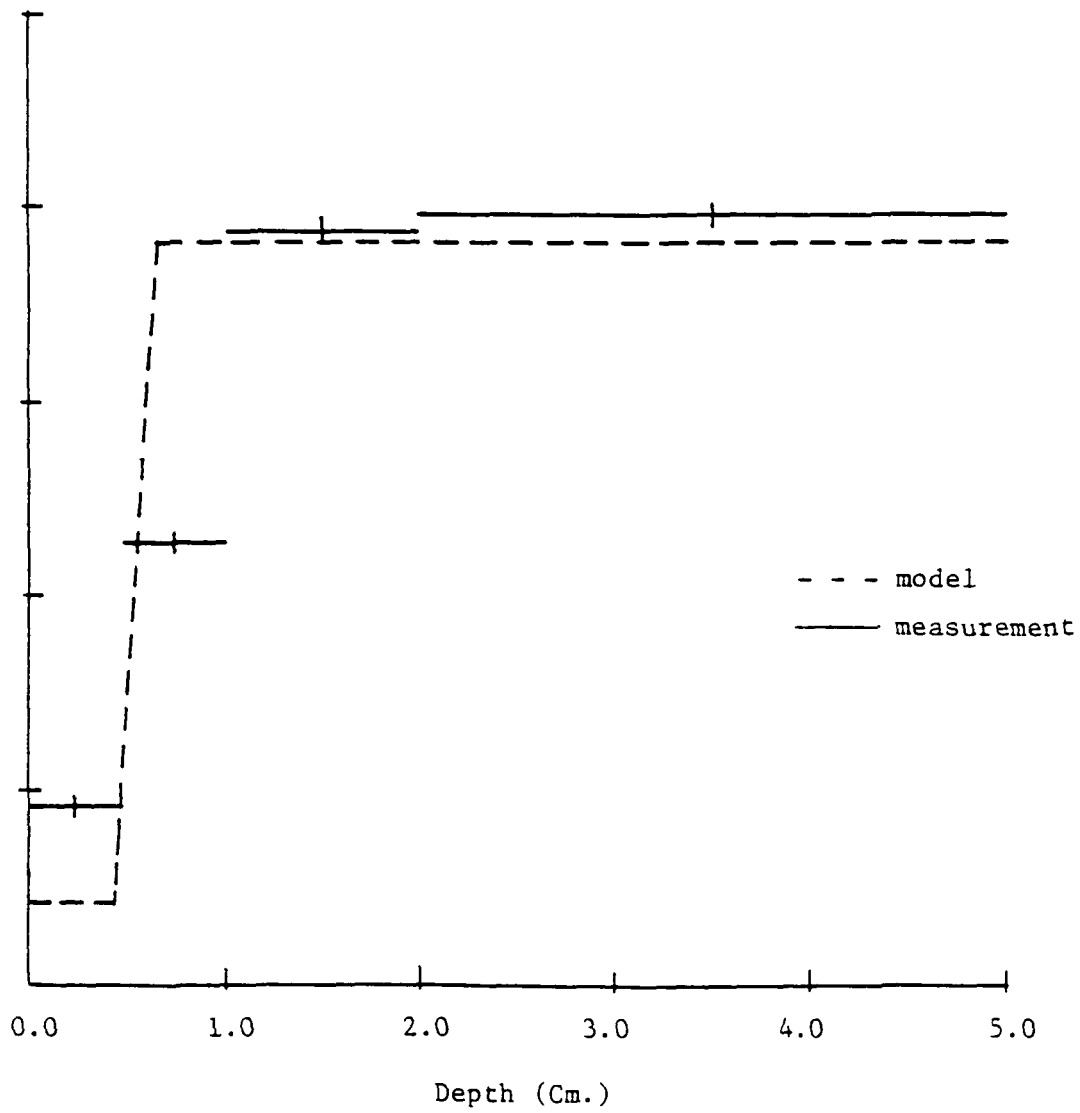
Figure 4.48   Measured and approximate soil moisture profile for
September 9, 1979 at 1415 hours.

day. However comparison of the modeled and measured soil moistures shows discrepancies between the two moisture profiles in the 0. - 1. cm. interval with close agreement in the deeper intervals. Since the predicted depth of the suspended moisture layer for the measurements is less than the 0. - .5 cm interval, it is possible that the soil samples contained a portion of the capillary border leading to the discrepancy between the profiles of the model and the measurement. This still does not account for the discrepancy between the model profile and the plot measurement in the .5 - 1.0 cm. sampling interval for these three days.

The measured soil moisture contents of the .5 - 1.0 cm. depth interval point to smaller capillary border moisture slopes than those predicted by the multi-layer reflectivity model. Modeled reflectivities from similar suspended moisture depths but with smaller capillary border moisture slopes, more comparable to the measured soil moisture profiles, would have minima of lesser magnitude occurring at lower frequencies. In order to obtain a possible reason for the differences in the capillary border moistures of the model and the measurement, it is necessary to investigate the individual soil samples in greater detail.

The soil moistures for each depth interval are the average of two soil samples. One sample from the west side of the soil test plot; the other sample from the east side of the test plot. The moisture contents of the .5 - 1.0 cm. sample interval for the east and west sides of the soil plot, respectively, are as follows: 8.4% and 20.6% for September 7 at 1430 hours, 11.6% and 16.4% for September 8 at 1430 hours; and 5.6% and 17.0% for September 9 at 1415 hours. Undoubtedly there are errors in the measurements due to the difficulty of sampling .5 cm. increments, however, these measurements indicate the west side of the soil plot

is decidedly wetter than the east side. This indicates a horizontal as well as vertical moisture gradient in the upper centimeter of the soil volume. This spatial variability could account for the discrepancies in magnitude of the modeled and measured reflectivities shown in Figures 4.43, 4.44 and 4.45. How the vertical moisture gradient varies across the soil plot is also brought into question because the model indicates soil moisture profiles more closely aligned with the higher moistures taken from the west side of the plot. To have substantiated the spatial variability would have required soil sampling of the area illuminated by the microwave antennas thereby destroying the area and interrupting the continuity of the experiment.

The multi-layer model is a function of the following parameters, ε_B, the permittivity of soil water; Z_1, the depth of the suspended moisture layer; Z_2, the depth at which the soil water horizon begins; and S, the slope of the capillary border moisture. Varying any of these five parameters can cause significant changes in the model reflectivity. Better agreement between the model and the measured reflectivities could possibly have been obtained by accounting for spatial variability in the suspended moisture layer and capillary border moisture. Better curve fits could also have possibly been obtained by including higher order terms in the expression for moisture in the capillary border. However, accounting for this further complicate an already complex model. Using only one soil moisture set (2.2%, 19.1%) and varying only the depth of the suspended moisture layer along with the slope of the capillary border moisture gives model results that generally agree with the measured soil moisture profile and movement of the soil moisture in the near soil surface.

Only one aspect of the soil volume remains to be investigated; surface structure. In the following chapter, the multi-layer model will be modified to include a parameter for roughness, and this rough surface multi-layer model will be compared with the measurement.

CHAPTER 5

THE EFFECT OF ROUGHNESS
ON THE SPECULARLY TRANSMITTED
ELECTRIC FIELD

5.1 Theory

The previous chapters have dealt with layered soil volumes with plane interfaces. The subject of this chapter will be the addition of small scale roughness at the air-soil interface. For the purposes of this chapter it is assumed that the only roughness occurs at the air-soil interface, that the roughness may be described by the small perturbations theory, and that there is no scattering within the volume.

Whether the boundary is smooth or rough the exact boundary condition for the electric field is that the tangential component of the field is continuous across the interface. For a smooth interface the solution for the total reflected field is straight-forward and given by the Fresnel reflection coefficient. However, for a rough surface the solution is complicated, with the total reflected field represented by a summation of scattered fields as given by the small perturbation theory. The total reflected field may also be viewed as the summation of a specularly reflected component and a diffuse component. The rough surface specular reflection coefficient is given by (Ruck et al, 1970)

$$\Gamma_{rough} = \rho \, \Gamma_{smooth} \tag{5.1}$$

where the roughness factor ρ is

$$\rho = e^{-2\left(\frac{2\pi h \cos\theta}{\lambda}\right)^2} \tag{5.2}$$

ϑ is the angle of incidence as measured from the normal of the plans of the rough surface, and h^2 is the mean-square roughness height.

The roughness factor ρ can be viewed as that fraction of the incident field contributing to the reflected field in the specular direction. Since only those field components at the specular angle of reflection are of interest, the boundary condition for a horizontally polarized electric field may be written as

Incident electric field contributing to the specular reflection	+	Reflected electric field at the specular angle	=	Transmitted electric field at the specular angle

This may be expressed for the rough surface by

$$\rho\, E_{incident} + \rho\, \Gamma_{smooth}\, E_{incident} = T_{rough}\, E_{incident}$$

or

$$\rho\,(1 + \Gamma_{smooth}) = T_{rough} \qquad (5.3)$$

where Γ_{smooth} is the smooth surface reflection coefficient and T_{rough} is the rough surface transmission coefficient at the specular angle of transmission. The smooth surface transmission coefficient, T_{smooth}, is given by the boundary condition

$$T_{smooth} = 1 + \Gamma_{smooth} \qquad (5.4)$$

Then from equation 5.3, the rough surface transmission coefficient will be related to the smooth surface transmission coefficient by

$$T_{rough} = \rho\, T_{smooth} \qquad (5.5)$$

111

Equations 5.1 and 5.5 simply state that at the specular angle both

the reflected and transmitted components of the field will be decreased

by the roughness factor ρ.

5.2 Correction to Models

The initial model correction for roughness will be for the two-

layer model of Chapter 3. Roughness correction of the multi-layer model

of Chapter 4 will follow directly since it is simply an extension of

the two-layer model.

5.2.1 Roughness Correction of the Two-layer Model.

Figure 5.1 shows the geometry of the two-layer model with roughness.

The assumptions for the two-layer model are the same as given in Chapter

3 with the addition that the rough surface height, $z = \zeta(x, y)$, is

random and varies only a small amount from $z = 0$ as required by the

small perturbation theory described in section 2.3. It is further assumed

that there is no scattering within the media and that the interface

betwen medium B and C is smooth. The roughness at the boundary between

media A and B gives rise to specular and diffuse components for both

the reflected and transmitted fields. The specular component of the

fields is dominant due to the assumption of a slightly rough surface

at the interface.

The derivation of the rough surface two-layer model is similar

to that of the smooth surface two-layer model development of Chapter

3. The only exceptions are that equations 5.1 and 5.5 are used to evaluate

the reflected and transmitted fields about the interface between media

A and B. The derivation of the rough surface two-layer model is
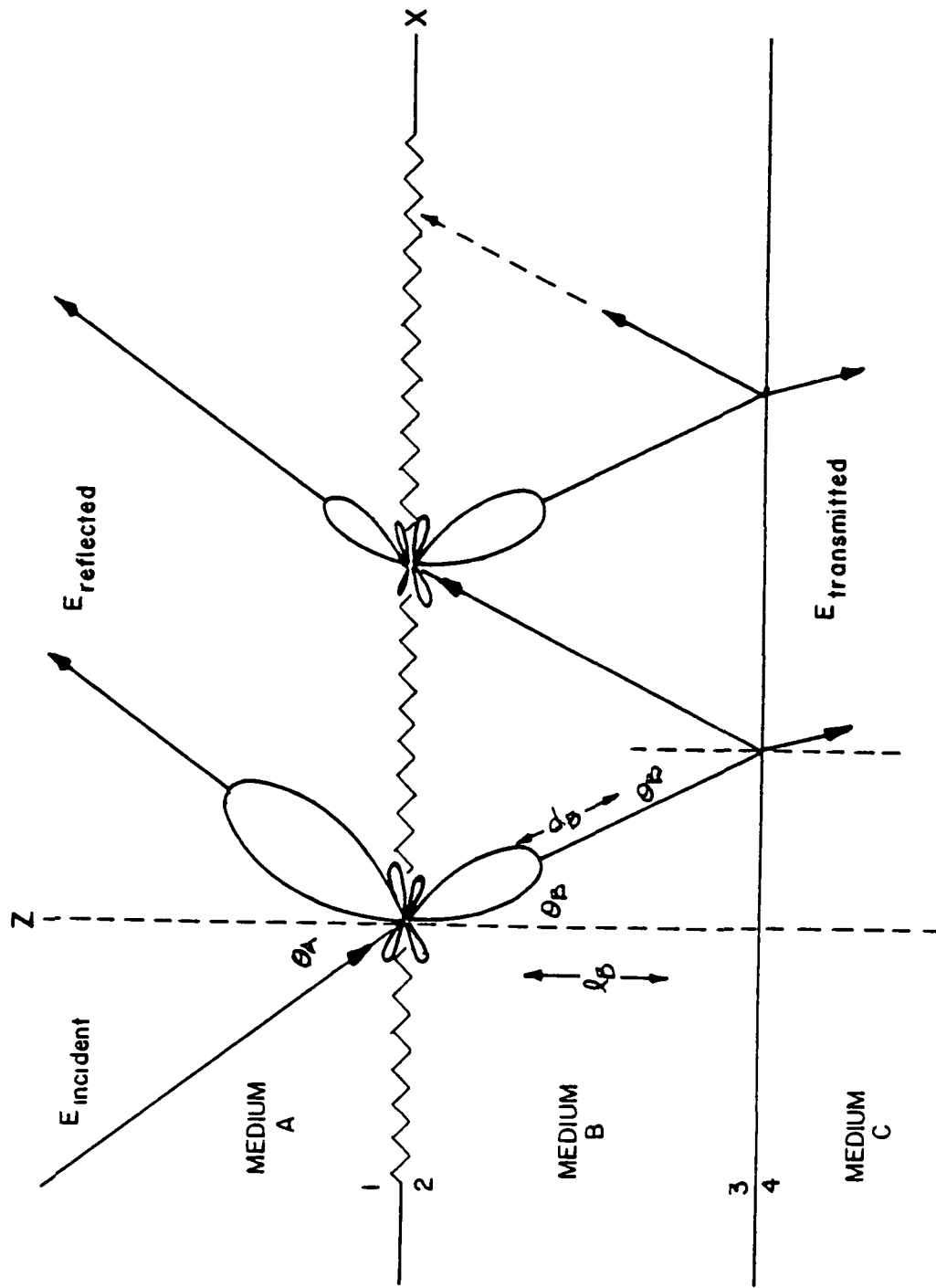
Figure 5.1 Geometry of the two-layer model with roughness.

given in Appendix B; and from Appendix B the total reflection is

$$\Gamma_{TOTAL} = \frac{\rho\,\Gamma_1 + \rho^2\,\Gamma_3\,e^{-2\gamma_B d_B}}{1.0 + \rho\,\Gamma_1\,\Gamma_3\,e^{-2\gamma_B d_B}} \tag{5.6}$$

where the roughness factor ρ is given by equation 5.2, the smooth surface
reflection coefficients Γ_1 and Γ_3 are given by equations 3.2 and 3.3,
respectively, γ_B is the propagation factor in medium B, and d_B is the
distance traversed by the fields in medium B.

As with the smooth surface two-layer model, the rough surface model
of equation 5.6 can be looked upon as the summation of a reflection
from the surface and a sub-surface reflection from the boundary formed
by media B and C, altered by the depth and permittivity of medium B.
The addition of roughness at the surface decreases the surface reflection
and also decreasing the subsurface contribution. The decrease of the
subsurface contribution is the square of the decrease in the surface
reflection, thus relatively large roughness will obscure the effects
of permittivity changes within the volume.

The reflectivity of the two-layer model with roughness can be expressed
as

$$\Gamma_{TOTAL}\,\Gamma_{TOTAL}^{*} = |\Gamma_{TOTAL}|^2$$

which is

$$|\Gamma_{TOTAL}|^2 = \frac{|\rho|^2|\Gamma_1|^2 + |\rho|^4|\Gamma_3|^2 e^{-4\alpha_B d_B} + 2|\rho|^3\Gamma_1||\Gamma_3|\,e^{-2\alpha_B d_B}\cos(2\beta_B d_B + \theta_1 - \theta_3 - \phi)}{1 + |\rho|^2|\Gamma_1|^2|\Gamma_3|^2 e^{-4\alpha_B d_B} + 2|\rho||\Gamma_1||\Gamma_3|\,e^{-2\alpha_B d_B}\cos(2\beta_B d_B - \theta_1 - \theta_3 - \phi)}$$

$$\tag{5.7}$$

114

where

$$\Theta_1 = Tan^{-1}\left(\frac{Im\,\Gamma_1}{Re\,\Gamma_1}\right)$$

$$\Theta_3 = Tan^{-1}\left(\frac{Im\,\Gamma_3}{Re\,\Gamma_3}\right)$$

$$\phi = Tan^{-1}\left(\frac{Im\,\rho}{Re\,\rho}\right)$$

α_B = attenuation factor of medium B

β_B = phase factor of medium B

d_B = depth traversed by the fields

Examination of equation 5.7 shows that roughness as well as lossy dielectrics can lead to shifts in the minima of the reflectivity if the roughness factor ω is complex. The roughness factor ω will be a complex function if the surface heights are not symmetrically distributed about a mean zero level (Beckmann and Spizzichino, 1963). Under the assumptions of the model used in the derivation of equation 5.7, the plane of the boundary between media A and B containing the surface roughness is placed such that the heights of the surface height distribution has zero mean. The effects of the lossy dielectric will be the same as discussed in Chapter 3.

5.2.2 Roughness Correction of the Multi-lyaer Model

The basic assumptions for the multi-layer model with roughness are similar to those of the two-layer model with roughness. The roughness occurs only at the air-soil interface, it can be described by the small pertubation theory of section 2.3, and there is no scattering within the soil volume. The development of the subsurface contribution due

to the varying permittivity of the capillary border moisture is the same as given in Chapter 4 which results in equation 4.7. The exact closed form of the reflection coefficient represented by equation 5.6 is used to translate the subsurface reflection through the suspended moisture layer. That is, the reflection coefficient Γ_3 due to the abrupt change in permittivity of equation 5.6 is replaced by the subsurface reflection, $\Gamma_{T,1}$, due to a varying permittivity as given by equation 4.7. Carrying out this operation and using notation consistant with the multi-layer model gives the total rough surface reflection as

$$\Gamma_{T,0} = \frac{\rho \, \Gamma_{1,0} + \rho^2 \sum_{i=0}^{N+1} \Gamma_{3,i} \, e^{-2 \sum_{m=0}^{i} \gamma_{B,m} d_{B,m}}}{1.0 + \rho \, \Gamma_{1,0} \sum_{i=0}^{N+1} \Gamma_{3,i} \, e^{-2 \sum_{m=0}^{i} \gamma_{B,m} d_{B,m}}}$$

(5.8)

where $\gamma_{B,m}$ denotes the propagation factor of a particular layer, $d_{B,m}$ the propagation distance within that layer, ρ the roughness factor of the surface, $\Gamma_{3,i}$ the smooth surface reflection coefficient at the interface of the layer given by equation 4.5, and $\Gamma_{1,0}$ the smooth surface reflection coefficient at the air-soil boundary given by equation 4.6.

5.3 Comparison of Rough Surface Model to Experimental Data

The following sections deal with roughness correction to both
the laboratory and field reflectivity measurements. The primary goal of
both experiments was to investigate using microwave swept frequency techniques
permittivity gradients within the soil volume. As such,
no direct estimate of the surface height variance was made for either
experiment since previous laboratory work (Hancock, 1976) involving roughness
at the surface of a homogeneous dielectric volume indicated that frequency
diversity could be used to correct for the effects of roughness. In both
of the following sections the estimate of the surface height deviation h
is made indirectly by parameterizing the models as a function of roughness and
obtaining the best agreement between the reflectivity of the roughness model
and measurement over the frequency ranges of 1.0 to 2.0 and 4.0 to
8.0 GHz.

5.3.1 Roughness Correction to Laboratory Measurements

Comparisons of the two-layer model with roughness as given by equation
5.6 and the laboratory measurements are presented in Figures 5.2, 5.3, and 5.4.
In each of these figures the modelled reflectivities are the solid curves
while the dashed curve is the measured reflectivity. The only difference
between these three figures and Figures 3.3, 3.4, and 3.5 is an additional
curve that is a function of the surface height deviation h. All other values
of the parameters for the model with roughness such as permittivity, depth of
the upper dry soil layer, and angle of incidence are the same as those of the
smooth surface two-layer model given in Chapter 3.

Figure 5.2 gives the reflectivities of the model and laboratory
measurement for the dry soil layer depth 1.9 cm. The two model curves

correspond to a smooth surface (h = 0.0) and to a slightly rough surface with a height deviation h of .3 cm. A comparison of the reflectivities shows that at low frequencies, in the span from 1.0 to 1.5 GHz, the two reflectivities coincide. This comparison also indicates that the model with roughness has frequency sensitivity in that the reflectivity shows a general decreasing trend as frequency increases. Also the magnitude of the reflectivity model with roughness is greater than that of the smooth surface indicating that the subsurface reflection is still dominant though lessened by the effect of the roughness. Comparing the model reflectivities and the reflectivity of the measurement shows the improvement given by the rough surface model. In the 1.0 to 2.0 GHz frequency range the agreement is good and becomes even better in the 4.0 to 8.0 GHz range with the roughness model showing a frequency sensitivity similar to that of the measurement. The magnitude of the minimum for the model reflectivity with h = .3 cm. is not as great as the measurement which is due to the subsurface permittivity of the model being slightly larger than the soil measurement.

Figure 5.3 is similar to Figure 3.4 with the exception that an additional model reflectivity curve with a surface height deviation of .3 cm. has been included. The depth of the upper soil layer for the reflectivities of Figure 5.3 is 3.0 cm. The model with roughness shows little improvement over the smooth surface model in the 1.0 to 2.0 GHz frequency range but in the 4.0 to 8.0 GHz range the reflectivities of the model with roughness h = .3 cm. and that of the measurement shows very good agreement.

The reflectivities of Figure 5.4 are for a soil volume with a dry upper depth of 3.6 cm. The two model reflectivity curves are for surfaces with height deviations, h, of 0.0 cm. (smooth surface) and 0.4 cm. As in

118

Figure 5.2 Laboratory measured and roughness corrected two-layer model reflectivity for a layer depth of 1.9 cm. (h = surface height deviation).
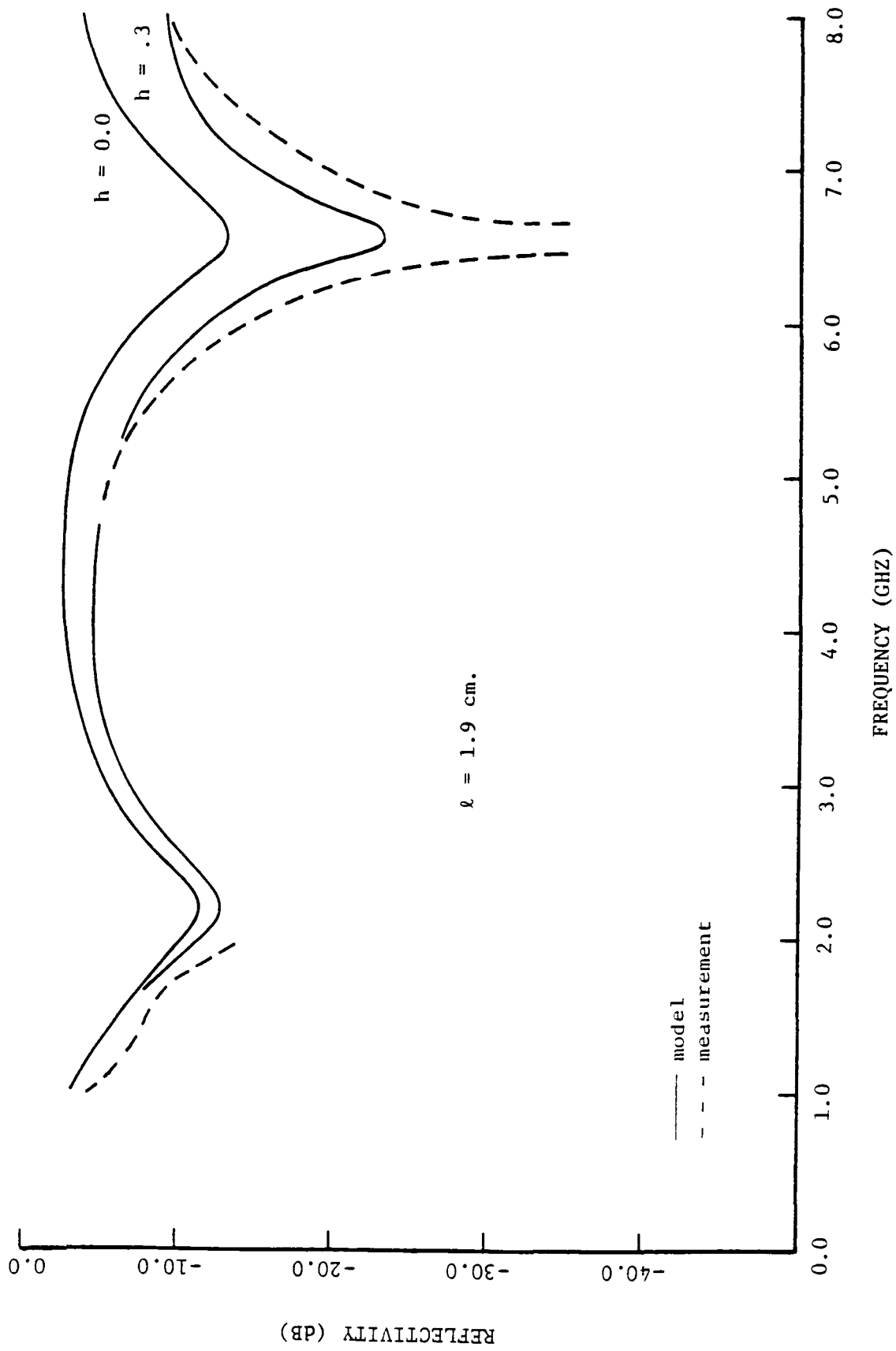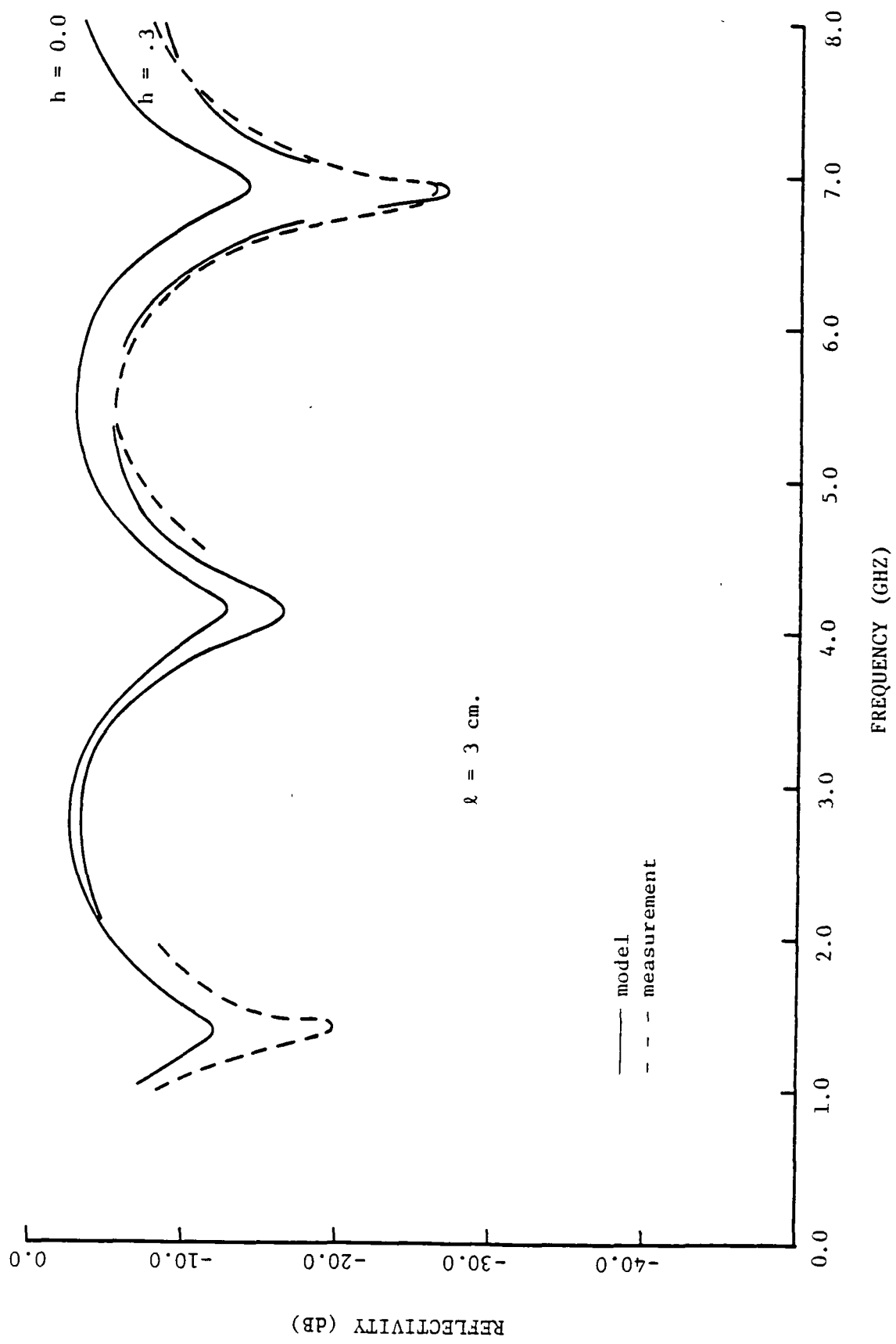
119

Figure 5.3 Laboratory measured and roughness corrected two-layer model reflectivity for a layer depth of 3.0 cm. (h = surface height deviation).
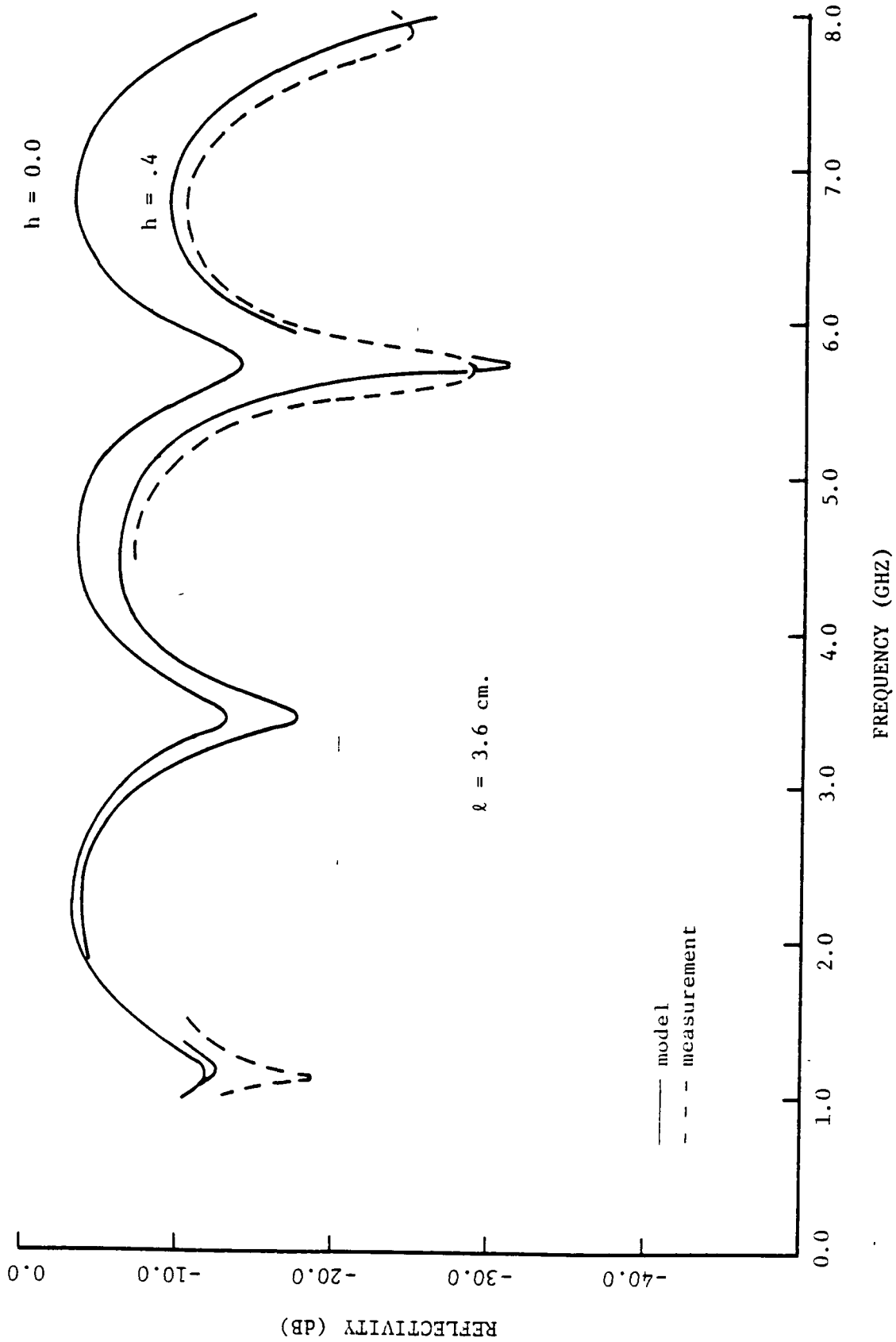
Figure 5.4 Laboratory measured and roughness corrected two-layer model reflectivity for a layer depth of 3.6 cm. (h = surface height deviation).

the two previous figures, roughness correction of the model gives considerable improvement over the smooth surface especially in the 4.0 to 8.0 GHz frequency range where the measured reflectivity shows the greater sensitivity with frequency. The offset in the frequency at which the minima of the two model reflectivity curves and the measurement reflectivity occur is due to the actual thickness of the soil volume being slightly deeper than the layer depth used in the model calculations.

A re-examination of Figures 5.2, 5.3, and 5.4 indicates that roughness correction to the two-layer model increases the sensitivity of the reflectivity to frequency yielding improved agreement with the measured reflectivity especially in the frequency range of 4.0 to 8.0 GHz. Some improvement is seen in the 1.0 to 2.0 GHz frequency range with roughness compared to the smooth surface model. This is to be expected since the roughness parameter (h/2) is small at these wavelengths for the surface height deviations used. The good agreement of the model with roughness and the measurement over the two frequency ranges of the experiment continues to affirm that swept frequency techniques can be used to correct for roughness as well as gain information about the electrical properties of soil volumes.

5.3.2 Roughness Correction to the Field Experiment

Comparisons of the multi-layer model with roughness as given by equation 5.8 are presented in Figures 5.5, 5.6, and 5.7. The model reflectivities are depicted by the solid curves while the reflectivity of the field measurement is given by the dashed curve. The field measurements of the figures were taken on September 22, 1979 at 0915, 1315 and 1610 hours, respectively. These figures correspond to Figures 4.37, 4.39, and 4.41 of

Figure 5.5 Measured and roughness corrected multi-layer model reflectivity for August 22, 1979 at 0915 hours (surface height deviation h = .3 cm.).
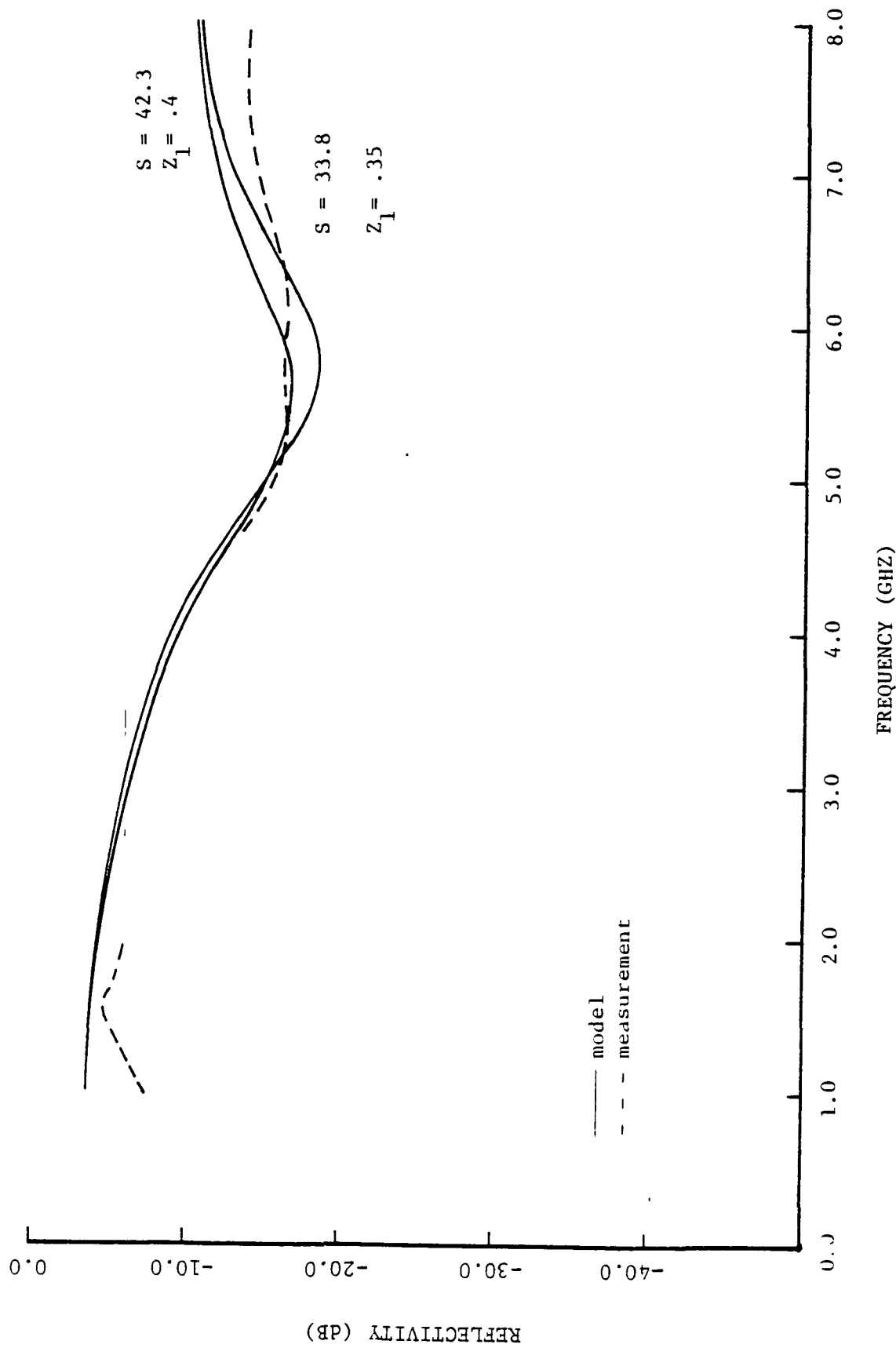
123

Figure 5.6 Measured and roughness corrected multi-layer model reflectivity for August 22, 1979 at 1315 hours (surface height deviation h = .3 cm.).
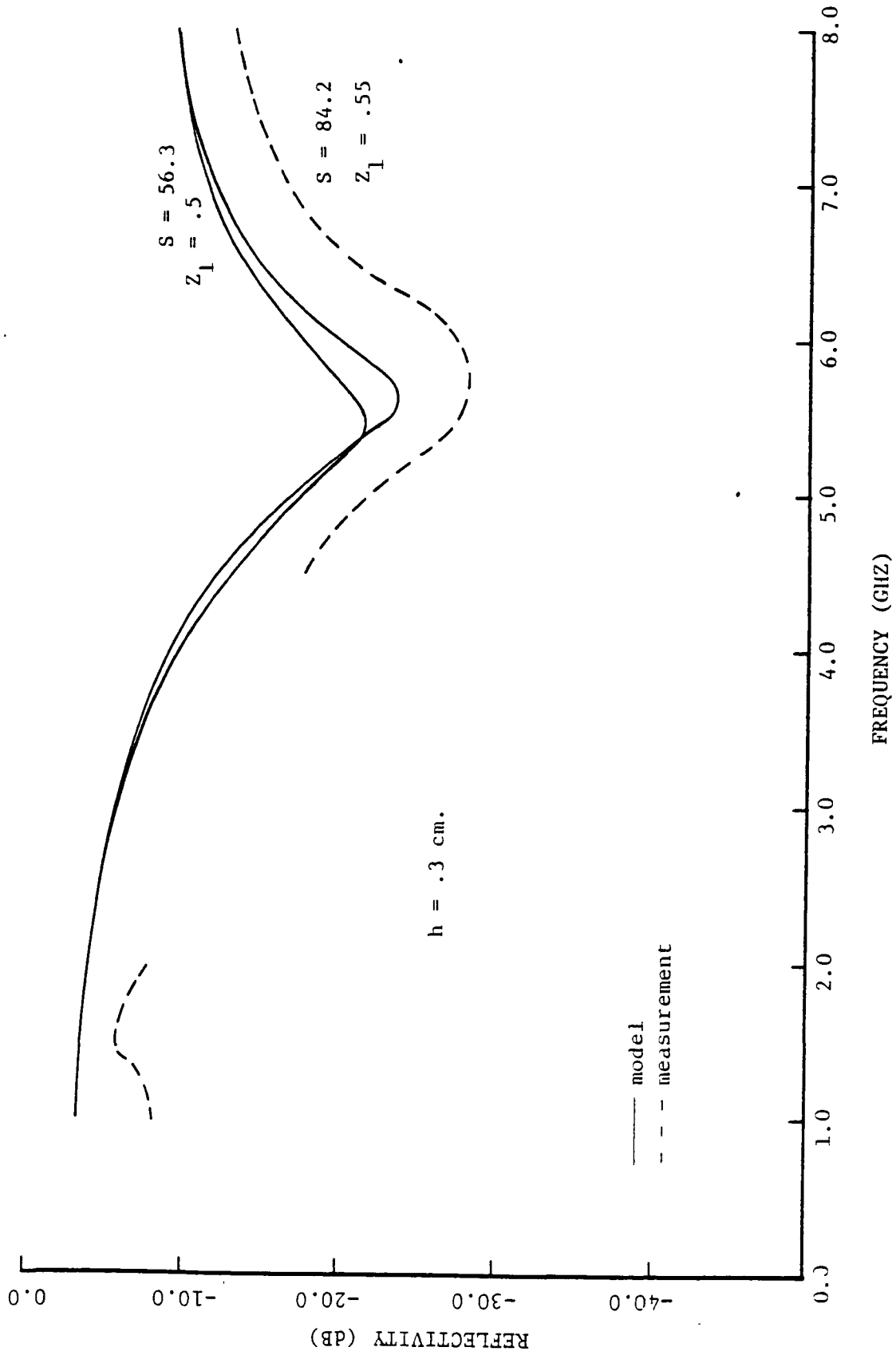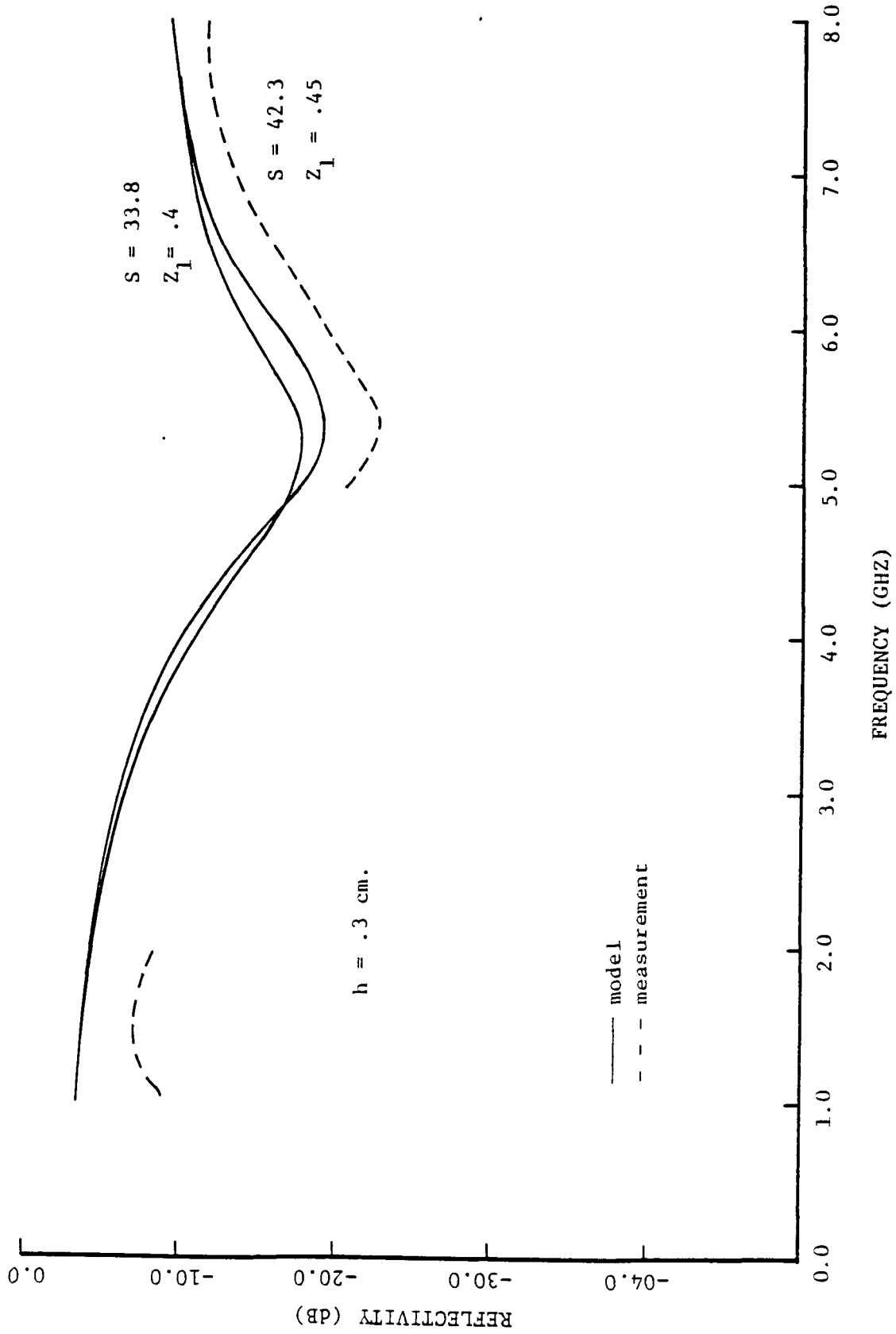
Figure 5.7 Measured and roughness corrected multi-layer model reflectivity for August 22, 1979 at 1610 hours (surface height deviation h = .3 cm.).

125

the smooth surface multi-layer model in depth of the suspended moisture layer, moisture slope of the capillary border, and soil moisture set (2.2%, 19.1%). The surface height deviation, h, used in determining all the reflectivities of the multi-layer model with roughness is 0.3 cm.

Figure 5.5 gives the reflectivity measurement of September 22, 1979 at 0915 hours. The effect of including roughness at the surface of the multi-layer model is to increase the sensitivity of the total reflectivity to frequency. The effect of roughness for the soil moisture set (2.2%, 19.1%) obscures the subsurface reflection leading to a decrease in the magnitude of the reflectivity at the minima indicating the dominance of the surface reflection for these figures. The additional sensitivity of the roughness model reflectivity to frequency is espeically noticeable in Figure 5.5 at frequencies greater than 6.0 GHz and gives improved agreement between the model reflectivity curves and the measurement. The best agreement is for the model reflectivity from a soil volume with a suspended moisture layer of .4 cm. and capillary moisture slope of 42.3%/cm.

The roughness model and field measurement reflectivities for September 22, 1979 at 1315 hours are given in Figure 5.6. A comparison of the roughness model curves of this figure and the smooth surface model reflectivities of Figure 4.39 shows that the roughness model has better overall agreement with the field measurement in shape and with less offset. The soil volume with a suspended moisture layer of .55 cm. and capillary moisture slope of 84.5%/cm. gives the best agreement between roughness model reflectivity and measurement.

Figure 5.7 gives the field reflectivity measurement for September 22, 1979 at 1610 hours. As in the previous two figures the magnitude of the reflectivity

at the minima of the model has been decreased by the effect of the surface roughness and the model reflectivity gives a frequency sensitivity similar to te measurement. The roughness model reflectivity curve showing the best agreement is from the soil volume with a capillary border mositure slope of 42.3 %/cm. and suspended moisture layer depth of .45 cm. The offset between this model reflectivity curve and the measurement is approximately 3 dB at the minima.

Figures 5.5, 5.6, and 5.7 indicate that the multi-layer model with roughness has good agreement with the reflectivity of the measurements. This agreement is better, with smaller overall differences, than the smooth surface model reflectivities of soil volumes with the same suspended moisture depth and capillary border moisture slopes.

CHAPTER 6

CONCLUSIONS

The frequency dependence of the reflectivity from soil volumes with both artificially created moisture discontinuities and with moisture gradients induced by the environment was measured and compared with models derived from transmission line theory. The comparison of the smooth surface models and the results of the experiments showed good agreement, however, the slight frequency dependence of the smooth surface models due to the imaginary part of the complex permittivity could not account for the much greater frequency dependence exhibited by the reflectivity measurements.

By using only one soil moisture set (2.2%, 19.1%) and varying only the depth of the suspended moisture layer and slope of the capillary border moisture good agreement with the measured soil moisture profile and movement of the soil moisture in the near surface was obtained. This substantiated the sensitivity of the reflectivity to moisture gradients within the soil. However, the sensitivity of the reflectivity to soil moisture was only discernible by using microwave swept frequency measurement techniques. These clearly showed minima in the reflectivity due to the subsurface reflection from the permittivity gradient in phase opposition to the surface reflection.

A rough surface transmission coefficient for the specular component of the electromagnetic field was obtained using concepts of the small perturbation theory. The basic premise of this model was that random surface roughness gives a diffuse and specular component to both the scattered and transmitted electromagnetic field. The rough surface transmission coefficient for the specular component was incorporated

128

into the derivation of the models, and the reflectivities of the roughness corrected models compared to the results of the experiments. This comparison showed further improvement in the agreement between the models and measurement especially in the 4.0 to 8.0 GHz frequency range. The excellent agreement between the models and measurements for both the laboratory and field experiment indicates that roughness is the dominant parameter contributing to the frequency dependence of the soil reflectivity and obscures the slight frequency dependence given by the complex permittivity. Most notable from the comparison of the roughness corrected models and the results of the experiments is that coherent phase effects due to the interference of the surface reflection and subsurface reflection can occur in the presence of roughness for the reflectivity from soil volumes even under the influence of natural environments.

In conclusion, microwave swept frequency measurement techniques can account for roughness effects of the surface and permittivity changes beneath the surface of soil volumes. Techniques measuring at only one frequency or even employing frequency diversity in which the operating frequencies are widely spaced may not be able to distinguish between coherent phase effect of moisture gradients and roughness.

6.1 Recommendations for Further Work

The recommendations for further work are:

1. The measurement of soil test plots should be continued using continuous swept frequencies from 1.0 to 10.0 GHz. The inclusion of the 2.0 to 4.0 Ghz and 8.0 to 10.0 GHz frequency ranges would allow for the characterization of a broader range of soil moisture profile while allowing for a more complete investigation of roughness effects.

2. The measurement of the soil test plots should be continued
   using angle diversity. The reflectivity models indicate that
   as the angle of incidence approaches normal to the surface for
   horizontal polarization the surface reflection will decrease.
   This would allow the subsurface reflection due to soil moisture
   gradients to make a greater contribution to the total soil reflec-
   tivity.

3. Increase the sensitivity of the measurement system to measure
   the diffuse component of the scattered energy. The capability
   to measure both the specular and diffuse components would permit
   the evaluation of the total transmittance of the soil volume
   as a function frequency. The transmittance of the soil could
   in turn be related to an emissivity that is solely dependent
   upon the permittivity of the soil volume.

4. Improve the mobility of the system in order to conduct measurement
   of the reflectivity from both bare and vegetated agricultural
   fields.

Appendix A

Derivation of the Total Reflection

Coefficient of the Two-layer Model

Consider a layered media with the geometry as given in Figure 3.1. Let the incident plane wave be given by

$$\bar{E}_i = E_0 \, e^{-\gamma_A (\bar{n} \cdot \bar{r})} \, \bar{a}_3$$

where E_0 is the magnitude of the incident plane wave, $\bar{n}$ is a unit vector in the direction of propagation, γ_A is propagation factor in medium A, $\bar{r}$ is the position vector, and $\bar{a}_z$ is a unit vector perpendicular to the plane of incidence signifying horizontal polarization. The reflection and transmission coefficient at the particular boundaries are defined as:

$$\Gamma_j = \frac{\text{Electric field reflected at the jth interface}}{\text{Electric field incident at the jth interface}}$$

$$\gamma_{j,k} = \frac{\text{Electric field transmitted between interfaces j and k}}{\text{Electric field incident at the jth interface}}$$

The total reflected electric in Medium A will be

$$\Gamma_{TOTAL} = \Gamma_1 + \gamma_{1,2} \, \Gamma_3 \, \gamma_{2,1} \, e^{-\gamma_B d_B} + \gamma_{1,2} \, \Gamma_3^2 \, \Gamma_2 \, \gamma_{2,1} \, e^{-4\gamma_B d_B} + \ldots$$

$$= \Gamma_1 + \gamma_{1,2} \, \gamma_{2,1} \, \Gamma_3 \cdot \sum_{n=0}^{\infty} (\Gamma_2 \, \Gamma_3 \, e^{-2\gamma_B d_B})^n$$

where γ_B is the propagation factor in medium B and d_B is the distance traversed by the electric field in medium B. Using the identity for a convergent series
$$\sum_{n=0}^{\infty} r^n = \frac{1}{1-r} , \quad \text{for } r < 1$$

131

and setting

$$r = \Gamma_2 \Gamma_3 e^{-2\gamma_B d_B} < 1$$

gives

$$\Gamma_{TOTAL} = \Gamma_1 + \frac{\tau_{1,2} \tau_{2,1} \Gamma_3 e^{-2\gamma_B d_B}}{1 - \Gamma_2 \Gamma_3 e^{-2\gamma_B d_B}}$$

(A.1)

Using the boundary conditions $\tau_{1,2} = 1 + \Gamma_1$ and $\tau_{2,1} = 1 + \Gamma_2$ along with the relationship $\Gamma_2 = -\Gamma_1$ in eq. A-1 gives

$$\Gamma_{TOTAL} = \Gamma_1 + \frac{(1 - \Gamma_1)^2 \Gamma_3 e^{-2\gamma_B d_B}}{1 + \Gamma_1 \Gamma_3 e^{-2\gamma_B d_B}}$$

or

$$\Gamma_{TOTAL} = \frac{\Gamma_1 + \Gamma_3 e^{-2\gamma_B d_B}}{1 + \Gamma_1 \Gamma_3 e^{-2\gamma_B d_B}}$$

(A.2)

APPENDIX B

DERIVATION OF THE TOTAL REFECTION
COEFFICIENT OF THE TWO-LAYER MODEL WITH ROUGHNESS

Consider a layered media with the geometry as given in Figure 5.1 and with roughness describable by the small perturbation theory at only the interface between mediums A and B. Let the incident plane wave be given by

$$\bar{E}_i = E_o \, e^{-\gamma_A (\hat{n} \cdot \bar{r})} \, \bar{a}_3$$

where E_o is the magnitude of the incident plane wave, $\bar{n}$ is a unit vector in the direction of propagation, $_A$ is the propagation factor in medium A, $\bar{r}$ is the position vector, and $\bar{a}z$ is a unit vector perpendicular to the plane of incidence signifying horizontal polarization. The reflection and transmission coefficients at the particular boundaries are now defined as:

Γ'_j = $\dfrac{\text{Electric field reflected from the } j^{\text{th}} \text{ interface at the specular angle}}{\text{Electric field incident at the } j^{\text{th}} \text{ interface in the specular direction}}$

$\tau'_{j,k}$ = $\dfrac{\text{Electric field transmitted between interfaces } j \text{ and } k \text{ at the specular angle}}{\text{Electric field incident at the } j^{\text{th}} \text{ interface in the specular direction}}$

The total reflection is defined as

Γ'_{Total} = $\dfrac{\text{Total reflected electric in medium A}}{\text{Electric field incident in medium B}}$

Then the total reflection in medium A will be

$$\Gamma'_{\text{TOTAL}} = \Gamma'_1 + \tau'_{1,2}\,\Gamma'_3\,\tau'_{2,1}\, e^{-2\gamma_B d_B} + \tau'_{1,2}\,\Gamma'^{2}_3\,\tau'_{2,1}\, e^{-4\gamma_B d_B} \, \ldots \ldots$$

$$= \Gamma'_1 + \tau'_{1,2}\,\tau'_{2,1}\,\Gamma'_3\, e^{-2\gamma_B d_B} \sum_{n=0}^{\infty} \left(\Gamma'_2 \Gamma'_3\, e^{-2\gamma_B d_B} \right)^n$$

133

where γ_B is the propagation factor in medium B and d_B is the distance traversed by the fields in Medium B. Using the identity for a convergent series

$$\sum_{n=0}^{\infty} r^n = \frac{1}{1-r}, \quad \text{for } r < 1$$

and setting

$$r = \Gamma_2' \Gamma_3' e^{-2\gamma_B d_B} < 1$$

gives

$$\Gamma_{TOTAL}' = \Gamma_1' + \frac{T_{1,2}' T_{2,1}' \Gamma_3' e^{-2\gamma_B d_B}}{1 - \Gamma_3' \Gamma_2' e^{-2\gamma_B d_B}} \tag{B.1}$$

which is in the same form as the smooth surface two-layer model except that Γ_1', Γ_2' $\tau_{1,2}'$, and $\tau_{2,1}'$ are now rough surface reflection and transmission coefficients. The rough surface transmission and reflection coefficients at the interfaces are related to the smooth surface transmission and reflection coefficients using equations 5.1 and 5.3 by the following relationships:

$$T_{1,2}' = \rho \left(1 + \Gamma_1 \right)$$
$$T_{2,1}' = \rho \left(1 + \Gamma_2 \right)$$
$$\Gamma_1' = \rho \, \Gamma_1$$
$$\Gamma_2 = -\Gamma_1$$
$$\Gamma_2' = \rho \, \Gamma_2 = -\rho \, \Gamma_1$$

where Γ_1 and Γ_2 are the smooth surface reflection coefficients. Since the interface between mediums B and C is considered to smooth, Γ_3' is given by the smooth reflection coefficient. Substituting the above relationships into equation B.1 gives the total reflection of the rough

134

surface two-layer model in terms of the roughness factor ρ and the smooth surface reflection coefficients as

$$\Gamma_{TOTAL} = \rho \Gamma_1 + \frac{\rho^2(1-\Gamma_1^2)\Gamma_3 e^{-2\gamma_B d_B}}{1 + \rho \Gamma_1 \Gamma_3 e^{-2\gamma_B d_B}}$$

or

$$\Gamma_{TOTAL} = \rho \left(\frac{\Gamma_1 + \rho \Gamma_3 e^{-2\gamma_B d_B}}{1 + \rho \Gamma_1 \Gamma_3 e^{-2\gamma_B d_B}} \right) \qquad (B.2)$$

BIBLIOGRAPHY

Ament, W. S., "Toward a Theory of Reflection by a Rough Surface,"
Proc. IRE, Vol. 41, pp. 142-146, 1953.

Basharinov, A. Ye. and Shutke, A. M., Model'nyye issledovaniya SVCh
radiatsionnykh kharakteristik pochv-gruntvo v usloviyakh uvlazhnenive
(Simulation Studies of the SHF Radiation Characteristics of Soils Under
Moist Conditions). Report of the IRE Academy of Sciences of the USSR,
1975.

Beckmann, P. and Spizzichino, A., The Scattering of Electromagnetic
Waves from Rough Surfaces, The MacMillan Co., New York, 1963.

Brekhovskikh, Waves in Layered Media, Academic Press Inc., New York, 1960.

Collin, R., Foundations for Microwave Engineering, McGraw-Hill Book Co.
1966.

Davies, H., "The Reflection of Electromagnetic Waves from a Rough Surface,"
Proc. IEEE, Vol. 101 (Part IV), page 209, 1954.

Hancock, G. D., "Broad Spectrum Microwave Measurements of Rough Discon-
tinuous Surfaces for the Determination of Moisture Content," M. S. Thesis,
University of Arkansas, Fayetteville, Arkansas, 1976.

Hancock, G. D., "Data Documentation for the Bare Soil Experiment at the
University of Arkansas July 9 - October 19, 1979," Elec. Eng. Dept.,
University of Arkansas, 1980.

Hillel, D., Soil and Water - Physical Principles and Processes, Academic
Press, Inc., New York, 1971.

Jackson, R. D., "Diurnal changes in Soil-Water Content During," Field
Soil Water Regime, Edited by R. R. Bruce et al., Spec. Publ. 5, pp. 37-55,
Soil Sci. Soc. Amer., Madison, Wisc., 1973.

Kraus, J. D. and Craver, K. R., Electromagnetics, McGraw-Hill Book Co.,
New York, 1973.

Lundien, J. R., "Terrain Analysis by Electromagnetic Means, Report 5,"
Technical Report No. 3-693, U.S. Army Engineer Waterways Experiment Station,
Vicksburg, Mississippi, February, 1971.

Lundien, J. R.. "Determining Presence, Thickness, and Electrical Properties
of Stratified Media Using Swept - Frequency Radar," Technical Report No.
M-72-4, U.S. Army Engineer Waterways Experiment Station, Vicksburg, Mississippi.
November, 1972.

Newton, R. W., "Microwave Remote Sensing and Its Application to Soil Moisture
Detection," Technical Report RSC-81, Texas A & M University, College
Station, Texas, 1977.

Peake, W. H., "The Interaction of Electromagnetic Waves with Some Natural Surfaces," Ph.D. Dissertation, Ohio State University, Columbus, Ohio, 1959.

Ramo, S., Whinnery, J. R., and Van Duzer, T., Fields and Waves in Communications Electronics, John Wiley & Sons, Inc., New York, 1967.

Reid, C. S., "The Utility of Microwave Remote Sensing Techniques for soil Moisture Profile Determination," M.S. Thesis, University of Arkansas, Fayetteville, Arkansas, 1977.

Rice, S. O., "Reflections of Electromagnetic Waves from Slightly Rough Surfaces," Communications in Pure and Applied Mathematics, Vol. 4, pp. 351-378, 1951.

Ruck, G. T., Barrick, D. E., Stuart, W. D. and Kichbaum, C. K., Radar Cross Section Handbook, Plenum Press, New York, 1970.

Stiles, W. H., "The Effect of Surface Roughness on the Microwave Measurement of Soil Moisture Content," M.S. Thesis, University of Arkansas, Fayetteville, Arkansas, 1974.

Stratton, J. A., Electromagnetic Theory, McGraw-Hill Book Co., New York, 1941.

Wait, J. R., Electromagnetic Waves in Stratified Media, The MacMillian Company, New York, 1962.

Waite, W. P., Cook, K. R., and Bryan, B. B., "Broad Spectrum Microwave Systems for Remotely Measuring Soil Moisture Content," Publication No. 18, Waiter Resources Research Center, University of Arkansas, Fayetteville, Arkansas, 1973.

Wang, J. R. and Schmugge, T. J., 'An Empirical Model for the Complex Dielectric Permittivity of Soils as a Function of Water Content, "NASA/GSFC Technical Memorandum 80597, 1978.

Wilheit, T. T., "Radiative Transfer in a Plane Stratified Dielectric," IEEE TRANS. on Geoscience Electronics," Vol. CE-16, No. 2, pp. 138-143, 1978.